THEORY, FABRICATION AND PERFORMANCE OF SOME INTEGRATED OPTICAL DEVICES

THESIS

by

Sasson R. Somekh

In Partial Fulfillment of the Requirements

for the Degree of

Doctor of Philosophy

California Institute of Technology

Pasadena, California

1974

(Submitted August 6, 1973)

TO MY DEAR PARENTS

ACKNOWLEDGMENTS

I wish to express my enormous gratitude to my advisor, Dr. Amnon Yariv, for his guidance, inspiration and friendship. His invaluable comments, suggestions, directions and criticism initiated and formed the contents of this work. I am also indebted to Dr. Elsa Garmire for her invaluable guidance and encouragement throughout the course of this work.

It has been a special privilege to have been a part of the quantum electronics group at Caltech. The collaboration between the members, the stimulating discussions and the helpful suggestions made the work pleasant and fruitful. I would like to thank my fellow students: Hal Stoll, Huan Wun Yen, and Avi Gover, as well as Dr. Michiharu Nakamura who spent the last year as a postdoctoral fellow at Caltech. The technical assistance of Desmond Armstrong is also greatly appreciated.

During the course of this work, our research group has had the good fortune of a close working relationship with the Hughes Research Laboratories in Malibu, California. I would like to thank in particular Dr. Hugh Garvin whose invaluable suggestions and talents have made dreams come true.

Special thanks are due to Dian Rapchak and Ruth Stratton for the masterful typing of the manuscript.

The financial support received from the Army Research Projects Agency (Monitored by the Army Research Office--Durham), the Office of Naval Research, and the Air Force Office of Scientific Research is greatly appreciated.

Finally, my thanks go to my wife, Eta, for her love and support.

ABSTRACT

Recent progress in the fabrication of low attenuation optical fibers raises the attractive possibility of optical communications via these waveguides. Integration of different optical functions on one substrate in the form of optical circuits will form ideal terminals for such a communication network. We shall discuss the theory, fabrication and performance of a few "building stones" of such optical circuits. Optical directional couplers capable of coupling light from one channel to another will be described and their use as switches will be discussed. Distributed feedback for integrated lasers will be analyzed. Laser action in a GaAs waveguide, in which distributed feedback was supplied by corrugations fabricated on the surface, will be described. Longitudinal and transverse mode control of such a laser will also be discussed. We shall conclude with an analysis of nonlinear interactions in thin films, pointing out new methods for phase matching and ways to implement them.

TABLE OF CONTENTS

I. INTRODUCTION

I.1 Optical Communications

One of the first exciting applications envisioned for the laser a decade ago was optical communication. The enormous information carrying capability of laser beams can be well understood by noting that at a wavelength of 1μ the frequency is $3 \cdot 10^5$ GHz.

This application has not materialized yet, largely because at the high optical frequency the laser beam is greatly attenuated in passage through a cloudy and rainy atmosphere. Optical waveguides in the form of small diameter (2-3 thousandths of an inch) glass fibers have been available for quite some time. However, the attenuation of the light propagating in those flexible fibers was so great that their use as "optical cables" was ruled out.

Recently low loss optical fibers have been fabricated. The fibers can be used for short distance communication systems like the ones between a computer and its peripheral equipment, or for medium and long distance communication systems with a repeater every several miles. They combine small size and light weight together with large bandwidths (several G bit/sec for a single mode fiber and several M bit/sec for a multimode fiber). Interference and pick-up problems are easily eliminated by coating the fiber with opaque material, and ground loop problems do not exist in fiber optics systems.

A review of the principles of operation of these fibers, their properties such as attenuation and bandwidth, and their input and output devices is given by S. Somekh and A. Yariv[1]. The enormous advances in the fabrication of low loss fibers can be appreciated by considering the spectral attenuation curve (Fig. I.1) for a multimode fiber fabricated by researchers at Corning Glass Works[2]. There are two important low loss attenuation spectral regions with loss as low as 4 db/km around 0.85μ (aluminum gallium arsenide laser and light emitters) and 1.06μ (neodynium YAG laser).

The low attenuation in these fibers together with their large bandwidth, revive again the hopes that optical communications will play an important role in the telephone network and in other types of communication networks such as the ones on aircrafts and ships, and the ones between a computer and its peripherals. Another potential application for fibers may very well be cable television.

These applications of the optical fibers call also for small, rugged and inexpensive terminals in which light will be generated and detected, and in which information will be imposed and extracted at high rates. It is also reasonable to believe that features such as switching and filtering of optical signals will have to be carried out at these terminals. These requirements have stimulated the work in the field known as "Integrated Optics."

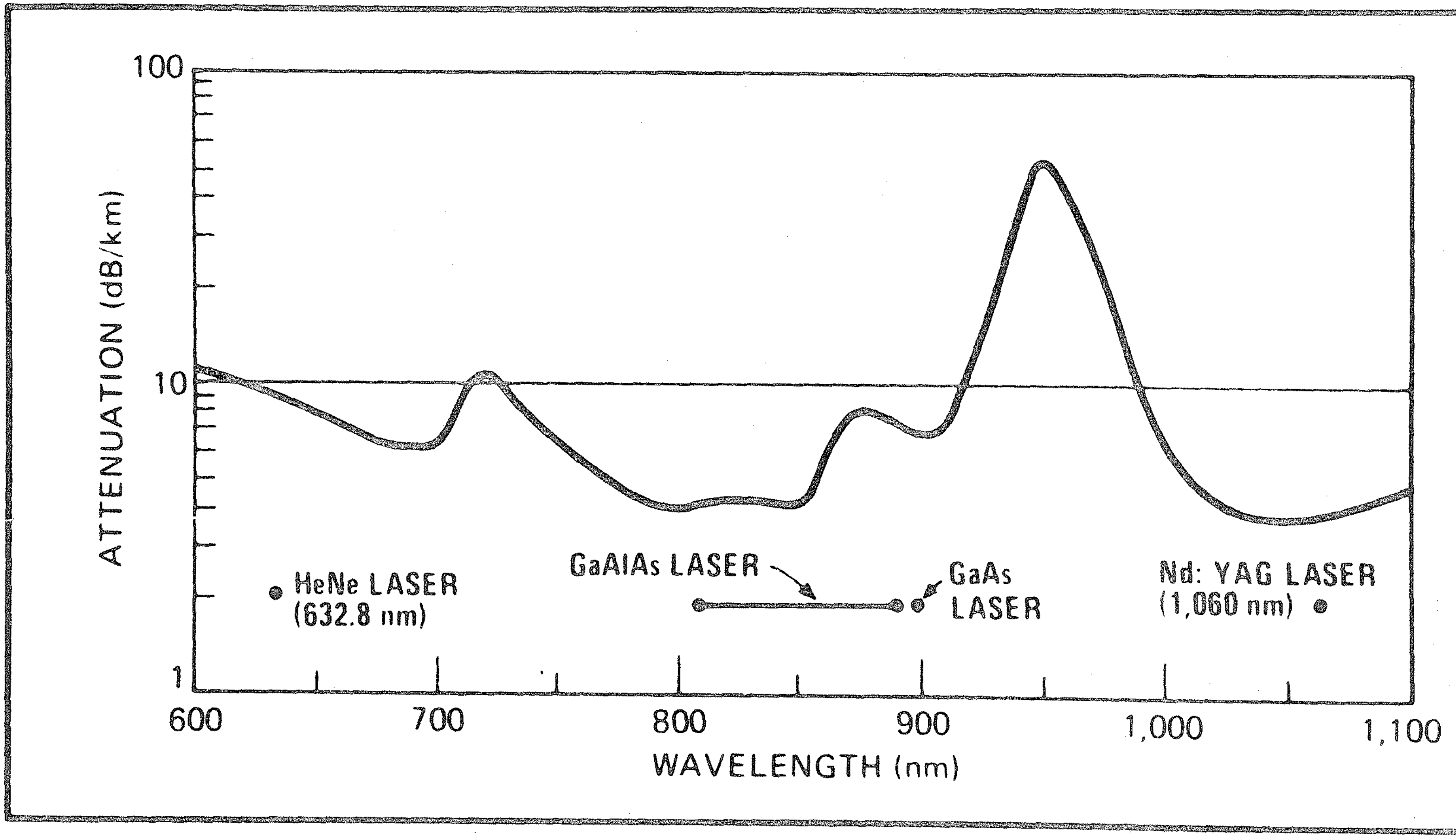

Fig. I.1 Spectral attenuation of a low loss multimode optical fiber (after Ref. 2).

I.2 Integrated Optics

A typical conventional "optical circuit" is described in Fig. 2. It consists of a light source, a modulator, an electronic driver for the modulator, polarizers and a lens. It is bulky, heavy, very often unreliable and expensive. In addition the interface between the solid state electronics and optics is complicated and usually limits the performance. The desire to overcome the same kind of problems as the ones faced by electronic circuits a decade ago has led to the development of a new research field called "integrated optics"[3-5]. The idea is to incorporate on a small substrate all the optical components required to make up the various optical circuits. Lasers, modulators and detectors, along with waveguides (the "optical wires") and the analog components to lenses, prisms, mirrors, polarizers, etc. are to be fabricated on a single chip yielding small, rugged, reliable and inexpensive optical circuits.

Let us examine, for example, some of the things that can be fabricated on a chip of GaAs. This material and its alloy $Al_xGa_{1-x}As$ are highly suitable for integrated optics purposes[4]. Waveguides can be easily constructed in GaAs; injection lasers are made of this material and a p-n diode when reverse biased is capable of detecting light. The electrooptic effect (change in the index n with the applied electric field) in GaAs is among the largest, thus allowing the use of efficient modulators. Finally, the possibility of incorporating fast electronic circuits together with optical circuits on the same chip would ease the interfacing problem.

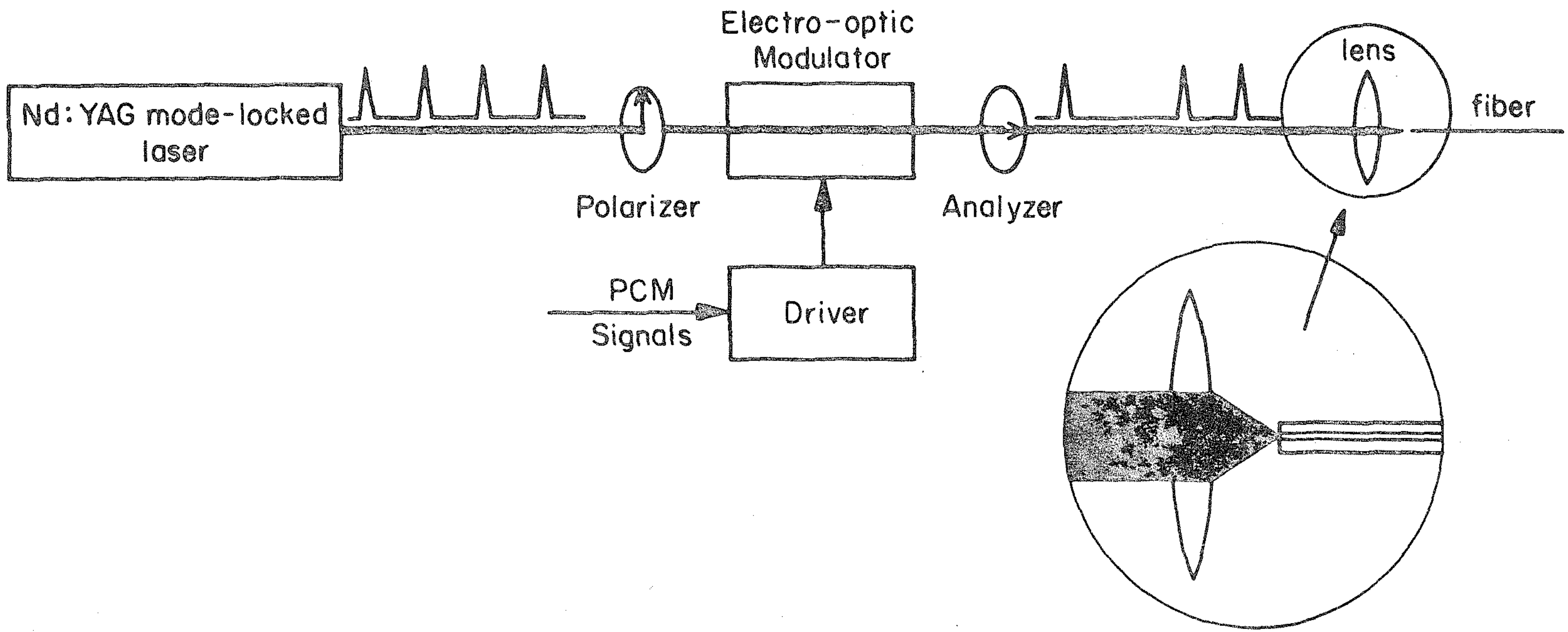

Fig. I.2 Fiber optics transmitter terminal employing a Nd:YAG laser and discrete components.

Since the field of integrated optics is in its first stages, most of the work in the field is concentrated on providing the building stones of the optical circuits. These building blocks include components and devices such as guides, directional couplers[16], modulators[7], detectors[8], surface lasers and cavities[9,10] mirrors, polarizers[11] and so on.

Chapters II and III deal with the theory, fabrication and performance of some of these components and devices. Figure I.3 describes two types of dielectric channel waveguides to be discussed. The one on the left is an embedded guide while the other is a ridged guide. When two guides are closely spaced so that the mode profiles overlap, optical coupling or tunneling occurs. Figure I.4 describes such a case. If the interaction length is appropriate, light entering the device in one channel will completely tunnel into the other channel and will emerge from there. This device is known as the directional coupler, and we shall describe the first experimental demonstration of the effect in embedded and ridged channels. Controlling the tunneling or the coupling between the two channels by applying electric field turns the device into a switch, capable of steering light pulses from one channel to the other on demand. This may find an important use in optical switching and multiplexing systems. We shall discuss this possibility in detail and point out a way of performing it with lower electric fields.

In our treatment of the theory we shall attempt to avoid elaborate solutions of Maxwell equations, but rather resort to

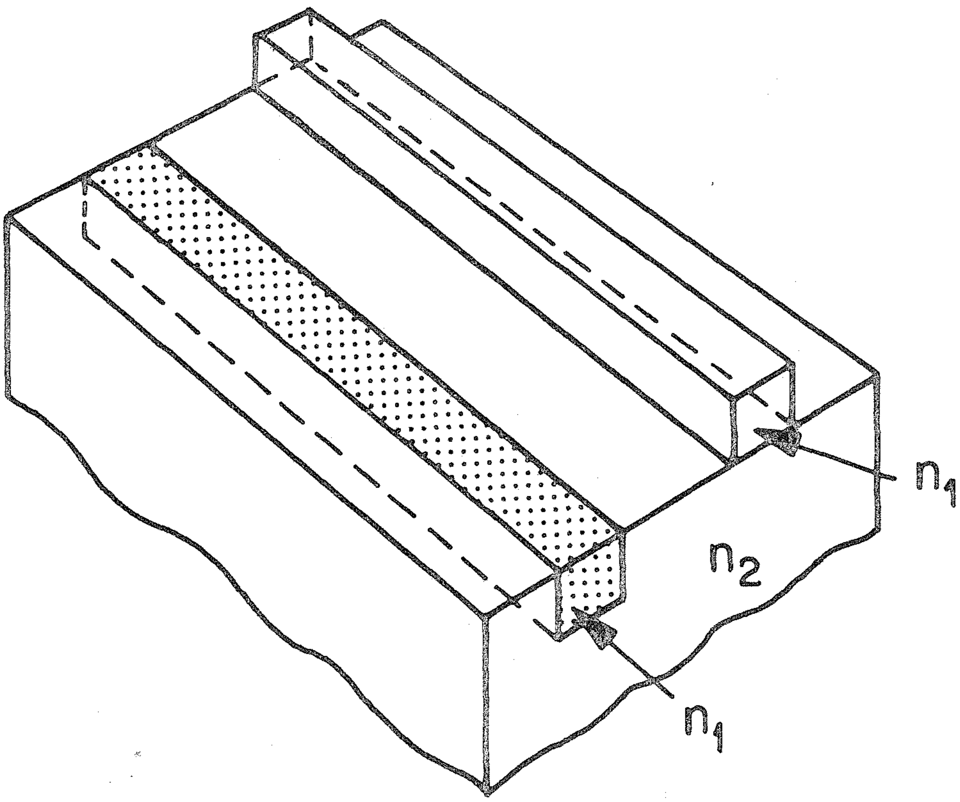

Fig. I.3 Embedded and ridged dielectric channel waveguides.

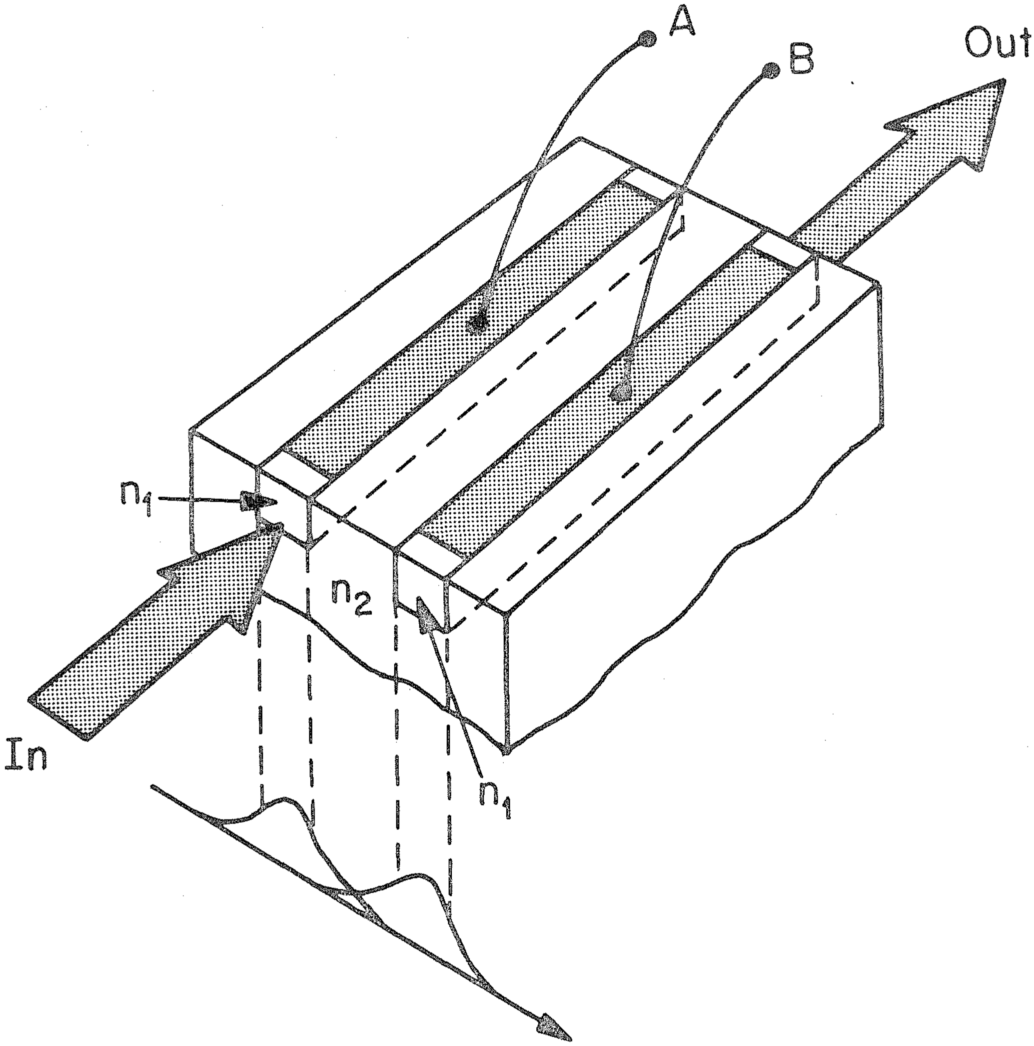

Fig. I.4 The optical directional coupler.

approximations that will enhance the physical understanding.

In Chapter III we shall concern ourselves with the linear applications of periodic structures in thin films. Our main interest will be in the formation of a suitable cavity for an integrated laser. The conventional GaAs laser is cleaved on both ends. The cleaving forms two distinct partial mirrors which have sufficient reflection to sustain the oscillation. This however is not compatible with the concept of integrated optical circuits, and alternatives will be examined. We shall describe a novel alternative which uses Bragg reflection from a mechanical corrugation on the surface of the waveguide as shown in Fig. I.5. When the corrugation period Λ satisfies:

$$\Lambda = \frac{\lambda}{2}$$

where λ is the wavelength of the guided propagating mode $\mathcal{E}_0$, the Bragg condition is fulfilled and backward reflection occurs. The intensities of the forward and backward propagating modes along a distributed mirror of length L are shown in Fig. I.5.

For GaAs ($\lambda_0 = 0.83\mu$, $n = 3.6$) a corrugation with a very small period of $\Lambda = 0.1150\mu$ is necessary and a method was devised to fabricate it. If the corrugation extends along the whole length of an amplifying medium a distributed feedback laser[9] may result. The frequency of oscillation of this laser is related to the corrugation period as in the last equation and can be varied by changing Λ. This effect is potentially useful for a frequency multiplexed communication network.

$$\Lambda = \frac{\lambda}{2}$$

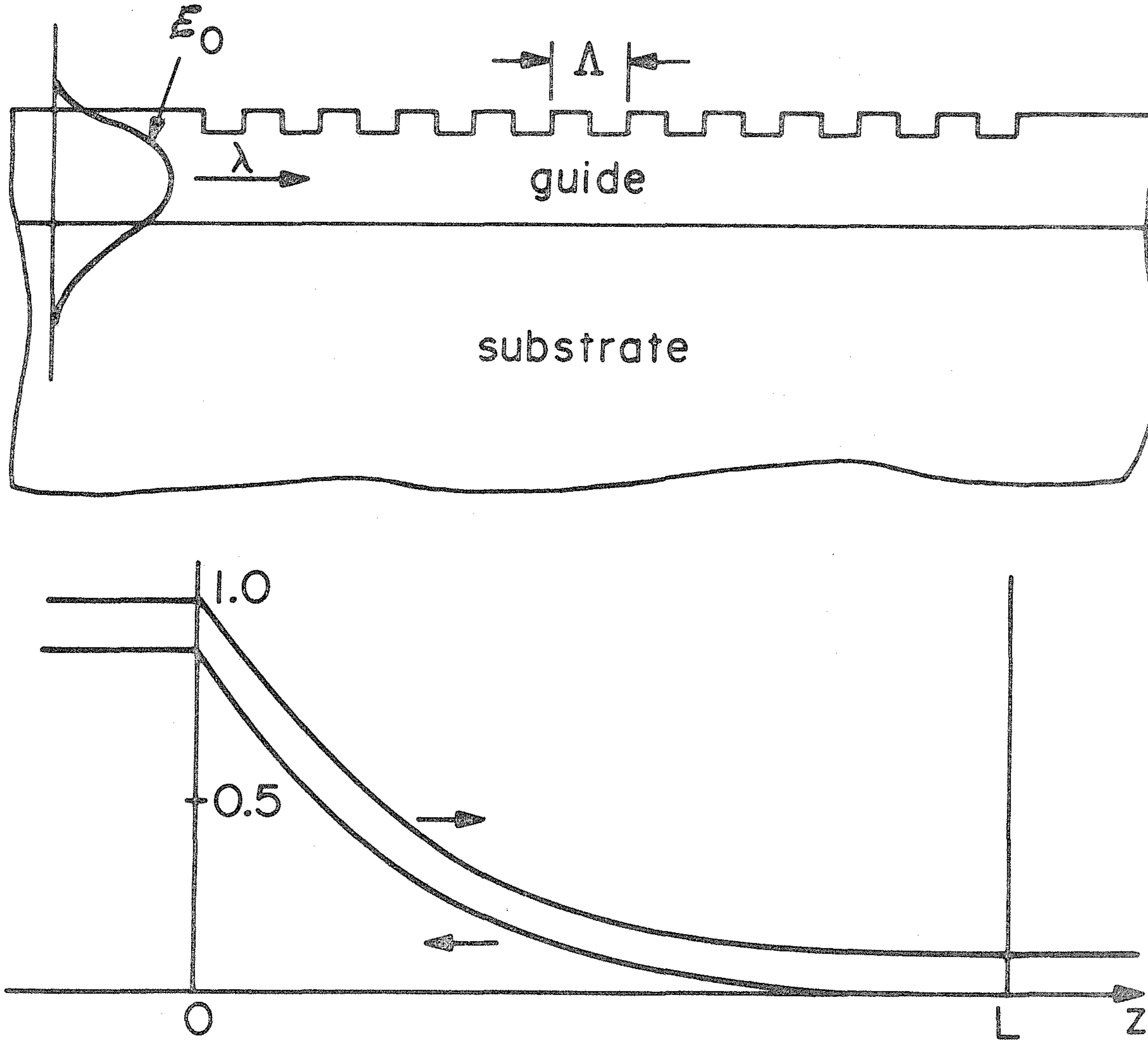

Fig. I.5 Bragg reflection from a distributed mirror, made of corrugation on the surface of the waveguide. The input beam decays as a function of z , giving rise to the reflected beam.

We shall describe the first observation of a distributed feedback laser in GaAs[10] and elaborate on longitudinal and transverse mode control.

Periodic structures in thin films are also useful for phase matching nonlinear interactions. This application will be discussed in the next section.

I.3 Nonlinear Interactions

The important application of integrated optics to optical communications shadows somewhat its interesting application to nonlinear optics. In the thin film configuration where the propagating power is confined to the guiding layer or channel, a moderate amount of total power yields a high power density. This power is confined to the guide and will propagate indefinitely with no diffraction, as opposed to the bulk devices. The high power density and the long interaction length are two factors that improve the efficiency of a nonlinear interaction and thus make the use of integrated optics attractive for nonlinear purposes.

Another advantage of the thin film configuration is related to the problem of phase matching which is also required for efficient nonlinear interactions. As an example, in the case of second harmonic generations the interaction is phase matched if the two interacting waves propagate with the same phase velocity. Because of material dispersion the phase velocities are usually not the same; however, in some cases it is possible to use the material birefringent for phase matching. This is usually done by picking an appropriate crystal orientation in which the two frequencies propagate with different polarizations but with the same phase velocities. For materials that are not birefringent and cannot therefore be phase matched by the above technique[12], thin films offer new methods for phase matching.

In Chapter IV we shall describe two new techniques for phase matching using periodic structures. One method[13] makes use of the same kind of corrugations encountered in the previous section, to generate space harmonics for each interacting wave. These space harmonics have each a different phase velocity. Some of these phase velocities can be matched when the period of the corrugation is appropriate. A second, more efficient method[14] we shall discuss, solves the problem of phase matching by modulation of the nonlinear coefficient of the guiding material. This method, however, is more difficult to realize and we shall describe a scheme for performing it. We shall conclude Chapter IV by describing the experiments performed to date.

I.4 Fabrication of Integrated Optics Components

We shall devote a whole chapter (Chapter V) to the fabrication of the devices we have discussed earlier, because, in my opinion, the fabrication problems will determine the rate at which the new field of integrated optics will develop. The dimensions of the channel guides are, as in their microwave counterparts, of the order of the wavelength. This means that structures with dimensions of a few microns have to be fabricated with high quality edge smoothness. As another example we recall that for a distributed feedback laser in GaAs a corrugation with a period of 0.1150μ has to be fabricated on the surface of GaAs.

We have used[15] the most sophisticated microfabrication methods such as electron beam lithography and ion beam milling. We have also devised new techniques, such as holographic exposure of photoresist combined with ion milling, for the fabrication of the small period corrugation.

References for Chapter I

1. S. Somekh and A. Yariv, "Fiber Optics Communications," Proceedings of the International Telemetering Conference (Los Angeles) VIII, 407 (1972).

2. D. B. Keck, R. D. Maurer, and P. C. Schultz, "On the Ultimate Lower Limit of Attenuation in Glass Optical Waveguides," Appl. Phys. Lett. 22, 307 (1973).

3. R. Shubert and J. H. Harris, "Optical Surface Waves on Thin Films and their Application to Integrated Data Processors," IEEE Trans. on Microwave Theory and Techniques, MIT-16, 1048 (1968). Also, S. E. Miller, "Integrated Optics: An Introduction," BSTJ, 48, 2059 (1969).

4. A. Yariv, "Active Integrated Optics," Proceedings, 1971 Esphahan Conference on Pure and Applied Physics (Wiley, N. Y.) in press.

5. P. K. Tien, "Light Waves in Thin Films and Integrated Optics," Appl. Optics, 10, 2395 (1971).

6. S. Somekh, E. Garmire, A. Yariv, H. L. Garvin and R. G. Hunsperger, "Channel Optical Waveguide Directional Couplers," Appl. Phys. Lett. 22, 46 (1972).

7. D. Hall, A. Yariv, and E. Garmire, "Optical Guiding and Electrooptic Modulation in GaAs Epitaxial Layers," Opt. Comm. 1, 403 (1970). Also, D. Hall, A. Yariv, and E. Garmire, "Observation of Propagation Cutoff and Its Control in Thin Optical Waveguides," Appl. Phys. Lett. 17, 127 (1970). Also F. K. Reinhart and B. I.

Miller, "Efficient GaAs-Al_xGa_{1-x}As Double Heterostructure Light Modulators," Appl. Phys. Lett. 20, 36 (1972).

8. H. Stoll, Ph.D. Thesis, California Institute of Technology, Pasadena, California, 1974.

9. H. Kogelnik and C. V. Shank, "Coupled Wave Theory of Distributed Feedback Lasers," J. Appl. Phys. 43, 2328 (1972).

10. M. Nakamura, A. Yariv, H. W. Yen, S. Somekh, and H. L. Garvin, "Optically Pumped GaAs Surface Laser with Corrugation Feedback," Appl. Phys. Lett. 22, 515 (1973). Additional work is to be published.

11. E. Garmire and H. Stoll, "Propagation Losses in Metal-Film-Substrate Optical Waveguides," IEEE Journal of Quantum Electronics, QE8, 763 (1972).

12. J. A. Giordmaine, "Mixing of Light Waves in Crystals," Phys. Rev. Lett. 8, 19 (1972). Also, P. D. Maker, R. W. Terhune, M. Nisenoff, and C. M. Savage, "Effects of Dispersion and Focusing on the Production of Optical Harmonics," Phys. Rev. Lett. 8, 21 (1962).

13. S. Somekh and A. Yariv, "Phase-Matchable Nonlinear Optical Interactions in Corrugated Thin Films," Appl. Phys. Lett. 21, 140 (1972).

14. S. Somekh and A. Yariv, "Phase Matching by Periodic Modulation of the Nonlinear Optical Properties," Opt. Comm. 6, 301 (1972).

15. H. L. Garvin, E. Garmire, S. Somekh, H. Stoll, and A. Yariv, "Ion Beam Micromachining of Integrated Optics Components," Appl. Optics 12, 455 (1973).

II. OPTICAL DIRECTIONAL COUPLERS

II.1 Introduction

The optical directional coupler, analogous to the microwave element(1) of the same name, consists of parallel channel optical waveguides sufficiently closely spaced that energy is transferred from one to another. For this coupling to take place cumulatively over a substantial length, the light must propagate with the same phase velocity in each channel. The fraction of the power coupled per unit length is determined by the overlap of the modes in the separate channels. Thus, it depends on the guides' separation, the mode penetration into the substrate, and the interaction length. Figure II.1 is an example of a multichannel directional coupler. It shows a diagram of a large number of coupled channel waveguides (produced by proton implantation) and typical intensity profiles of the guided light. The incident light is focused into a single channel at $z = 0$, but is coupled into the adjacent guides as it propagates.

A theoretical analysis of the coupling between dielectric waveguides usually involves a formal solution of Maxwell's equations(2). We shall attempt here to derive an expression for the coupling coefficient and its sign from an intuitive physical point of view without resorting to an elaborate mathematical solution. We shall also derive the power distribution as a function of propagation distance for two coupled guides and an infinite number of coupled guides.

Experimental results of a dual channel directional coupler and a multichannel coupler will be given. These channels were embedded

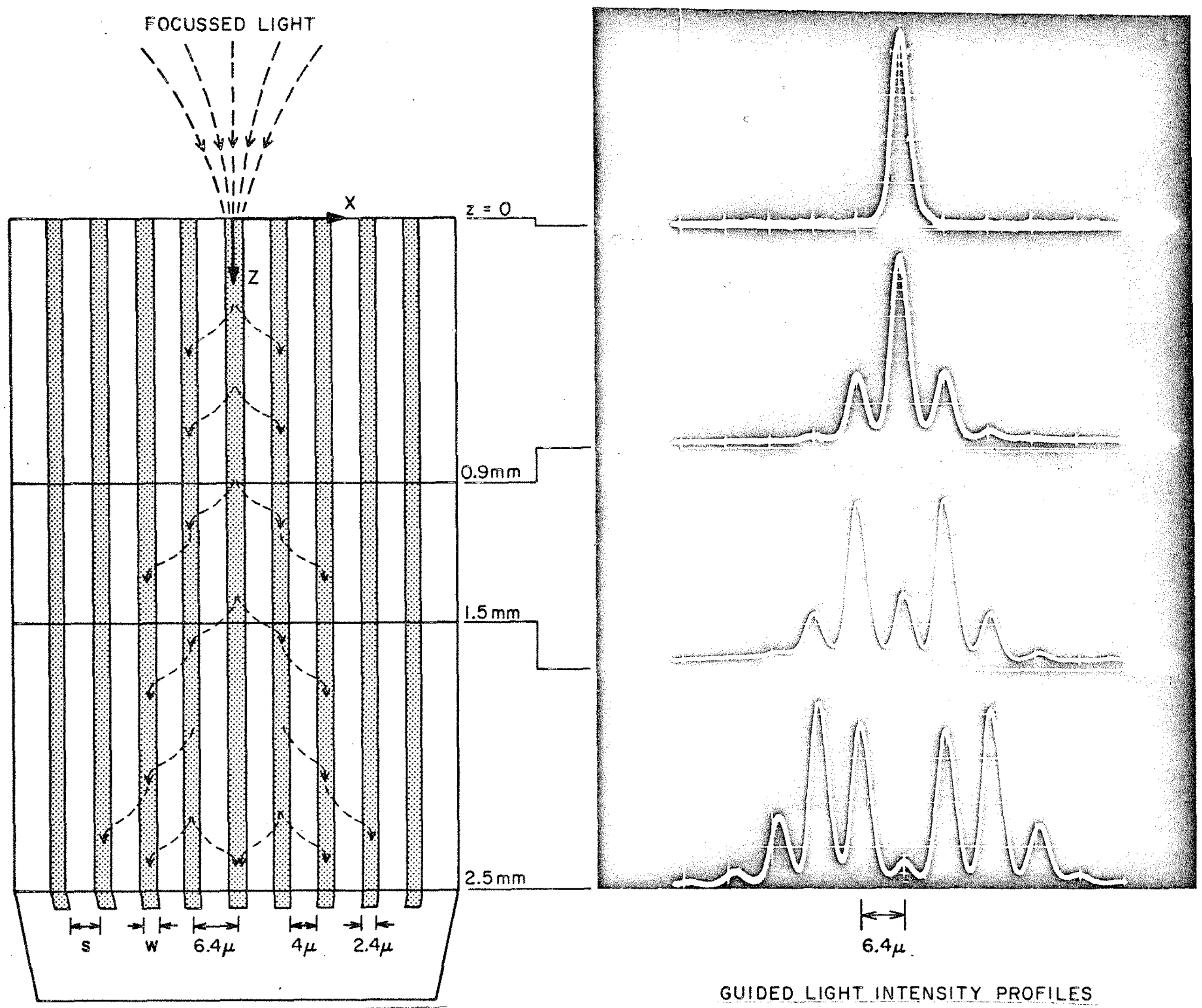

Fig. II.1 Sketch of channel optical waveguide directional coupler showing flow of light energy into adjacent channels. To the right are photographs of guided light intensity profiles for various lengths. Intensity scale is arbitrary.

at the surface of GaAs by proton implantation. A different type of directional coupler suitable for ridged waveguides is also described. We conclude with an account of the different applications of these devices in an integrated optics circuit, such as couplers, modulators, multiplexers and polarizers.

II.2 Coupled Mode Formalism

Let us consider the two waveguides shown in Fig. II.2a. The waveguides can have an arbitrary cross section; however, for the sake of simplicity, we consider only guides with rectangular cross sections. The electric field of a propagating mode in a guide is described by the complex amplitude $A(z)$ which includes the phase term $e^{i\beta z}$, and by the mode $\vec{\mathcal{E}}(x,y)$ solved for in the absence of the other guide. We thus have:

$$\vec{E}(x,y,z) = A(z)\ \vec{\mathcal{E}}(x,y) \qquad \text{(II.2.1)}$$

The mode profiles $\mathcal{E}(x,y)$ are always normalized to carry one unit of power; the power carried by $E_1(x,y,z)$ (where the subindex 1 denotes the guide number), at a given z is

$$P_1(z) = |A_1(z)|^2 = A_1(z)\ A_1^*(z) \qquad \text{(II.2.2)}$$

Employing the coupled mode formalism[1], we write the general coupled mode equations for the amplitudes of the two modes

$$\frac{dA_0(z)}{dz} = -i\beta_0 A_0(z) + K_{01}A_1(z) \qquad \text{(II.2.3)}$$

$$\frac{dA_1(z)}{dz} = -i\beta_1 A_1(z) + K_{10}A_0(z) \qquad \text{(II.2.4)}$$

β_0 and β_1 are the propagation constants of the modes in the two guides (an imaginary part in β describes loss or gain that may exist in the guides). K_{01} and K_{10} represent the coupling between the two modes, and a great deal of the theory in this chapter will be devoted to their derivation. Before going into that, let us consider a theoretical and an experimental example of the coupled mode behavior.

II.3 Dual Channel Directional Coupler-Theory and Experiment

Consider the guides shown in Figure II.2a. We assume that the guides are identical and that both have an exponential loss constant of α. Thus the propagation constant of the guide is given by

$$\beta = \beta_r - i\,\frac{\alpha}{2} \qquad \text{(II.3.1)}$$

As we shall see later the coupled mode equation for this case can be written as:

$$\frac{dA_0(z)}{dz} = -i\beta\, A_0(z) - iKA_1(z) \qquad \text{(II.3.2)}$$

$$\frac{dA_1(z)}{dz} = -i\beta\, A_1(z) - iKA_0(z) \qquad \text{(II.3.3)}$$

where K, the coupling coefficient, is a real quantity. We also assume that at $z = 0$ light is coupled into guide 0 so that the

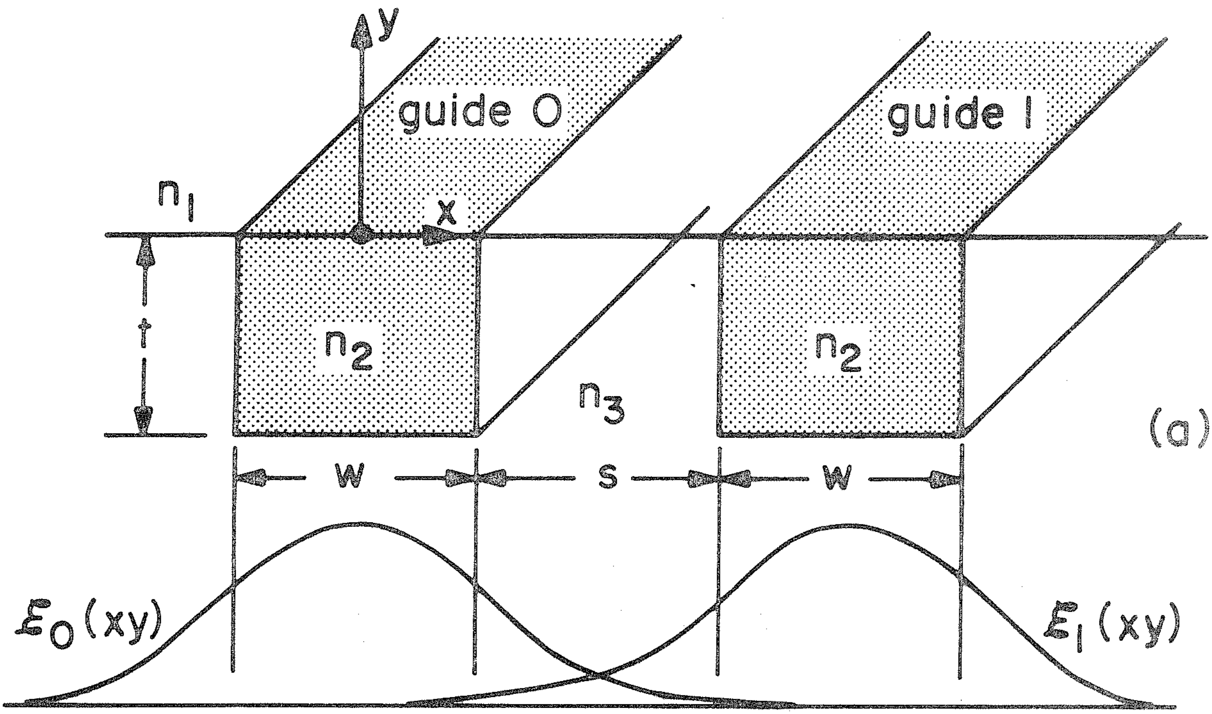

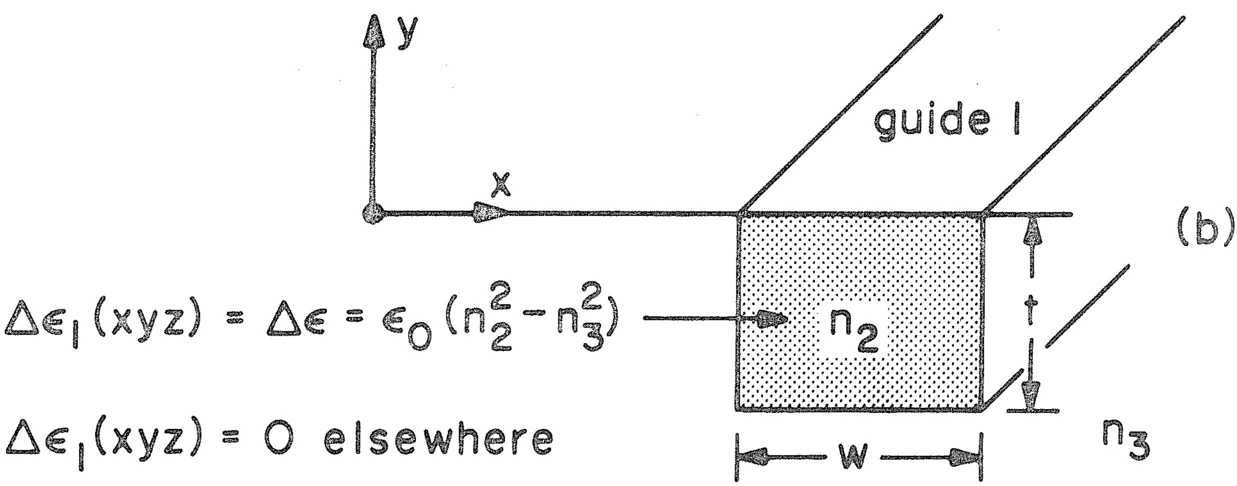

Fig. II.2 (a) Sketch of two adjacent rectangular waveguides and their propagating modes.

(b) Definition of the dielectric discontinuity $\Delta\varepsilon_1(xyz)$.

boundary conditions for the problem are given by

$$A_0(0) = 1 \qquad\qquad A_1(0) = 0 \tag{II.3.4}$$

The solution is described by:

$$A_0(z) = \cos Kz\ e^{i\beta z} \tag{II.3.5}$$

$$A_1(z) = -i \sin Kz\ e^{i\beta z} \tag{II.3.6}$$

The power flow in the guides therefore is

$$P_0(z) = A_0(z)\ A_0^*(z) = \cos^2 Kz\ e^{-\alpha z} \tag{II.3.7}$$

$$P_1(z) = A_1(z)\ A_1^*(z) = \sin^2 Kz\ e^{-\alpha z} \tag{II.3.8}$$

From II.3.7 and II.3.8 we learn that the power will oscillate back and forth between the two guides as shown in Fig. II.3. Because of the losses present in the guide, the power will also decay exponentially as a function of the propagation distance. The length necessary for a complete transfer of power from one guide to the other is given by

$$L = \frac{\pi/2}{K} \tag{II.3.9}$$

Such a directional coupler that allows the transfer of light from one channel to another is one of the building blocks of optical integrated circuits. We shall describe in what follows the first

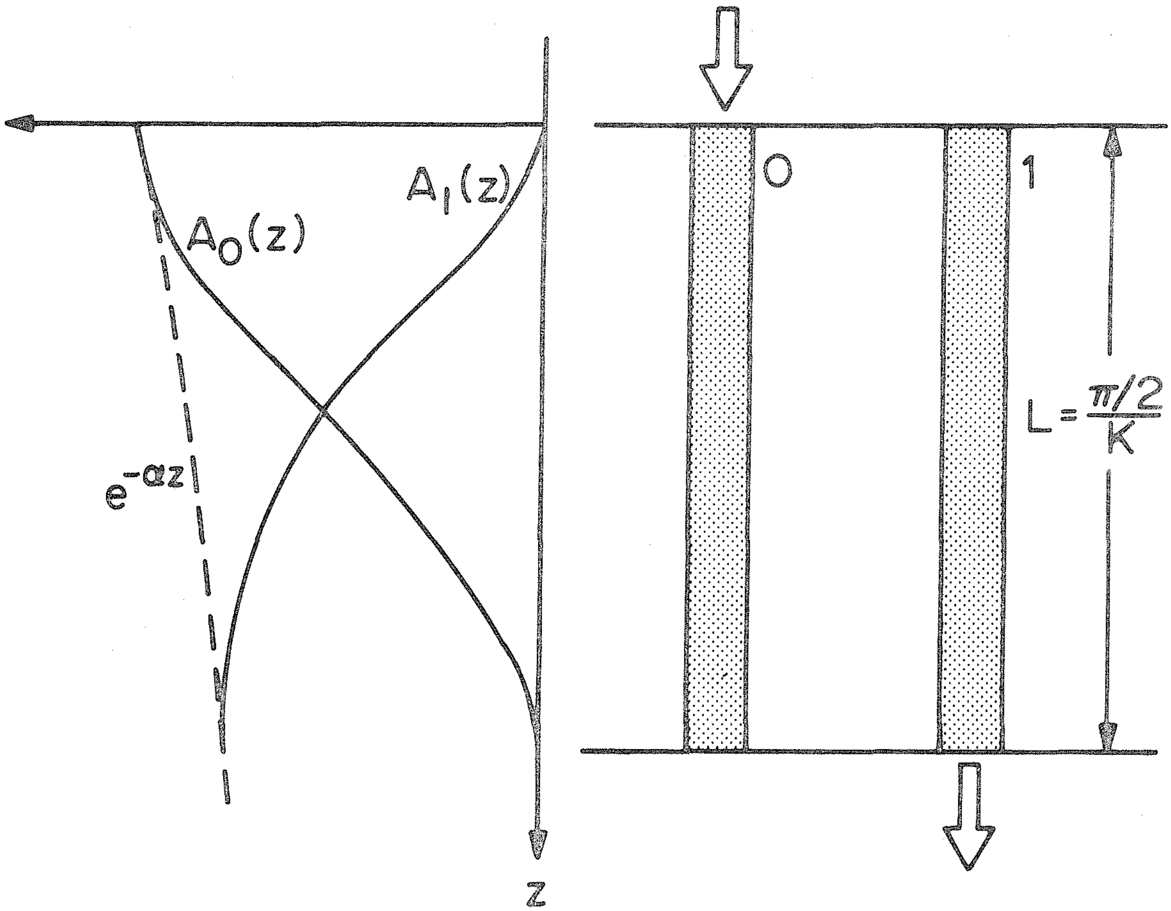

Fig. II.3 Sketch of a dual optical directional coupler showing flow of light energy between the guides.

operation of such a device in the optical regime.

The dual channel directional coupler was fabricated by proton implantation in GaAs[3] in a fashion described in detail in Chapter V. The channel guides were formed by implanting the protons through a gold mask with the appropriate slit openings in it. Bombardment causes defect centers in the material, which trap the free carriers. This compensation of the free carriers eliminates their negative plasma contribution to the index of refraction, and thus increases the index for the samples used here ($N_{substrate} \approx 2 \times 10^{18}$) by $\Delta n \simeq .005$. The cross section of the gold mask on top of the GaAs substrate is shown in Fig. II.4a. This way the guides embedded at the surface have a cross section of about $3 \times 3\mu$, an index discontinuity of about $\Delta n \simeq .005$, and a separation of 3μ between the guides.

Fig. II.5 describes three pair of such directional couplers. On the left is the input plane of the device and the black dot indicates the point at which the input light was focused. On the right is a series of scans of the light distribution at the output plane, taken by the set-up described in Ref. (3). Let us confine our attention to the directional coupler at the center. The second row from the top shows that when the input light is coupled into the channel on the right, it emerges at the output plane from both channels. Similarly, the second row from the bottom indicates that the light also emerges from both channels when it is coupled into the left channel. Since the intensity of the emerging light from both channels is about equal, we can write for this sample,

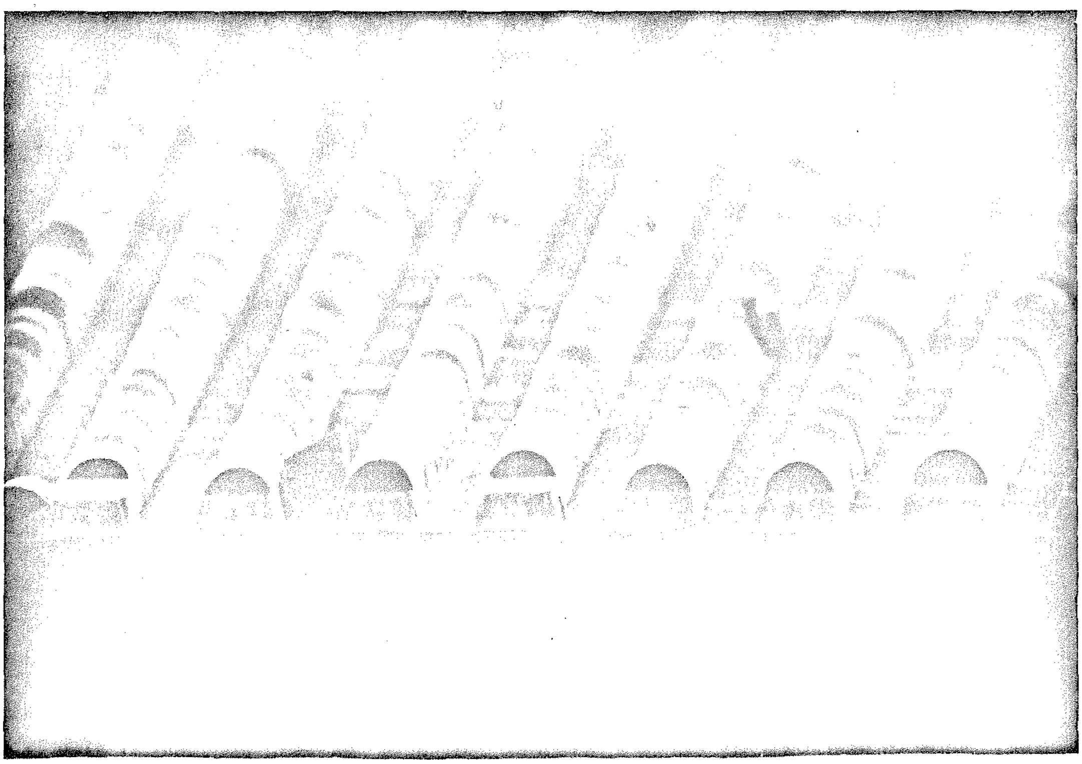

Fig. II.4 Scanning electron microscope photograph of the gold mask on the GaAs substrate used in the fabrication of the (a) dual directional coupler, (b) multichannel directional coupler. The remains of the photoresist can be seen on top of the gold stripes.

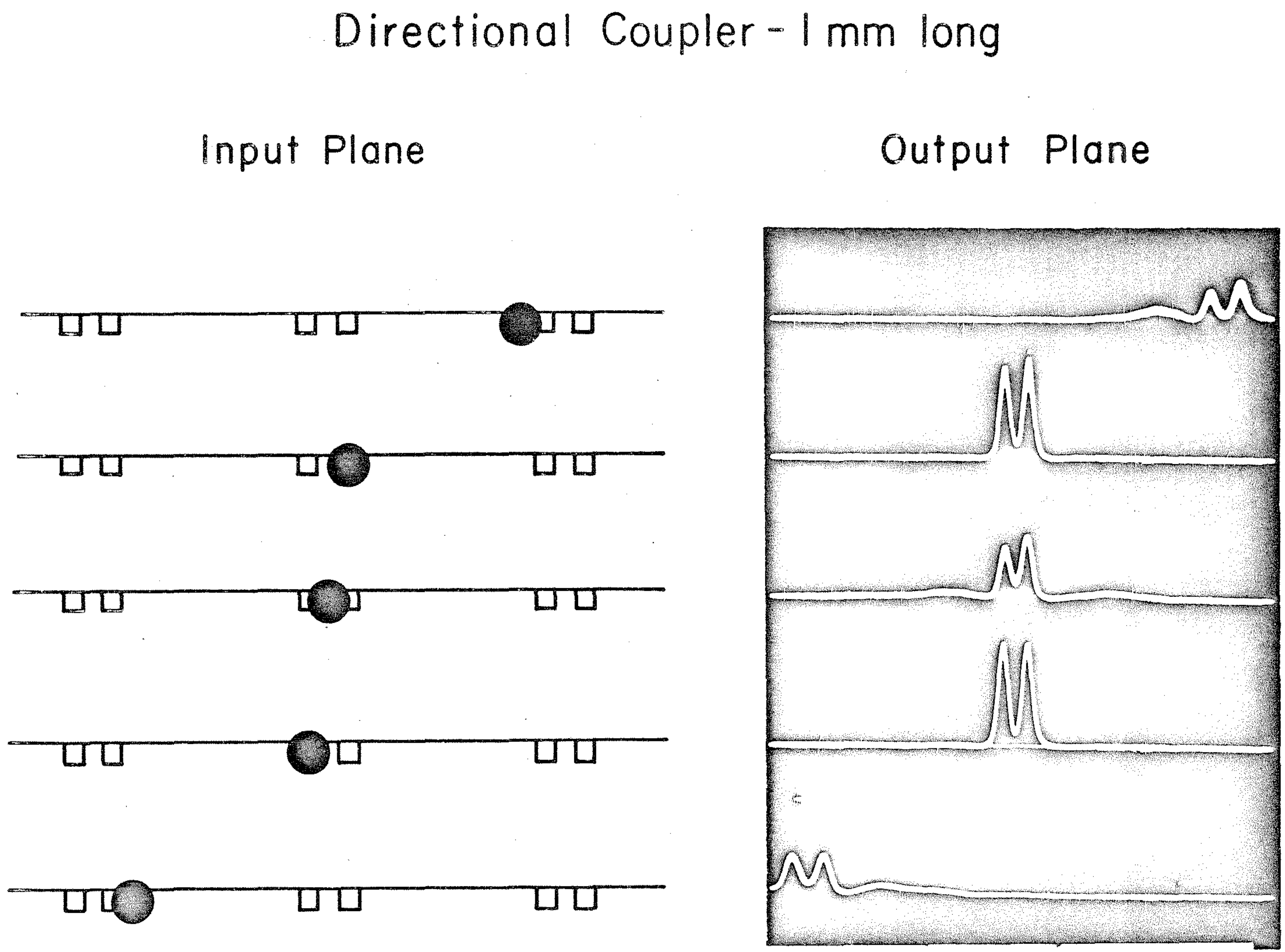

Fig. II.5 Sketch of the input plane of a 1 mm long directional coupler. On the right are photographs of guided light intensity profiles at the output for various input conditions

$$K\ell \simeq \frac{\pi}{4}$$

$$\ell = 1 \text{ mm} \qquad \Rightarrow \qquad K \simeq 0.79 \text{ mm}^{-1}$$

By increasing the length of the sample by about a factor of two, a complete transfer of power should be observed because

$$KL = \frac{\pi}{2}$$

This is shown in Fig. II.6. The second row from the top describes a situation in which light coupled into the left channel emerges from the one on the left, and the second row from the bottom shows the transfer of power from left to right.

This device can be turned into a switch by controlling K, the coupling coefficient, with the application of an electric field through the electrooptic effect. This exciting possibility will be discussed in detail later.

Let us go back now and derive theoretical expressions for the value of the coupling coefficient.

II.4 Derivation of the Coupling Coefficient

We consider again the coupled mode equations:

$$\frac{dA_0(z)}{dz} = -i\beta_0 A_0(z) + K_{01} A_1(z) \qquad \text{(II.2.3)}$$

$$\frac{dA_1(z)}{dz} = -i\beta_1 A_1(z) + K_{10} A_0(z) \qquad \text{(II.2.4)}$$

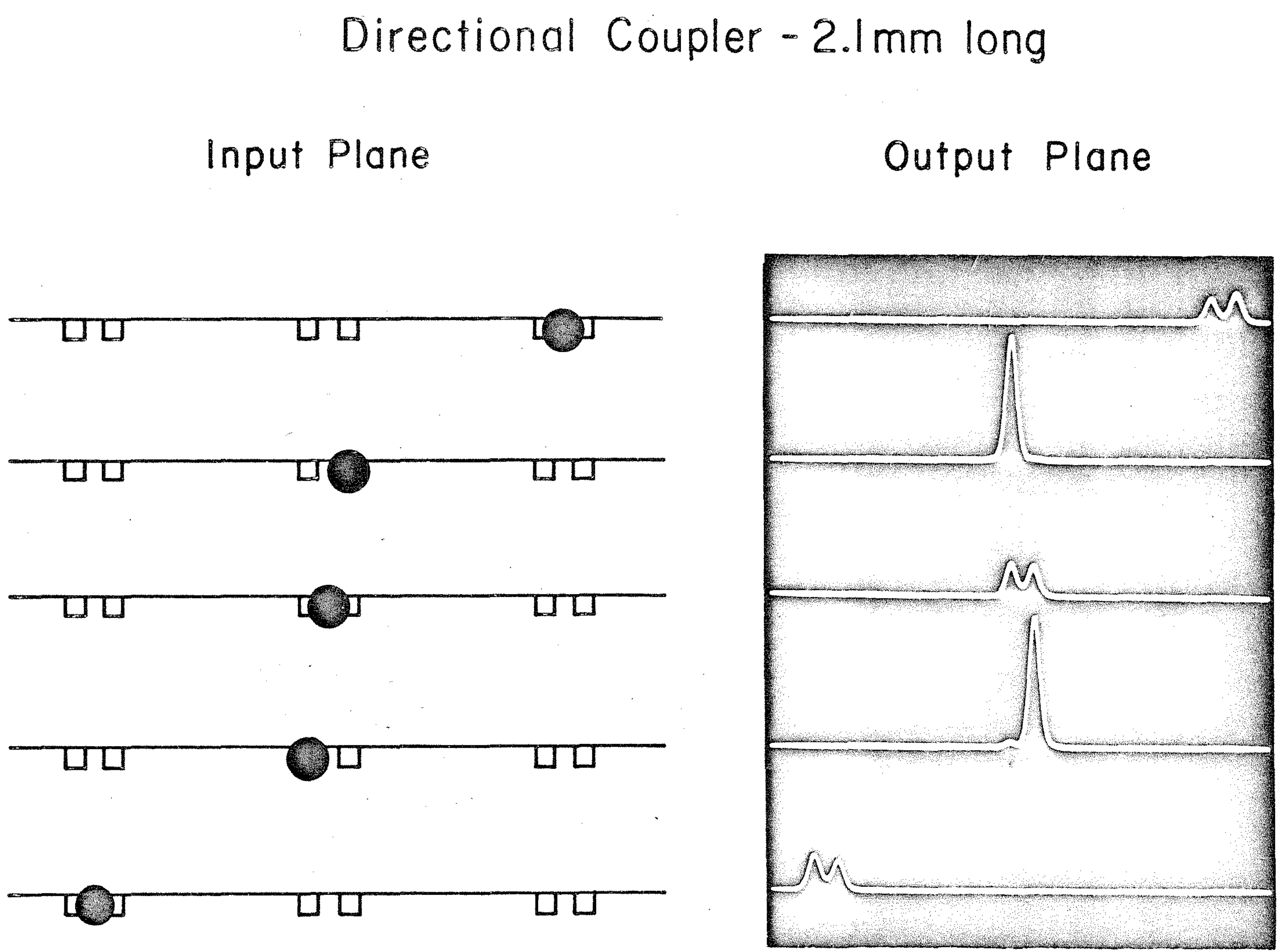

Fig. II.6 Sketch of the input plane of a 2.1 mm long directional coupler. On the right are photographs of guided light intensity profiles at the output for various input conditions.

We also recall that the electric field in a guide is given by

$$\vec{E}(x,y,z) = A(z)\ \vec{\mathcal{E}}(xy) \tag{II.2.1}$$

and that the power carried by $\vec{E}_1(x,y,z)$, for example, is

$$P_1(z) = |A_1(z)|^2 = A_1(z)\ A_1^*(z) \tag{II.2.2}$$

Next we obtain the rate of power growth in mode 1 due to the coupling from mode 0. (For this purpose we assume that β is real.) To do this we multiply II.2.4 by $A_1^*(z)$ and the complex conjugate of II.2.4 by $A_1(z)$. This gives

$$A_1^*(z)\ \frac{dA_1(z)}{dz} = -i\beta_1 A_1(z)\ A_1^*(z) + K_{10}A_0(z)A_1^*(z) \tag{II.4.1}$$

$$A_1(z)\ \frac{dA_1^*(z)}{dz} = i\beta_1 A_1^*(z)\ A_1(z) + K_{10}^* A_0^*(z)A_1(z) \tag{II.4.2}$$

Summing the two equations thus yields

$$\frac{d[A_1(z)\ A_1^*(z)]}{dz} = 2\ \mathrm{Re}[\,A_1(z)\ K_{10}^*\ A_0^*(z)\,] \tag{II.4.3}$$

Using II.2.2 gives

$$\frac{dP_1(z)}{dz} = 2\ \mathrm{Re}[A_1(z)\ K_{01}^*\ A_0^*(z)] \tag{II.4.4}$$

We shall now obtain a different expression for the rate of power growth in guide 1 from a simple minded physical point of view, in the following manner. Guide 0 in the absence of guide 1 supports a mode with a mode profile given by $\mathcal{E}_0(xy)$. This mode, in spite of having a long tail in the x and y directions, suffers no loss, and propagates with a constant power. When guide 1 is introduced, the tail of $\mathcal{E}_0(xy)$ penetrates into guide 1 and generates additional polarization because of the higher index inside the guide. This perturbation in the polarization in turn drives the mode in guide 1.

The net power per unit volume expended by an electric field on the electric polarization is given by the well known relation

$$\frac{\text{Power}}{\text{Volume}} = \overline{E \frac{\partial P}{\partial t}} \qquad \text{(II.4.5)}$$

where E is the field, P is the polarization, and the horizontal bar denotes time averaging.

We can thus express the power generation, due to the perturbation in the polarization at a given point in guide 1, by changing the sign on the right of equation II.4.4 yielding

$$\frac{dP_1}{dV} = \overline{-E_1(xyzt) \cdot \frac{\partial P_{10}(xyzt)}{\partial t}} \qquad \text{(II.4.6)}$$

where P_{10} is the driving polarization caused by the mode in guide 0. This perturbation in the polarization can be approximated by multiplying the electric field of mode 0 by the disturbance of the dielectric constant caused by the introduction of guide 1.

$$P_{10}(xyz) = \vec{E}_0(xyz) \cdot \Delta\varepsilon_1(xyz) \qquad (II.4.7)$$

Over the cross section of guide 1, $\Delta\varepsilon_1(xyz)$ has a constant value, independent of z, of

$$\Delta\varepsilon = \varepsilon_2 - \varepsilon_3 = \varepsilon_0(n_2^2 - n_3^2)$$

and is zero elsewhere as shown in Fig. II.2b. Using II.2.3, II.4.7 and time dependence of $e^{i\omega t}$, II.4.6 becomes:

$$\frac{dP_1}{dV} = \overline{-A_1(z)e^{i\omega t}\mathcal{E}_1(xy)\Delta\varepsilon_1(xy)i\omega A_0(z)e^{i\omega t}\mathcal{E}_0(xy)} \qquad (II.4.8)$$

Performing the time averaging yields

$$\frac{dP_1}{dV} = \tfrac{1}{2}\mathrm{Re}\left\{A_1(z)\mathcal{E}_1(xy)[-i\omega\Delta\varepsilon_1(xy)\mathcal{E}_0(xy)A_0(z)]^*\right\} \qquad (II.4.9)$$

The growth of the total power P_1 carried by the mode in guide 1 can now be derived by simply integrating over x and y. We obtain

$$\frac{dP_1(z)}{dz} = \tfrac{1}{2}\mathrm{Re}\left\{A_1(z)[i\omega\int \mathcal{E}_1(xy)\Delta\varepsilon_1^*(xy)\mathcal{E}_0{}^*(xy)dxdy]A_0^*(z)\right\}$$

(II.4.10)

This can also be written as:

$$\frac{dP_1(z)}{dz} = \tfrac{1}{2}\mathrm{Re}\left\{A_1(z)\left[-i\omega\int \mathcal{E}_1^*(xy)\Delta\varepsilon_1(xy)\mathcal{E}_0(xy)dxdy\right]^* A_0^*(z)\right\} \qquad (II.4.11)$$

A comparison of II.4.4 and II.4.11 immediately reveals that

$$K_{10} = \frac{-i\omega}{4}\int \mathcal{E}_1^*(xy)\Delta\varepsilon_1(xy)\mathcal{E}_0(xy)dxdy \qquad (II.4.12)$$

Similarly one obtains

$$K_{01} = \frac{-i\omega}{4}\int \mathcal{E}_0^*(xy)\Delta\varepsilon_0(xy)\mathcal{E}_1(xy)dxdy \qquad (II.4.13)$$

where $\Delta\varepsilon_0(xy)$ as opposed to $\Delta\varepsilon_1(xy)$, is equal to $\Delta\varepsilon$ over the cross section of guide 0 , and is zero elsewhere.

From II.4.12 and II.4.13 it is evident that as long as $\Delta\varepsilon$ is real and the guides are similar,

$$K_{10} = -K_{01}^* \qquad (II.4.14)$$

As shown in Appendix II this is a general property of lossless co-directional coupling. It is interesting to note that this relation holds also for lossy propagation in which β is complex but $\Delta\varepsilon$ is real (such a case may occur when the absorption in the guide and in the substrate are the same, or when the losses are caused by scattering). In the cases we consider $\Delta\varepsilon$ is mainly real. In general a complex $\Delta\varepsilon$ will modify, for example, the solutions described in Fig. II.3 for two modes, by causing the two modes to carry the same power when z is sufficiently large[4].

Equations II.4.12 and II.4.13 are identical to those obtained by Marcuse[4] who solved the Maxwell equations using perturbation theory. They are independent of the guide geometry and can be applied to various cross section guides once the profile of the propagating mode is known.

The problem of coupling between the guides can be approached from a different point of view, in which the coupling coefficient is derived by solving for the propagation constants of the two eigenmodes of the two guide directional coupler, as shown in Fig. II.7. The two modes of a symmetric coupler are a symmetric one $\mathcal{E}_s$ and an anti-symmetric one $\mathcal{E}_a$, with propagation constants β_s and β_a. If at $z = 0$ light is coupled into the 0 guide only, the two modes are excited equally in such a way that they add on the 0 guide side and cancel over guide number 1 side. Since $\beta_s \neq \beta_a$ the two modes drift out of phase as they propagate along the z direction. At a distance L which is given by

$$\Delta\beta L = (\beta_s - \beta_a)L = \pi \tag{II.4.15}$$

the two modes are 180° out of phase, cancel over guide number 0 and add over guide number 1, as shown in Fig. II.7. The net result is a complete transfer of power from guide 0 to guide 1. From a comparison of II.4.15 and II.3.9 we find that $\Delta\beta$ is related to the coupling coefficient by

$$K = \frac{\Delta\beta}{2} \tag{II.4.16}$$

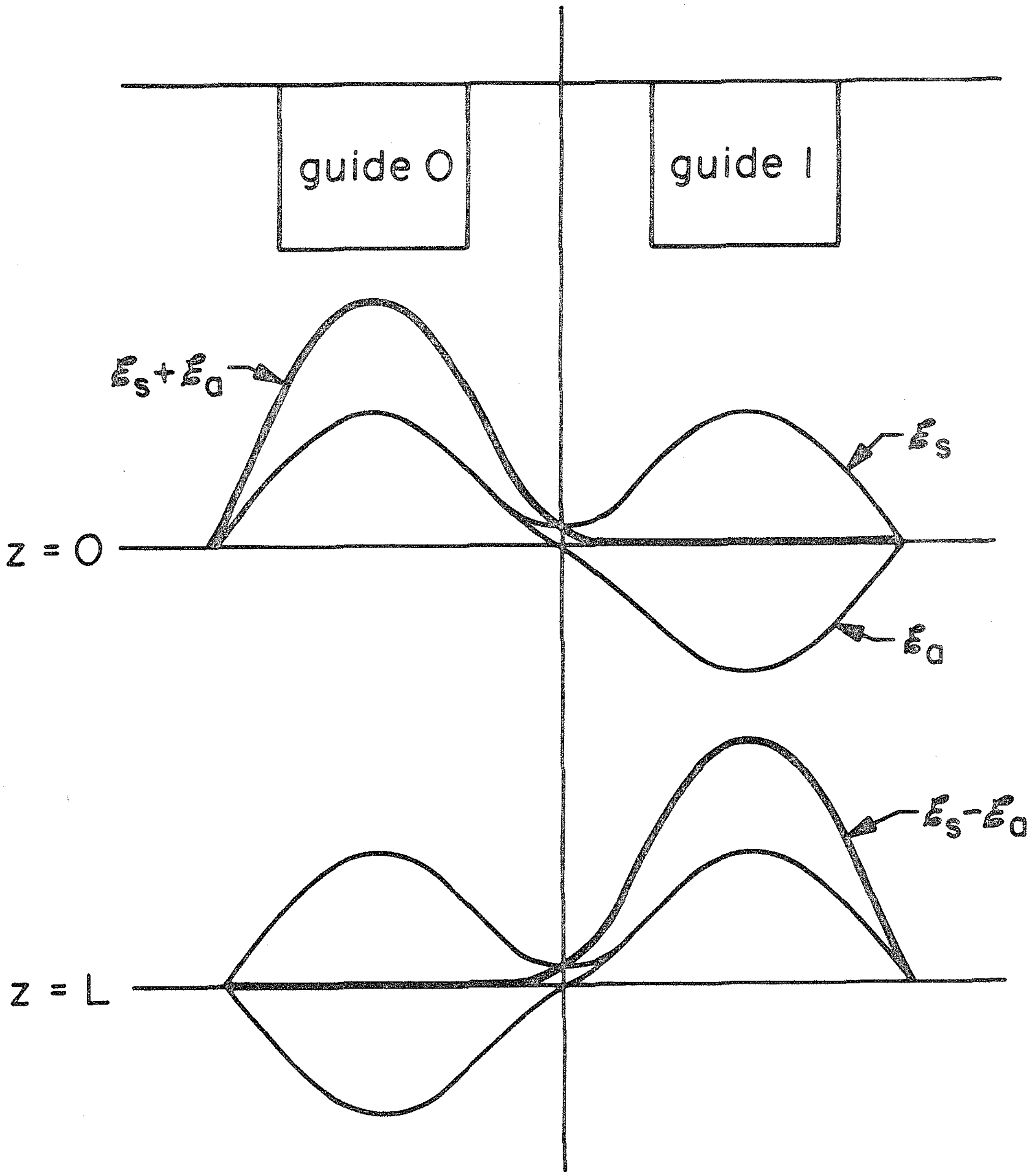

Fig. II.7 The symmetric and antisymmetric eigen modes of a dual directional coupler. Power is transferred from one channel to another because of not identical propagation constants.

Let us obtain an expression for K by deriving $\Delta\beta$. We consider again the geometry shown in Fig. 2a. We recall that the modes in the individual guides, $\mathcal{E}_0(xy)$ and $\mathcal{E}_1(xy)$ are given by the wave equation

$$\nabla_t^2\mathcal{E}_0(xy) + \frac{\omega^2}{c^2} n_0^2\mathcal{E}_0(xy) = \beta_0^2\mathcal{E}_0(xy)$$
$$\nabla_t^2\mathcal{E}_1(xy) + \frac{\omega^2}{c^2} n_1^2\mathcal{E}_1(xy) = \beta_1^2\mathcal{E}_1(xy) \tag{II.4.17}$$

where

$$\nabla_t^2 = \frac{\partial^2}{\partial x^2} + \frac{\partial^2}{\partial y^2} \tag{II.4.18}$$

and n_0 is the index of refraction distribution in the absence of guide 1, while n_I is the distribution in the absence of guide 0. For effective exchange of power between the two guides the propagation constants must be similar. In section II.10 we shall treat, from a coupled modes point of view, a case where they are not similar. Let us therefore confine our attention now to a case where

$$\beta_0 = \beta_1 \equiv \beta \tag{II.4.19}$$

As will be discussed in section II.6 we can assume that the modes have one main component of the electric field, say in the y direction, and therefore a mode can be normalized to carry one unit of power by imposing (see Appendix I):

$$\frac{\beta}{2\omega\mu}\int_{-\infty}^{\infty}|\mathcal{E}_i(xy)|^2 dxdy = 1 \qquad i = 0,1 \tag{II.4.20}$$

We now approximate the modes of the two guide directional coupler by the sum and difference of the individual modes.

$$\mathcal{E}_s(xy) = \frac{1}{(a^2 + b^2)^{\frac{1}{2}}} [a\mathcal{E}_0(xy) + b\mathcal{E}_1(xy)]$$

$$\mathcal{E}_a(xy) = \frac{1}{(a^2 + b^2)^{\frac{1}{2}}} [b\mathcal{E}_0(xy) - a\mathcal{E}_1(xy)] \qquad (II.4.21)$$

To ensure the orthonormality of these two modes we have to assume a small overlap of the individual modes.

$$\int |\mathcal{E}_1(xy)\mathcal{E}_0(xy)|dxdy \ll \int |\mathcal{E}_0(xy)|^2 dxdy \qquad (II.4.22)$$

The orthogonality of $\mathcal{E}_s$ and $\mathcal{E}_a$ is important because it ensures the conservation of energy, once a combination of these modes is excited and propagates in the z direction.

To find the propagation constants of the above modes, β_s and β_a, we insert them into the appropriate wave equation.

$$\nabla_t^2\mathcal{E}_s + \frac{\omega^2}{c^2} n_{II}^2\mathcal{E}_s = \beta_s^2\mathcal{E}_s$$

$$\nabla_t^2\mathcal{E}_a + \frac{\omega^2}{c^2} n_{II}^2\mathcal{E}_a = \beta_a^2\mathcal{E}_a \qquad (II.4.23)$$

where n_{II} is the index distribution when both guides exist and is shown in Fig. II.2a.

Let us consider the equation for $\mathcal{E}_s$. With the aid of II.4.17 and II.4.21 we can write the upper equation in II.4.23 as

$$\frac{\omega^2}{c^2}(n_{II}^2 - n_0^2)a\mathcal{E}_0 + \frac{\omega^2}{c^2}(n_{II}^2 - n_I^2)b\mathcal{E}_1 = (\beta_s^2 - \beta_0^2)(a\mathcal{E}_0 + b\mathcal{E}_1) \qquad (II.4.24)$$

We recall that $(n_{II}^2 - n_0^2)$ and $(n_{II}^2 - n_I^2)$ are actually the perturbations in the dielectric constant we have discussed earlier. We can thus write

$$n_{II}^2 - n_0^2 = \Delta\varepsilon_1/\varepsilon_o$$
$$n_{II}^2 - n_I^2 = \Delta\varepsilon_0/\varepsilon_o \qquad (II.4.25)$$

where $\Delta\varepsilon_1$ is shown for example in Fig. II.2b and ε_o is the free space dielectric constant. Next we obtain two expressions by multiplying II.4.24 by $\mathcal{E}_0^*$ or $\mathcal{E}_1^*$ and integrating over x and y . Using II.4.25 and $c^2 = \frac{1}{\mu\varepsilon_0}$ we get

$$\omega^2\mu b\int_{-\infty}^{\infty}\mathcal{E}_0^*\Delta\varepsilon_0\mathcal{E}_1 dxdy + \omega^2\mu a\int_{-\infty}^{\infty}\mathcal{E}_0^*\Delta\varepsilon_1\mathcal{E}_0 dxdy = (\beta_s^2-\beta^2)\int_{-\infty}^{\infty}\mathcal{E}_0^*(a\mathcal{E}_0+b\mathcal{E}_1)dxdy \qquad (II.4.26)$$

$$\omega^2\mu a\int_{-\infty}^{\infty}\mathcal{E}_1^*\Delta\varepsilon_1\mathcal{E}_0 dxdy + \omega^2\mu b\int_{-\infty}^{\infty}\mathcal{E}_1^*\Delta\varepsilon_0\mathcal{E}_1 dxdy = (\beta_s^2-\beta^2)\int_{-\infty}^{\infty}\mathcal{E}_1^*(a\mathcal{E}_0+b\mathcal{E}_1)dxdy \qquad (II.4.27)$$

The second integrals on the left are second order terms because $\Delta\varepsilon_1$, for example, is different from 0 only where $|\mathcal{E}_0|^2$ is very close to zero. Thus using II.4.22 we can write II.4.26 and II.4.27 as

$$\omega^2\mu b\int_{-\infty}^{\infty}\mathcal{E}_0^*\Delta\varepsilon_1\mathcal{E}_1 dxdy = a(\beta_s^2-\beta^2)\int_{-\infty}^{\infty}\mathcal{E}_0^*\mathcal{E}_0 dxdy \qquad (II.4.28)$$

$$\omega^2\mu a\int_{-\infty}^{\infty}\mathcal{E}_1^*\Delta\varepsilon_1\mathcal{E}_0 dxdy = b(\beta_s^2-\beta^2)\int_{-\infty}^{\infty}\mathcal{E}_1^*\mathcal{E}_1 dxdy \qquad (II.4.29)$$

Taking the ratio of the two equations we get

$$\frac{a^2}{b^2} = \frac{\int_{-\infty}^{\infty}\mathcal{E}_0^*\Delta\varepsilon_1\mathcal{E}_1 dxdy}{\int_{-\infty}^{\infty}\mathcal{E}_1^*\Delta\varepsilon_0\mathcal{E}_0 dxdy} \qquad (II.4.30)$$

In a similar fashion, starting with the equation for $\mathcal{E}_a$ in II.4.23, we find

$$\frac{b^2}{a^2} = \frac{\int\limits_{-\infty}^{\infty} \mathcal{E}_0^* \Delta\varepsilon_1 \mathcal{E}_1 dxdy}{\int\limits_{-\infty}^{\infty} \mathcal{E}_1^* \Delta\varepsilon_0 \mathcal{E}_0 dxdy} \qquad \text{(II.4.31)}$$

From II.4.30 and II.4.31 we can conclude that for the existence of a solution in the form of II.4.21 we must require

$$\int\limits_{-\infty}^{\infty} \mathcal{E}_0^* \Delta\varepsilon_1 \mathcal{E}_1 dxdy = \int\limits_{-\infty}^{\infty} \mathcal{E}_1^* \Delta\varepsilon_0 \mathcal{E}_0 dxdy \qquad \text{(II.4.32)}$$

which yields

$$a = b \qquad \text{(II.4.33)}$$

We can now obtain β_s by adding II.4.28 and II.4.29. We also assume that $\beta_s - \beta \ll \beta$ and with the help of II.4.20 we get

$$\beta_s - \beta = \frac{\omega}{8} \left[\int\limits_{-\infty}^{\infty} \mathcal{E}_0^* \Delta\varepsilon_0 \mathcal{E}_1 dxdy + \int\limits_{-\infty}^{\infty} \mathcal{E}_1^* \Delta\varepsilon_1 \mathcal{E}_0 dxdy\right] \qquad \text{(II.4.34)}$$

In the same fashion we obtain for β_a

$$\beta_a - \beta = -\frac{\omega}{8}\left[\int\limits_{-\infty}^{\infty} \mathcal{E}_0^* \Delta\varepsilon_0 \mathcal{E}_1 dxdy + \int\limits_{-\infty}^{\infty} \mathcal{E}_1^* \Delta\varepsilon_1 \mathcal{E}_0 dxdy\right] \qquad \text{(II.4.35)}$$

The coupling coefficient can now be obtained from II.4.16, II.4.34 and II.4.35

$$K = \frac{\beta_s - \beta_a}{2} = \frac{\omega}{8} \left[\int\limits_{-\infty}^{\infty} \mathcal{E}_0^* \Delta\varepsilon_0 \mathcal{E}_1 dxdy + \int\limits_{-\infty}^{\infty} \mathcal{E}_1^* \Delta\varepsilon_1 \mathcal{E}_0 dxdy\right] \qquad \text{(II.4.36)}$$

The value of K is in agreement with the expression derived earlier. It is reasonable to assume that II.4.36 yields a good approximation for K also in a case where the guides are not identical and II.4.32 is violated.

It is interesting to note that from the above point of view it is possible to easily obtain an upper limit for the value of the coupling coefficient K . Clearly, this value reaches its upper limit as the two guides are brought closer and closer together. Eventually they form one guide with twice the width. The symmetric mode turns into the lower order mode of the wide guide and the antisymmetric mode turns into its higher order mode. The calculation of the propagation constants of the new modes is straightforward and yields the upper limit for $\Delta\beta$.

II.5 Coupling between Planar Guides

As a first example we apply our result to the planar waveguides shown in Fig. II.8. The mode profile of a single planar waveguide can be derived analytically (see Appendix I). We consider a TE mode which has its electric field in the y direction, carries a unit power per unit length in the y direction, and is given by[4]:

$$\mathcal{E}_0(x) = \left(\frac{4\omega\mu}{\beta(w + \frac{2}{p_x})} \right)^{\frac{1}{2}} \cos h_x x \; , \quad |x| \le \frac{w}{2} \, , \quad -\infty \le y \le -\infty$$

$$\mathcal{E}_0(x) = \left(\frac{4\omega\mu}{\beta(w + \frac{2}{p_x})} \right)^{\frac{1}{2}} \cos h_x t \; e^{-p_x(|x| - \frac{w}{2})} \, , \quad |x| \ge \frac{w}{2} \, , \quad -\infty \le y \le -\infty \qquad \text{(II.5.1)}$$

where k_0 is the free space wave number and

$$h_x = (n_2^2 k_0^2 - \beta^2)^{\frac{1}{2}}$$

$$p_x = (\beta^2 - n_3^2 k_0^2)^{\frac{1}{2}} \qquad \text{(II.5.2)}$$

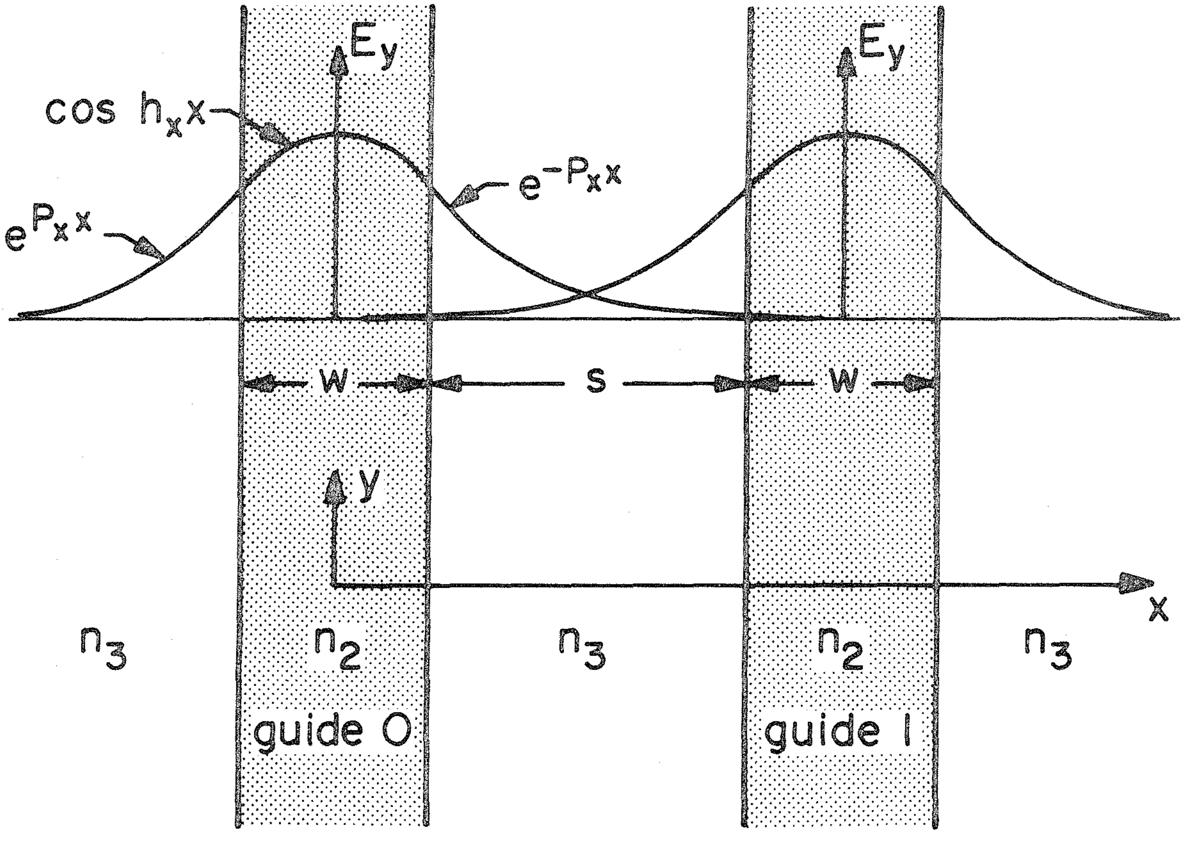

Fig. II.8 Sketch of two adjacent planar guides and their propagating modes.

In addition, the eigenvalue equation imposes the relation for the mth order mode (m+1 is the number of extrema)

$$h_x w = (m+1)\pi - 2 \tan^{-1} \frac{h_x}{p_x} \tag{II.5.3}$$

A similar profile describes the mode in guide number 1, the only difference being that the center of the mode is at $x = w+s$ rather than $x = 0$.

Knowing the mode profiles we can obtain the coupling coefficient between the guides with the help of equation II.4.12. We note first that $\Delta\varepsilon_1$ for this case is given by

$$\Delta\varepsilon_1(xy) = \varepsilon_2 - \varepsilon_3 = \varepsilon_0(n_2^2 - n_3^2) \quad \text{for} \quad s + \frac{w}{2} \le x \le s + \frac{3w}{2}, \quad -\infty \le y \le -\infty \tag{II.5.4}$$

$$\Delta\varepsilon_1(xy) = 0 \quad , \quad \text{elsewhere}$$

We thus obtain the following expression for the coupling coefficient:

$$K_{10} = K_{01} = -iK = -i \frac{2h_x^2 p_x}{\beta(w+\frac{2}{p_x})(h_x^2+p_x^2)} e^{-p_x s} \tag{II.5.5}$$

In the derivation of this expression, the y integration is performed over one unit length and we have assumed that

$$|p_x \cos h_x \tfrac{w}{2} + h_x \sin h_x \tfrac{w}{2}| \gg |p_x \cosh_x \tfrac{w}{2} - h_x \sinh_x \tfrac{w}{2}| e^{-p_x w} \tag{II.5.6}$$

which is always true for well confined modes.

Equation II.5.5 is the same as approximate expressions for the coupling coefficient between planar waveguides given in Refs. 4,5,6.

In Ref. 5 a comparison of this expression to the exact solution of the problem is made and a good agreement is shown.

II.6 Coupling between Channel Guides

A rigorous solution for the mode profile at a rectangular cross section channel waveguide requires a computer[7]. However, once the mode profile is known, II.4.12 can be applied for the calculation of the coupling coefficient. Marcatili[2] has shown that it is possible to introduce a drastic simplification in the derivation of the mode profile which enables one to get a simple solution. Consider the waveguide shown in Fig. II.9. Most of the power propagates in the high index region and the fields decay exponentially in the x and y directions. Consequently, for a reasonably confined mode only a small part of the power propagates in the four shaded areas. This means that in matching the boundary conditions the field along the edges of the shaded area can be ignored.

The solution of the simplified problem yields modes that are essentially of the TEM kind and can be grouped in two families, $\mathcal{E}^{x}_{mn}$ and $\mathcal{E}^{y}_{mn}$. The first family has most of the electric field in the x direction and the magnetic field in the y direction, while the second family has most of the electric field in the y direction and the magnetic field in the x. Our notation is such that $m+1$ and $n+1$ indicate

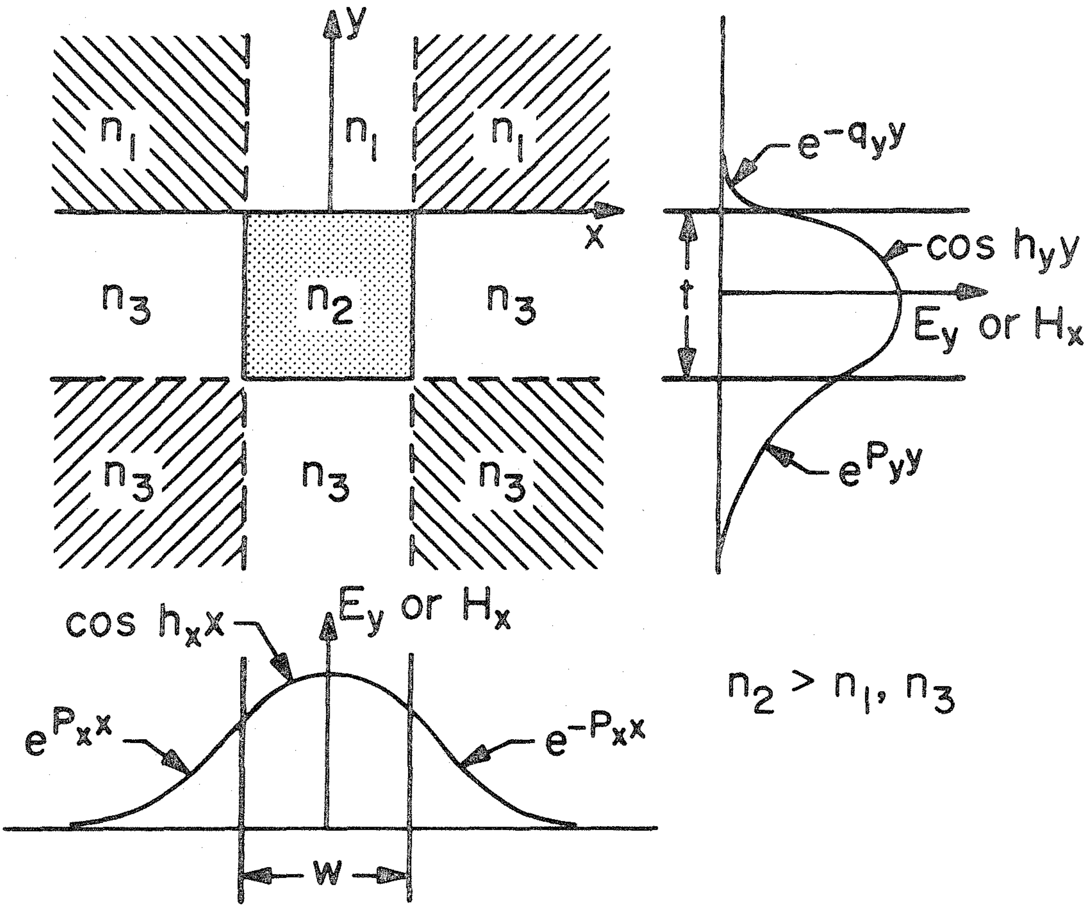

Fig. II.9 Mode profile of a rectangular channel guide.

the number of extrema of the fields in the x and y directions.) Furthermore the solution of the problem indicates that mode profiles in the x and y directions are actually given by two equations, each of which is identical to the eigenvalue equations one obtains for a one-dimensional (planar) waveguide. For example, we consider an $\mathcal{E}^y$ mode in the guide shown in Fig. II.9. The eigenvalue equation for the x direction is identical to that of a TE mode in a symmetric planar guide (see Appendix I). It is given by

$$h_x w = (m+1)\pi - 2 \tan^{-1} \frac{h_x}{p_x} \tag{II.6.1}$$

where

$$h_x^2 + p_x^2 = (n_2^2 - n_3^2)k_0^2$$

The eigenvalue equation for the y direction is identical to that of a TM mode in an asymmetric planar guide (see Appendix I) and is given by

$$h_y t = (n+1)\pi - \tan^{-1} \frac{n_3^2 h_y}{n_2^2 p_y} - \tan^{-1} \frac{n_1^2 h_y}{n_2^2 q_y} \tag{II.6.2}$$

where

$$h_y^2 + p_y^2 = (n_2^2 - n_3^2)k_0^2 \quad ; \quad h_y^2 + q_y^2 = (n_2^2 - n_1^2)k_0^2 \tag{II.6.3}$$

The propagation constant along the z direction is therefore given by

$$\beta^2 = n_2^2 k_0^2 - h_x^2 - h_y^2 \tag{II.6.4}$$

We can therefore approximate the propagating mode by regarding only the main components of the fields and using the mode profiles as given by II.6.2 and II.6.3. The validity of this approximation can be determined by comparing the value of the expression

$$\frac{\beta^2-n_3^2k_0^2}{n_2^2k_0^2-n_3^2k_0^2} = \frac{(n_2^2-n_3^2)k_0^2 - h_x^2 - h_y^2}{(n_2^2-n_3^2)k_0^2} \qquad \text{(II.6.5)}$$

with that derived by computer calculation[7]. For

$$\frac{\beta^2-n_3^2k_0^2}{n_2^2k_0^2-n_3^2k_0^2} \geq 0.3 \qquad \text{(II.6.6)}$$

according to the figures in Ref. 2, the approximation is within a few percent of the exact value. Equation II.6.6 also indicates what modes are supported by the guide, because only modes for which the expression is positive are above cutoff.

Figure II.9 shows the mode profile of the $\mathcal{E}_{00}^y$ mode. This mode profile after the appropriate normalization can be used in conjunction with II.4.12 to calculate the coupling coefficient.

We shall attempt to get a good estimate for the coupling coefficient without going through the above process. We note that the profile of the mode in the x direction is the same as that of the planar guide we have dealt with before. The major difference is that the planar guide and its propagating modes are independent of y. This basically means that $\Delta\varepsilon_1(xy)$ (which is defined for the planar guide case by II.5.4) has the same value for any value of y to which the modes of the guides extend. This would also be the case in a channel waveguide if the modes were very well confined in the y direction $\left(\frac{1}{q_y}+\frac{1}{p_y} \ll 1\right)$. In this case $\Delta\varepsilon_1(xy)$ is defined as

$$\Delta\varepsilon_1(xy) = \varepsilon_2 - \varepsilon_3 = \varepsilon_0(n_2^2 - n_3^2) \quad \text{for} \quad s + \frac{w}{2} \le x \le s\,\frac{3w}{2} \;; \quad -t \le y \le 0$$

$$\Delta\varepsilon_1(xy) = 0 \qquad \text{elsewhere} \tag{II.6.7}$$

Thus if the mode is very well confined in the y direction it extends only from $y = 0$ to $y = -t$ which is the region at which $\Delta\varepsilon(xy)$ has a constant value. For this case II.5.5 can be used to express the coupling between the two channels. We can modify II.5.5 to include coupling between modes that are not very well confined, but satisfy II.6.6. This is done by multiplying II.5.5 by a factor which is the ratio of the mode power propagating between $y = 0$ and $y = -t$ (the region where $\Delta\varepsilon_1(xy) \neq 0$) and the total mode power. This factor can be roughly approximated by

$$\frac{t}{(t + \sin^2 h_y t/p_y)} \tag{II.6.8}$$

where $\frac{1}{p_y} \gg \frac{1}{q_y}$ the penetration depths of the modes into the upper and lower boundaries satisfy. The expression for the coupling coefficient between two channel guides thus becomes:

$$K_{10} = K_{01} = -iK = -i \frac{2h_x^2\, p_x\, t\, e^{-p_x s}}{(t + \sin^2 h_y t/p_y)(w + \frac{2}{p_x})(h_x^2+p_x^2)} \qquad \text{(II.6.9)}$$

For a very well confined mode

$$t \gg \frac{1}{p_y} \quad \text{and} \quad w \gg \frac{2}{p_x}$$

and II.6.9 reduces to

$$K_{10} = K_{01} = -iK = -i \frac{2h_x^2 p_x e^{-p_x s}}{\beta w(h_x^2+p_x^2)} \qquad \text{(II.6.10)}$$

which, aside from its negative sign, is the expression derived by Marcatili(2).

Before comparing the theoretical expressions for the coupling coefficient with the experimental results, let us consider a geometry which allows an accurate measurement of the coupling coefficient.

II.7 Multichannel Directional Coupler - Coupling Coefficient Measurement

In Section II.3 we have considered a directional coupler made of two channels in which the power oscillates back and forth between the channels as a function of propagation distance. We consider now an infinite number of identical guides each coupled to its adjacent guides, as shown on the left of Fig. II.1. When light is coupled into a central channel (defined as $n = 0$) it will leak to the sides. Because of the large number of channels, it is clear that the full power will not appear again in the central channel, but will constantly flow to the sides.

The coupled mode equation for the nth channel is given by:

$$\frac{dA_n(z)}{dz} = -i\beta A_n(z) = ikA_{n-1}(z) - ikA_{n+1}(z) \qquad \text{(II.7.1)}$$

where β is the propagation constant which includes the guide attenuation α

$$\beta = \beta_r - i\,\frac{\alpha}{2} \qquad \text{(II.7.2)}$$

n is the guide number ($n=0, \pm1, \pm2, \ldots$), and K (a real number) is the coupling coefficient between two adjacent guides. (The coupling coefficient between non-adjacent guides is negligibly small). When light is coupled into the 0 channel only, the boundary conditions become

$$A_0(0) = 1 \qquad\qquad A_{n\neq0}(0) = 0 \qquad \text{(II.7.3)}$$

The solution of II.7.1 is

$$A_n(z) = (-i)^n\, J_n(2Kz)\, e^{-i\beta z} \qquad \text{(II.7.4)}$$

and the power flow in the guides therefore is:

$$P_n(z) = A_n(z)\, A_n^+(z) = J_n^2(2Kz)\, e^{-\alpha z} \qquad (II.7.5)$$

where J_n represents the Bessel function of nth order.

A multichannel direction coupler(8) was fabricated by proton implantation through an appropriate gold mask on the surface of the GaAs substrate as shown in Fig. II.4b. The width of the embedded channels can be estimated by the width of the notches in the mask to be about 2.4μ separated by 3.9μ. Their depth is determined by the known penetration of the 300 KeV protons in GaAs which is 3μ. The index discontinuity as measured in a fashion described in Chapter V, is about .005 at 1.15μ and about 10% larger at 1.06μ.

Figure II.1 describes the multichannel directional coupler with the input light coupled into a central guide and the output light scanned at different sample lengths. The argument of the Bessel functions at each of the scans was determined by fitting the square root of the normalized intensities of the light in the different channels, to a plot of the Bessel functions as shown in Fig. II.10. The experiment was performed with light having a wavelength of $\lambda = 1.15\mu$ (from a HeNe laser) and $\lambda = 1.06\mu$ (a Nd:YAG laser). The coupling coefficient can be deduced quite readily and accurately now, simply by plotting the argument of the Bessel functions against the distance of propagation, and measuring the slope.

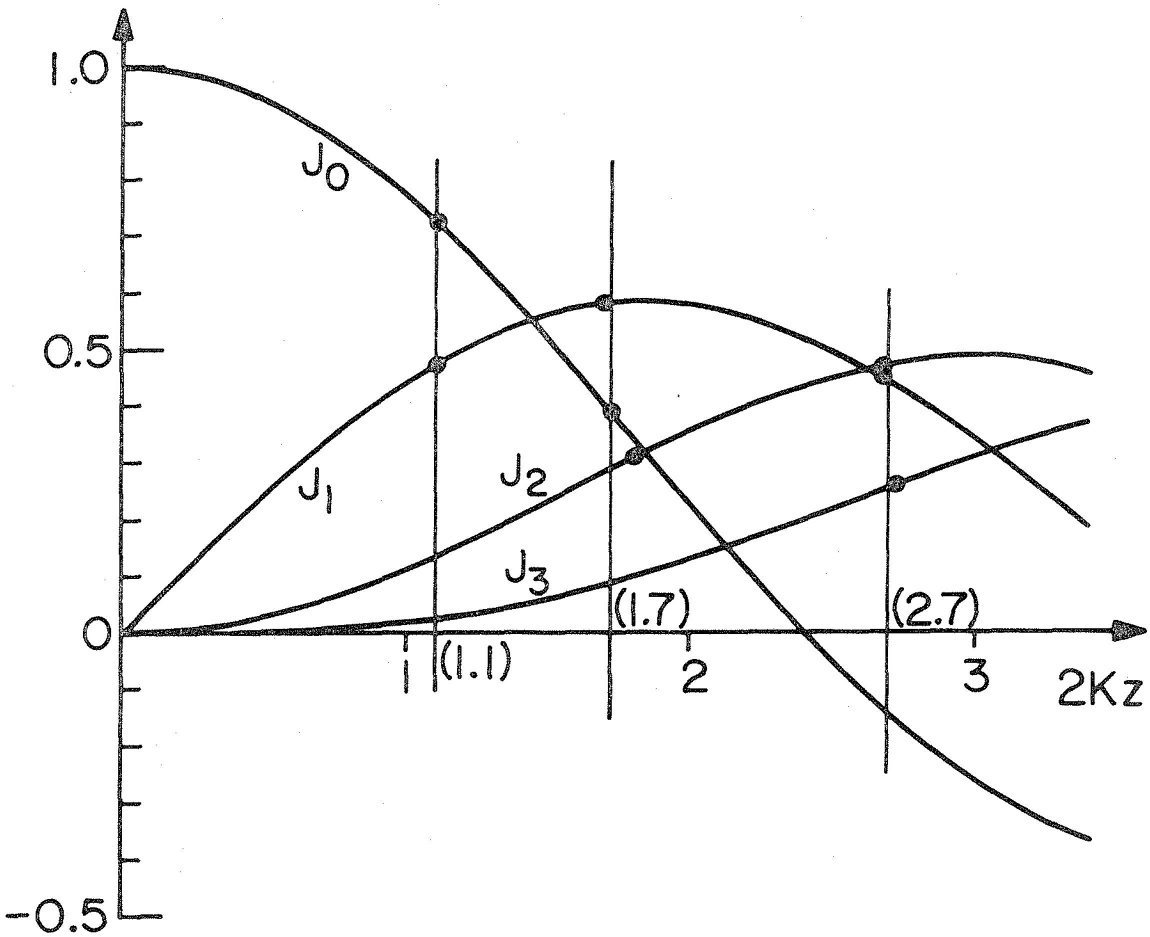

Fig. II.10 Sketch of various orders Bessel functions to which the square root of the amplitudes in Fig. II.1 are fitted.

Using II.7.4 the coupling coefficient is thus given by:

$$K = \text{slope}/2 \qquad \text{(II.7.6)}$$

A series of measurements at 1.15μ and 1.06μ is plotted in Fig. II.11. By measuring the slopes we find that for the same directional coupler,

$$K_{1.15\mu} = 0.52 \pm 0.01 \text{ mm}^{-1} \qquad K_{1.06\mu} = 0.30 \pm 0.01 \text{ mm}^{-1} \qquad \text{(II.7.7)}$$

It has also been found that different polarizations (E^x or E^y) of the input beam had no noticeable effect on K .

Only a qualitative comparison between theory and experiment can be made with these samples. The modes in these guides are not well confined modes, to which the theory of Section II.6 pertains. Besides, the dielectric discontinuity may not be uniform across the guide's cross section and the accuracy in measuring it is not high. However, the coupling coefficients calculated on the basis of the dimensions given earlier in (II.6.9) are quite close to the actual values. The theoretical results are (for both polarizations):

$$K_{1.15} = 0.32 \text{ mm}^{-1} \qquad K_{1.06} = 0.21 \text{ mm}^{-1} \qquad \text{(II.7.8)}$$

Considering the limitations mentioned above, these results are in good agreement with (II.7.7).

The absorption of the propagating light is relatively high in

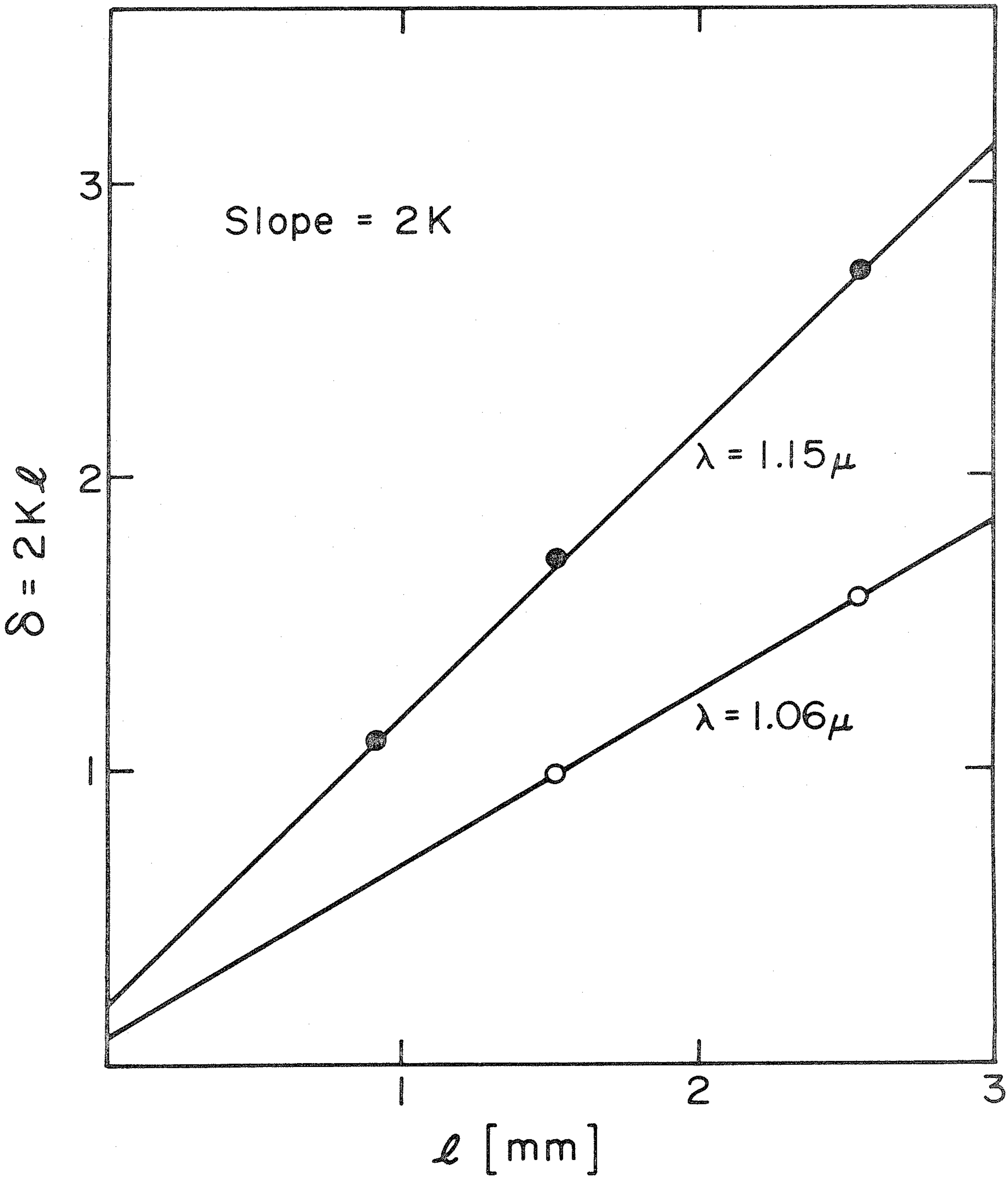

Fig. II.11 Plot of the arguments of the Bessel functions against the distance of propagation.

these ion implanted waveguides. It amounts to about $5\ cm^{-1}$ which is the same as the absorption of planar ion implanted guides[3]. It is caused by the absorption of the defect centers created by the implantation and by the free carrier absorption in the substrate. Other methods for fabrication of directional couplers will be discussed in Section II.9.

II.8 The Sign of the Coupling Coefficient

Let us consider again the dual directional coupler shown in Fig. II.3. The amplitude of the fields in the two guides are given by II.3.5 and II.3.6 as:

$$A_0(z) = \cos Kz\ e^{i\beta z} \tag{II.3.5}$$

$$A_1(z) = -i \sin Kz\ e^{i\beta z} \tag{II.3.6}$$

From these equations we learn that a distinct phase difference exists between the two guides. We also find that the phase of the guide in which the power is increasing will always lag 90° behind the phase of the guide in which the power is decreasing. Formally this is a direct correspondence of the sign of the coupling as given in II.4.12. Physically the reason for the time lag is the necessary phase relation between the polarization (caused by the field in guide zero), and the field in guide 1, if power is to be generated in guide 1. It is well known[9] that power dissipation in a dielectric occurs when the polarization lags the field. Therefore, in our case, for power generation in guide 1 the field there has to lag the polarization, which is caused by the field of guide 0 and has its phase. This reasoning thus gives the same result as the above equations.

The phase relation between the two guides might be of importance in an optical circuit in which the phase of the light as well as its amplitude may be used to carry information. In Ref. 2 the coupling coefficient appears to have an opposite sign to the one in II.4.12. Such a sign will cause a time lead in guide 1 rather than time lag. The following experiment was carried out to find whether the phase difference is time lead or time lag.

Phase information can be acquired by interference. In this case the interference was performed in the fashion described in Fig. II.12. Drawing (b) describes a geometry in which the input beam is focused with an objective into the central channel of the multichannel directional coupler. The input face at the channels is in the focal plane of the objective and the spot size of the beam is small enough to couple into one channel only. The distribution of light at the output plane, caused by the coupling effect, is shown at the top of the drawing.

By moving the objective in or out, the focal plane will not coincide with the input plane of the sample, the spot size will increase and light will be coupled into the adjacent guides as well as the central guide. When the lens is moved toward the sample, the curvature of the phase fronts of the beam is such that the light coupled into the side channels at the input plane has a time lead (as shown in drawing a).

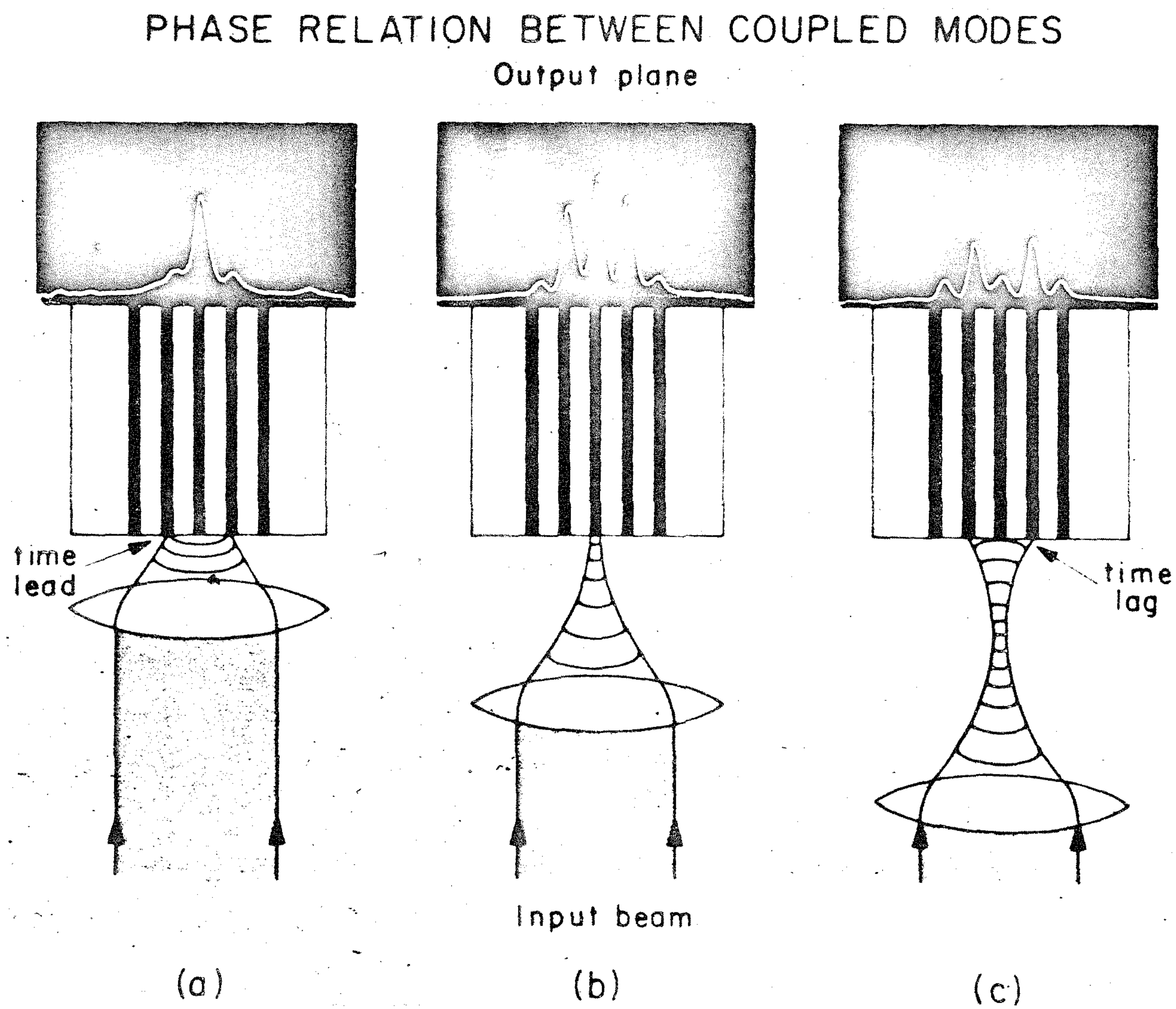

Fig. II.12 Phase relation between coupled modes is obtained by interference. (See text for details.)

On the other hand, when the beam is moved away from the sample (drawing c) the light coupled into the adjacent channels suffers a time lag. This input light will interfere, as it propagates with the light coupled into the channels from the central one. The intensity of the light in the output plane, with respect to the central guide indicates where this interference was a constructive or destructive one. For example, in Fig. II.12a we find that the intensity of the light in the adjacent channels is close to zero, while in (c) it is very strong. This indicates that there is a constructive interference in case (c) and the light coupled via the directional coupling effect suffers a time lag.

II.9 Ridged Channel Waveguides and Directional Couplers

A variety of thin films suitable for optical waveguiding has been reported so far. These films include epitaxial layers of high resistivity on low resistivity GaAs[10], composite structure of GaAs-GaAlAs[11], composite structure ADP-KDP[12], and single crystal garnet films[13]. These layers can be grown with a high degree of purity and offer the attractive feature of modulation[10,11,14].

All these layers are planar guides which confine the light in one dimension only, and therefore as such are not compatible with the concept of optical circuitry. To form a channel waveguide in which the radiation is confined in the two dimensions perpendicular to the direction of propagation, it is possible as shown earlier, to use ion implanatation or diffusion[15]. It is interesting to investigate the possibility of fabricating a channel guide by a removal of the superfluous sections of the epilayer (as shown in Fig. II.13). Because of the large dielectric discontinuity the scattering losses in this guide are very sensitive to the smoothness of its walls as well as its top surface. For example, a 3μ wide waveguide in GaAs will suffer roughly a loss of $4\ cm^{-1}$ when the roughness of the walls is $500Å$ rms. This rough estimate[16] based on the Rayleigh criterion indicates that special care has to be taken in the fabrication of these guides. An extreme case of rough walls and top surface is shown in Fig. II.14a. This guide (3μ high, 7μ wide) scattered away most of the propagating light in a sample less than 1 mm long.

Smoother channels were fabricated by exposing the photoresist with a better mask, and ion polishing the sample after the ion machining (details are given in Chapter IV). Figure II.14b shows a channel (1.4μ high, $2\ \mu$ wide) with much smoother walls.

The number of modes supported by a ridged guide, as discussed in Section II.6, can be controlled for a given dimension by choosing an appropriate guide substrate dielectric discontinuity or by covering the guide with an appropriate index material.

We have discussed earlier directional couplers made of single mode waveguides embedded in the surface of GaAs. In that case the coupling between two adjacent guides is caused by the overlap of the propagating modes as shown in Fig. II.15a. Figure II.15b shows single mode ridged waveguides in which the modes are very well confined in the x direction (because of the large dielectric discontinuity) and two

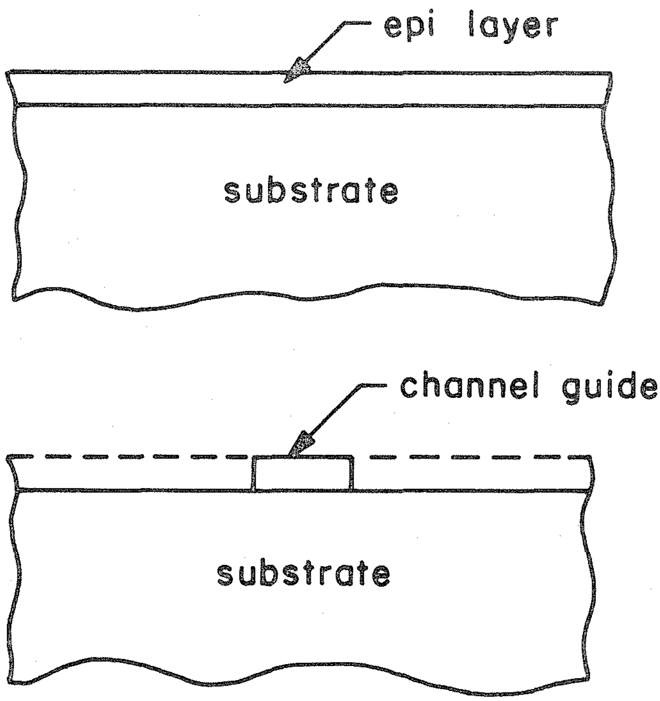

Fig. II.13 Channel waveguide fabrication by removal of superfluous sections of an epilayer.

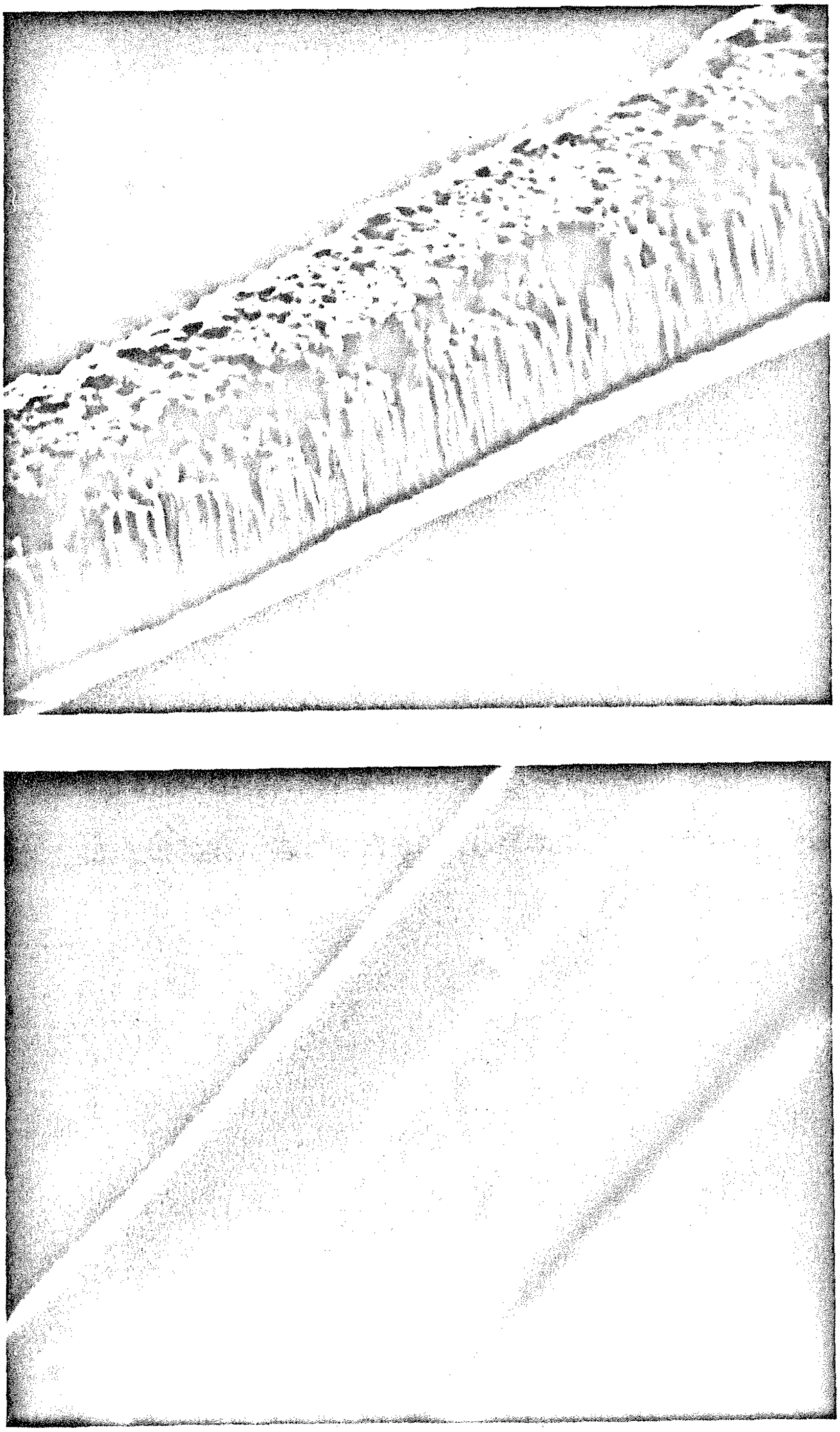

Fig. II.14 (a) An extreme example of a guide with rough walls and top surface. (The guide is 3μ high and 7μ wide.)

(b) Good quality channel waveguide fabricated by using holographically prepared mask and ion polishing. (The guide is 1.4μ high and 2μ wide.)

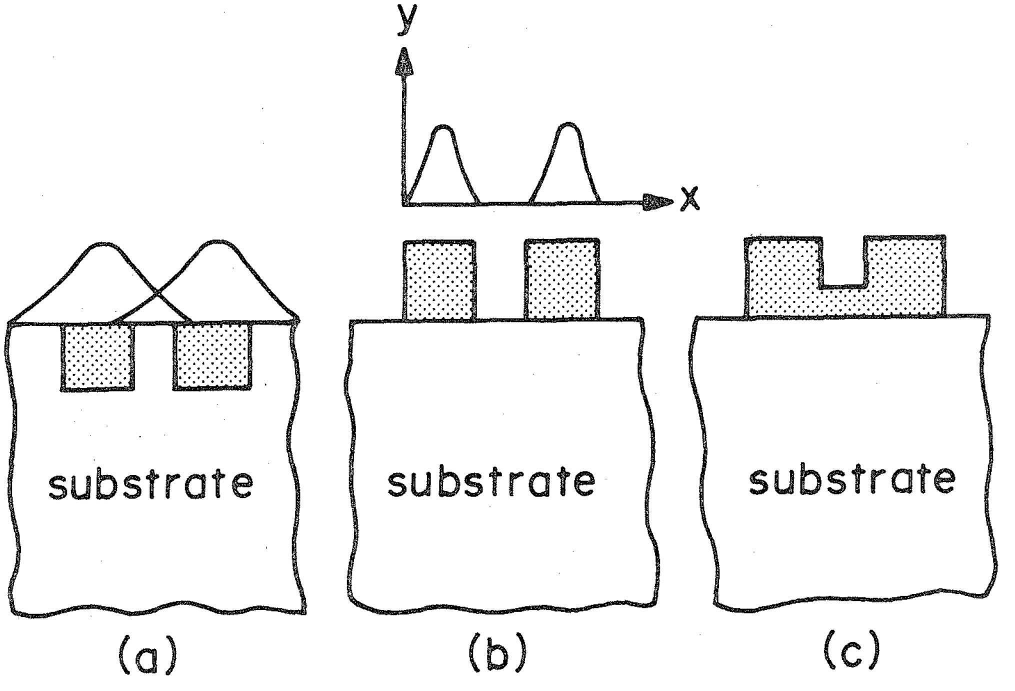

Fig. II.15 Directional couplers fabricated in GaAs.

(a) Single mode embedded guides directional coupler.

(b) Two single mode ridged guides with no coupling.

(c) Ridged guides with increased degree of coupling.

closely spaced guides will thus have a negligible coupling. To increase the coupling between the guides, only a partial removal of the epilayer between them was performed as shown in Fig. II.15c. Fig. II.16 is an indication of the coupling. It shows the cross section of a high resistivity GaAs epilayer (about 8μ thick) that was machined down to the substrate to form a large number of isolated channels. Light coupled into one channel emerges at the other end of the sample from that channel only (bottom photograph). However, when the same epilayer is only partially machined (Fig. II.16b), light coupled into one guide emerges from three guides.

II.10 Directional Coupler--Switch Modulator

As mentioned earlier, one of the most exciting applications of the directional coupler is the switch modulator in which the amount of light coupled from one channel to the other is controlled by electric signal applied to the guides. Such a device can be used to modulate the light propagating in one guide or to switch light from one channel to another. The latter property is an important mean for multiplexing (or demultiplexing) two signals into one, or for switching light in an opto-electronic switchboard of an optical communication network.

The merit of a modulator is determined by two factors: the speed at which it can impose the information on the light beam and the electrical power it consumes in order to do so. The speed of the crystalline electrooptic modulator is determined by the response of the electrical circuit, and this response is limited by the capacitance of

MULTIMODE DIRECTIONAL COUPLER

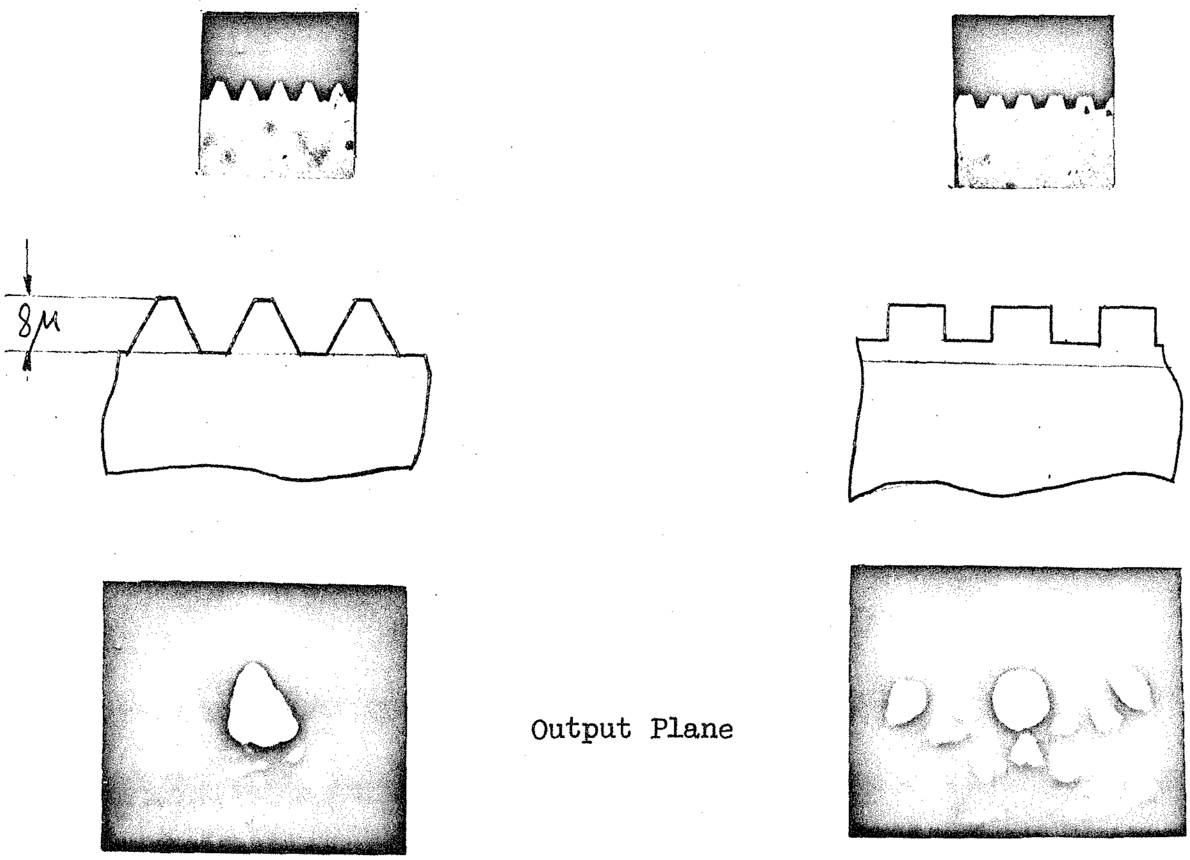

(a) (b)

Fig. II.16 Directional coupler fabricated by ion machining in a GaAs epilayer.

(a) Isolated channels. (b) Coupled channels.

the device. The capacitance of a $3 \times 3\mu$ rectangular guide, 1 cm long, is about ≈ 10 pF allowing subnano-second response. We shall thus limit our attention to the relative magnitude of voltage necessary for deriving different schemes of modulation. First we recall that for the linear electrooptic effect

$$\delta n \propto E \Rightarrow \delta n \propto V \qquad \text{(II.10.1)}$$

where δn is the index of refraction caused by the applied field E and where V is the applied voltage. We also recall that for polarization modulation[9] (in which the polarization of the propagating light is rotated by 90° as a result of the applied field) the change $\delta\beta$ in the propagation constants of the TE and TM modes must be such that:

$$(\delta\beta_{TE} - \delta\beta_{TM})L = \pi \qquad \text{(II.10.2)}$$

where L is the length of the modulator.

For the sake of simplicity we assume

$$\delta\beta_{TM} = 0 \qquad \text{(II.11.3)}$$

and that $\delta\beta_{TE}$ can be written as

$$\delta\beta_{TE} = \delta n \cdot k_0 \qquad \text{(II.10.4)}$$

Using II.10.4 and II.10.2 we can write that:

$$\delta n = \frac{\pi}{k_0 L} \qquad (II.10.5)$$

Our task now is to compare this δn which is required for a 100% modulation in the polarization modulator (as well as mode conversion modulator[17]) with the one needed for a directional coupler modulator.

Let us therefore consider a typical example. It is the directional coupler whose cross section is shown in Fig. II.17. The material is assumed to be GaAs (n = 3.5). Because of the relatively large dielectric discontinuity ($\Delta n = .01$) the modes are well confined, yielding (with the use of II.6.9 for the 3 x 3μ guides) the following value for the coupling coefficient at $\lambda = 1.15\mu$

$$K = 0.155\text{mm}^{-1} \qquad (II.10.6)$$

We choose the modulator length to be the length necessary for complete transfer of power. According to II.3.9

$$L = \frac{\pi/2}{K} \approx 10\text{mm} \qquad (II.10.7)$$

Thus light entering the device at the left channel will emerge from the one on the right. In order to turn the device into a switch modulator Marcaliti[2] has suggested changing the coupling coefficient (by changing the dielectric discontinuity, through the electrooptic effect) to a new value K_1 such that

$$K_1 = \frac{\pi}{L} \qquad (II.10.8)$$

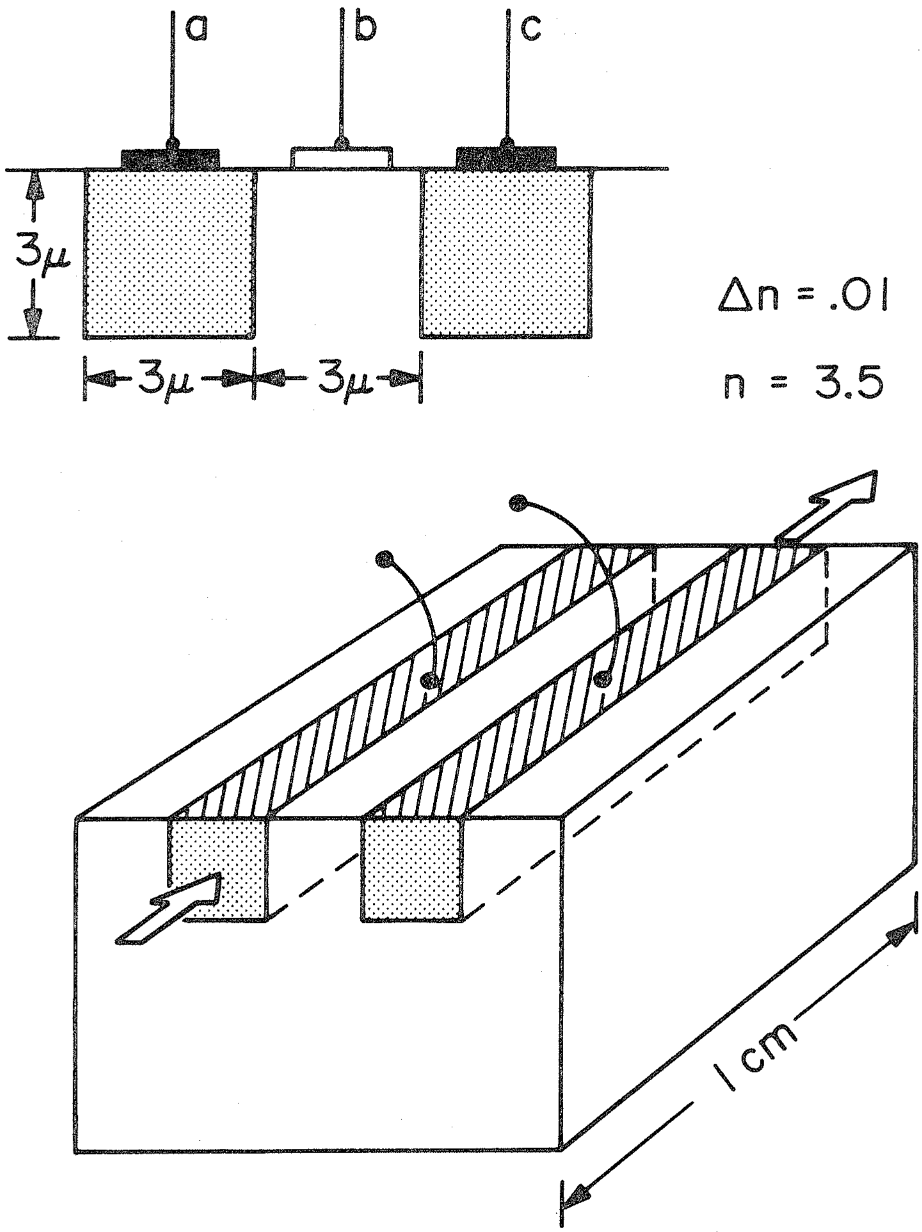

Fig. II.17 Example of a directional coupler modulator.

According to II.3.7, this will cause the light to be coupled back to the original channel resulting in a 100% switch modulation. The coupling coefficient can be varied by applying field to the section between the two guides (schematically via electrode b in Fig. II.17), or alternatively by applying the field to the guides (electrodes a and c). To obtain the above value of K_1 the dielectric discontinuity of the guide has to be reduced from $\Delta n = .01$ to $\Delta n = .007$. Thus the change in the index of refraction required for switching is:

$$\delta n \approx .003 = 52 \frac{\pi}{k_0 L} \tag{II.10.9}$$

The conclusion drawn from this extreme example is very disappointing. It indicates that the electrical power necessary to drive this directional coupler modulator is 2500 times larger than the driving power of a regular polarization modulator II.10.5. A smaller δn can be achieved for a given length geometry by decreasing the dielectric discontinuity and increasing the separation between the guides. This however reduces the confinement of the propagating modes.

In order to devise a new scheme that will allow directional coupling switching with less drive power, let us consider again the coupled mode equations (II.3.2 and II.3.3), but this time allowing for different propagation constants β_0 and β_1 for the two guides.

$$\frac{dA_0(z)}{dz} = -i\beta_0 A_0(z) - iK\, A_1(z) \tag{II.10.10}$$

$$\frac{dA_1(z)}{dz} = -i\beta_1 A_1(z) - iK\, A_0(z) \tag{II.10.11}$$

Using the regular boundary conditions

$$A_0(0) = 1 \qquad\qquad A_1(0) = 0 \tag{II.10.12}$$

we obtain the solution:

$$A_0(z) = \left[\cos\left(K^2+\left(\frac{\Delta\beta}{2}\right)^2\right)^{\frac{1}{2}} z - i\,\frac{\Delta\beta/2}{\left(K^2+\left(\frac{\Delta\beta}{2}\right)^2\right)^{\frac{1}{2}}}\sin\left(K^2+\left(\frac{\Delta\beta}{2}\right)^2\right)^{\frac{1}{2}} z\right]\cdot e^{-i(\beta_0-\frac{\Delta\beta}{2})} \tag{II.10.13}$$

$$A_1(z) = -\left[\frac{-i\,K}{\left(K^2+\left(\frac{\Delta\beta}{2}\right)^2\right)^{\frac{1}{2}}}\sin\left(K^2+\left(\frac{\Delta\beta}{2}\right)^2\right)^{\frac{1}{2}} z\right] e^{-i(\beta_1+\frac{\Delta\beta}{2})z} \tag{II.10.14}$$

where $\Delta\beta$ is

$$\Delta\beta = \beta_0 - \beta_1 \tag{II.10.15}$$

This solution becomes identical to II.3.7 and II.3.8 when $\Delta\beta = 0$.

Going back to our previous example, where with two identical guides $(\Delta\beta = 0)$ we had a complete transfer of power in a length L $(A_1\,(L) = 1)$, it is possible by applying field to one of the guides only to destroy the identity between the guides so that $\Delta\beta \neq 0$ any more. According to II.10.14 if

$$\left(K^2 + \left(\frac{\Delta\beta}{2}\right)^2\right)^{\frac{1}{2}} L = \pi \tag{II.10.16}$$

we will get

$$A_1(L) = 0$$

$$A_0(L) = 1$$

This means that for such a $\Delta\beta$ there is no power transfer, and thus a 100% switch modulation is achieved. Equations II.10.16 and II.10.7 give the value of $\Delta\beta$ needed for destroying the coupling between the guides:

$$\Delta\beta L = \sqrt{3}\,\pi \qquad \text{(II.10.17)}$$

and the necessary change δn is thus

$$\delta n \approx 1.73 \frac{\pi}{k_0 L} = 1.10^{-4} \qquad \text{(II.10.18)}$$

This δn is much smaller than the previous one II.10.9 and is approaching the value required for polarization modulation. It is interesting to note that II.10.18 applies to the ridge directional couplers described in Section II.9 as well as the embedded ones.

A directional coupler can be made polarization sensitive by choosing an appropriate guiding plane (for example 100 in GaAs) in which application of field causes a certain δn for TE modes but $\delta n = 0$ for TM mode (or vice versa). Thus in our example, before the application of the field, TE as well as TM modes are coupled from one guide to the other. However with the application of the field, the coupling of the TE mode is destroyed while the coupling of the TM mode remains the same. Such a device with a D.C. electric field is capable of separating the two polarizations of an incoming optical signal into two different channels. As such it can turn a polarization modulator (or a mode converter) into a directional coupler switch, as shown in Fig. II.18a. This composite device will have a low modulating power together with a directional coupler switch capability. Reversing the pulse's direction of propagation (Fig. II.18b) enables the devices to combine (multiplex) into one output channel pulse, with the appropriate polarizations from two input channels.

We can apply electric fields in a semiconductor[18] guide by back-biasing a metal-semiconductor junction (Schottky barrier). The field is supported in a depletion region which is swept free of carriers to a depth d, given by $d = \varepsilon E/eN$, where N is the free carrier concentration (assumed independent of depth) and E is the peak value of the electric field. In this depletion region the field falls off linearly with depth. The maximum depth to which a field can be applied in such a junction is given by the field at which the material breaks down. In GaAs the breakdown field is roughly independent of doping level, and has a value $E_B \simeq 5 \times 10^5$ V/cm. This means that the maximum depletion width is inversely proportional to the carrier concentration. Numerically the maximum depth d_m in microns is related to the carrier concentration N in cm^{-3} by

$$d_m = 3.5 \times 10^{16}/N \qquad \text{(II.10.19)}$$

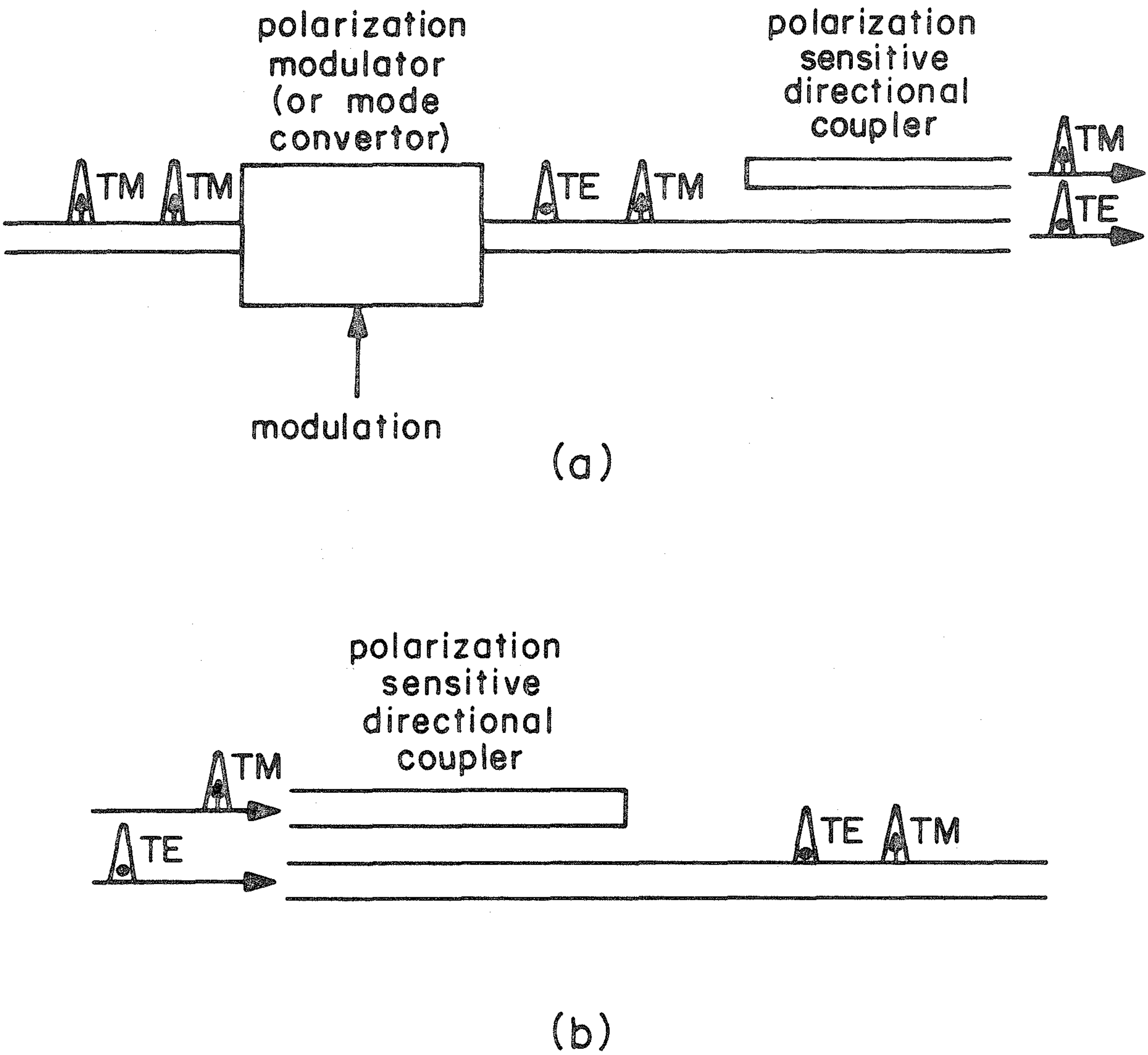

Fig. II.18 (a) Combination of a phase modulator and a polarization sensitive directional coupler.

(b) Polarization sensitive directional coupler as a multiplexer.

This indicates that in order to penetrate about 3μ into the guiding layer, its concentration must be lower than

$$N < 10^{16} cm^{-3}$$

Unfortunately the free carrier concentration of the proton implanted waveguides after the anneal (which is necessary for low optical attenuation) is about $10^{17} cm^{-3}$, thus preventing the penetration of the field into the bulk of the guide. GaAs epitaxial layers with low carrier concentration have been grown[10], but are not yet readily available. A ridged directional coupler (Section II.9) made of such an epitaxial layer may be a suitable candidate for a modulator.

In a GaAs guide in the (100) plane TM modes are unchanged by the applied field. TE modes, however, experience a change in refractive index

$$\delta n = \tfrac{1}{2} n^3 r_{41} E \quad , \tag{II.10.20}$$

where r_{41} is the electrooptic coefficient and n is the index of refraction. Substituting the value of n_4 and r we get:

$$\delta n = 3 \cdot 10^{-9} \cdot E \tag{II.10.21}$$

where E is the applied field in V/cm.

To achieve a $\delta n = 10^{-4}$ which is necessary for the directional coupler switching, we need an average electric field of:

$$E = 3.3 \cdot 10^4 \frac{V}{cm} = 3.3 \frac{V}{\mu}$$

and voltage required for a 3μ thick guide is thus

$$V = 10V$$

In the next section we shall discuss the use of this switch and a similar device for multiplexing and demultiplexing of optical pulses.

II.11 Light Multiplexing by Directional Coupling

The high optical frequency of the laser radiation enables it to carry large amounts of information. However, imposing a high rate of information on a laser beam is a difficult matter. One of the ways around this difficulty is to modulate the information on a number of beams at a relatively moderate rate, and then to multiplex these beams into one beam as shown in Fig. II.19a. We shall assume for the following discussion that the laser radiation is in the form of very short pulses with a period T, and that they appear in the different channels with the appropriate shift in time so that they can be multiplexed with no overlap between them. Such pulses can be generated, for example, by mode locking[9] an Nd:YAG laser, and the appropriate shift in time between the channels can be achieved by coupling the pulses to the channel via optical fibers with different lengths. Another method is to have an array of injection lasers on the same substrate as part of an integrated optical circuit, where each one of these lasers is pulsed at a moderate

rate but with an appropriate shift in time.

Let us examine the operation of the directional coupler switch described in the previous section as a two channel multiplexer. Figure II.19b shows the channels into which the two already modulated (pulse code modulation-PCM) beams are coupled. In order to combine the two beams into one that will propagate in the lower guide, we have to see to it that when a pulse appears in the upper guide it is completely coupled into the lower guide, but a T/2 seconds later when a pulse appears in the lower guide it is not coupled into the upper one but keeps propagating in the lower guide. This can be accomplished by choosing the coupling coefficient and the length of the two guides to be such that with no application of electric field a complete transfer of power from one channel to the other is possible $(KL = \frac{\pi}{2})$. On the other hand to prevent the coupling of pulses from the lower to the upper channel, we have to apply field with the appropriate strength for destroying the coupling whenever a pulse in the lower guide is due. This can be done by driving the directional coupler with a sinusoidal wave whose period is exactly T as shown in Fig. II.19b. To perform multiplexing the same configuration can be used but the direction of propagation of the pulses is reversed.

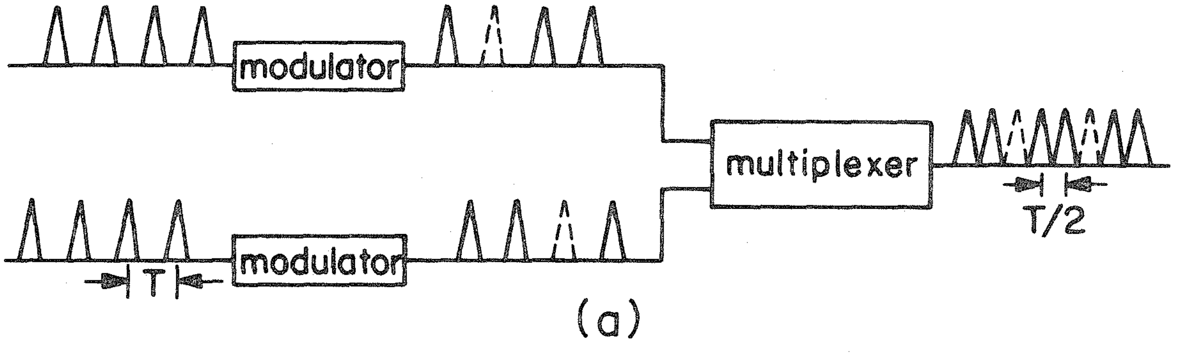

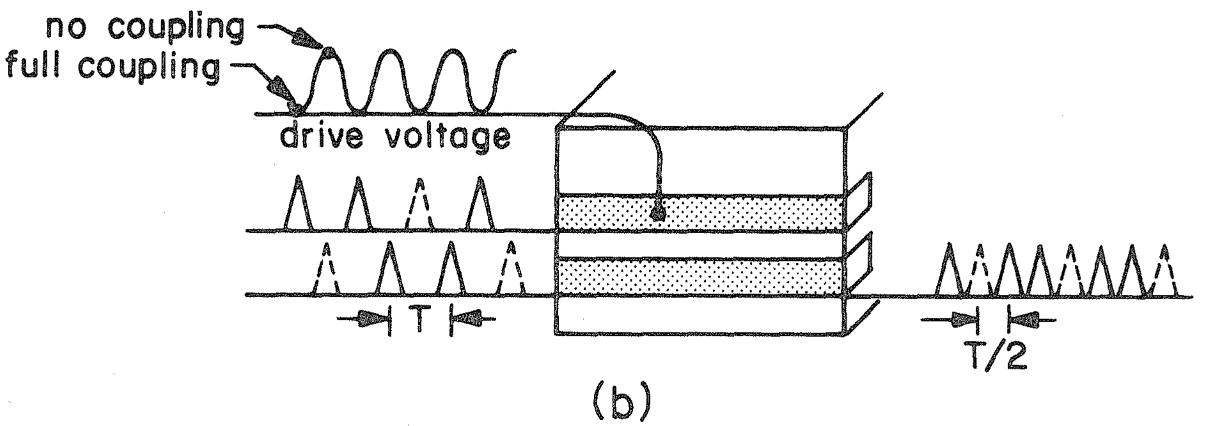

Fig. II.19 (a) Multiplexing scheme for a higher rate of information modulation.

(b) Directional coupler multiplexer.

References for Chapter II

1. See for example, J. R. Pierce, "Coupling of Modes of Propagation," J. Appl. Phys. 25, 179 (1954).
2. E. A. J. Marcatili, "Dielectric Rectangular Waveguide and Directional Coupler for Integrated Optics," BSTJ 48, 2071 (1969).
3. E. Garmire, H. Stoll, A. Yariv, and R. G. Hunsperger, "Optical Wave-Guiding in Proton-Implanted GaAs," Appl. Phys. Lett. 21, 87 (1972).
4. D. Marcuse, "The Coupling of Degenerate Modes in Two Parallel Dielectric Waveguides," BSTJ 50, 1791 (1971).
5. M. F. Bracey, A. L. Cullen, E. F. F. Gillespie, and J. A. Staniforth, "Surface-Wave Research in Sheffield," IRE Trans. Antennas and Propagation AP-7, Special Supplement, S219 (1959).
6. N. S. Kapany, Fiber Optics, New York: Academic Press (1967).
7. J. E. Goell, "A Circular-Harmonic Computer Analysis of Rectangular Dielectric Waveguides," BSTJ 48, 2133 (1969).
8. S. Somekh, E. Garmire, A. Yariv, H. L. Garvin, and R. G. Hunsperger, "Channel Optical Waveguide Directional Coupler," Appl. Phys. Lett. 22, 46 (1973).
9. See for example, A. Yariv, Introduction to Optical Electronics, New York: Holt, Rinehart and Winston, 1971.
10. D. Hall, A. Yariv, and E. Garmire, "Optical Guiding and Electrooptic Modulation in GaAs Epitaxial Layers," Opt. Comm. 1, 403 (1970).

Also, D. Hall, A. Yariv, and E. Garmire, "Observation of Propagation Cutoff and Its Control in Thin Optical Waveguides," Appl. Phys. Lett. 17, 127 (1970).

11. F. K. Reinhart and B. I. Miller, "Efficient GaAs-$Al_xGa_{1-x}As$ Double-Heterostructure Light Modulators," Appl. Phys. Lett. 20, 36 (1972).

12. V. Ramaswamy, "Epitaxial Electrooptic Mixed Crystal $(NH_4)_xK_{1-x}H_2PO_4$ Film Waveguide," Appl. Phys. Lett. 21, 183 (1972).

13. P. K. Tien, R. J. Martin, S. L. Blank, S. H. Wemple and L. J. Vernerin, "Optical Waveguides of Single-Crystal Garnet Films," Appl. Phys. Lett. 21, 207 (1972).

14. P. K. Tien, R. J. Martin, R. Wolfe, R. C. LeCraw, and S. L. Blank, "Switching and Modulation of Light in Magneto-Optic Waveguides of Garnet Films," Appl. Phys. Lett. 21, 394 (1972).

15. W. E. Martin and D. B. Hall, "Optical Waveguides by Diffusion in II-VI Compounds," Appl. Phys. Lett. 21, 325 (1972).

16. P. K. Tien, "Light Waves in Thin Films and Integrated Optics," Appl. Optics 10, 2395 (1971).

17. A. Yariv, "Coupled Mode Theory for Guided-Wave Optics," to be published in IEEE JQE, (1973).

18. E. Garmire, "Integrated Optics in Semiconductors," Presented at the Solid State Circuits Conference, NEREM 1972.

III. PERIODIC CORRUGATIONS IN OPTICAL WAVEGUIDES

III.1 Introduction

The interaction of radiation with man-made periodic structures is of great importance in the microwave and optical regions. The traveling wave tube is a good example of a device in the microwave region which is based on this kind of interactions. In the optical region one finds devices such as the diffraction grating, the acousto-optic modulator and deflector, and the hologram.

In this chapter we shall discuss the interaction between periodic corrugations on the surface of a dielectric waveguide and the wave propagating in the guide. In Chapter V we shall describe methods which were devised to enable us to fabricate these periodic structures, with periods as low as 0.11μ (1100Å).

In general a wave propagating in a periodic structure consists of space harmonics. These space harmonics have the same frequency as the original wave but a different propagation constant β . Considering the first order space harmonics only, we can write

$$\beta_{\text{space harmonic}} = \beta \pm \frac{2\pi}{\Lambda} \qquad \text{(III.1.1)}$$

where Λ is the corrugation period. The space harmonics are thus shifted in k space by the length of the k vector of the structure $-\eta$

$$\eta \equiv \frac{2\pi}{\Lambda} \qquad \text{(III.1.2)}$$

If the propagation constant of the space harmonic happens to coincide with the propagation constant of a different mode, coupling of power from one mode to the other becomes possible.

Let us consider the guide shown in Fig. III.1a; the ω-β diagram is shown in Fig. III.1b. The guide (which is discussed in Appendix I) is assumed to support two guided modes 0 and 1. The propagation constants of these modes at a given ω, are β_0 and β_1. As can be seen from the diagram (we have assumed $n_3 > n_1$)

$$n_2k_0 > \beta_0 > \beta_1 > n_3k_0 \qquad \text{(III.1.3)}$$

The β's are less than n_2k_0 in order to allow the cosine or sine variation of the modes inside the guide along the thickness direction. Outside the waveguide the mode profile should fall exponentially for a guided mode. This is taken care of by requiring $\beta > n_3k_0$ where n_3k_0 is the free wave propagation constant in the substrate.

In this waveguide it is possible to cause coupling between the two guided modes[1] by having a corrugation whose period satisfies

$$\frac{2\pi}{\Lambda} \equiv \eta = \beta_0 - \beta_1 \qquad \text{(III.1.4)}$$

This condition is illustrated on the right branch of Fig. III.1b by η_1. The value of the coupling coefficient which depends on the corrugation depth, the modes' profiles and so on, will be discussed later. If we decrease the corrugation period and thus increase the value of its vector η, it becomes possible to couple light from a

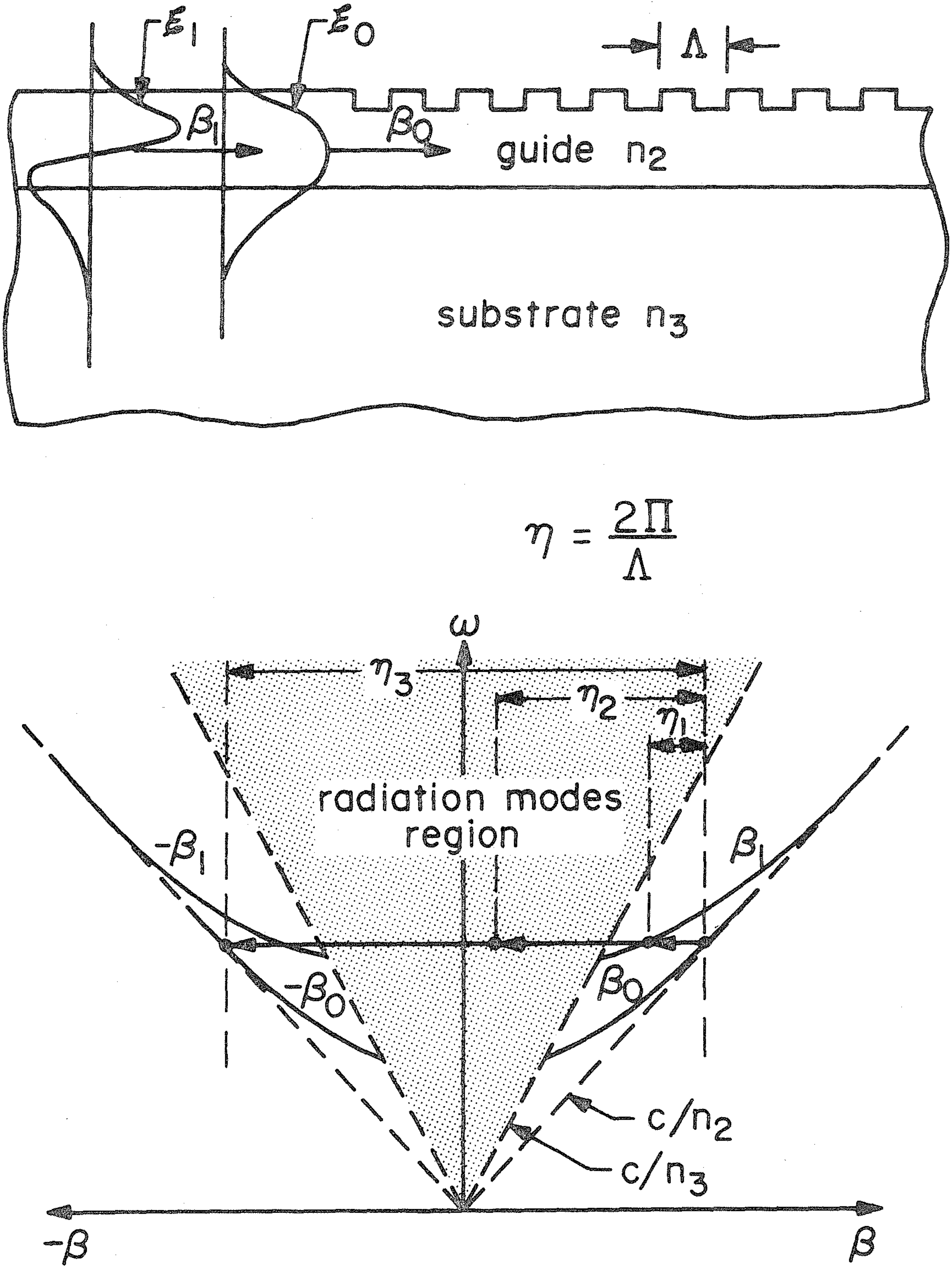

Fig. III.1. (a) Periodically corrugated dielectric waveguide.

(b) Mode dispersion and possible interactions in the above guide.

guided mode, say the 0 mode, to a continuum of radiation modes[1]. These radiation modes have a propagation constant in the z direction which is

$$\beta_r < n_3 k_0 \qquad \text{(III.1.5)}$$

This means that they do not decay exponentially in the x direction and are able to carry power away from the guide. The case is illustrated by η_2 in Fig. III.1b. The coupling from the 0 order mode will be to a cluster of radiation modes whose propagation constant in the z direction is close enough to

$$\beta_r = \beta_0 - \eta \qquad \text{(III.1.6)}$$

This effect can be used to couple light in and out of a waveguide and is known as the grating coupler[2,3].

If Λ is further decreased so that

$$\frac{2\pi}{\Lambda} \equiv \eta = 2\beta_0 \qquad \text{(III.1.7)}$$

coupling occurs between a forward propagating mode and the same backward mode. This effect is illustrated by η_3 in Fig. III.1b. It results in a distributed mirror whose behavior was described by Fig. I.5 and will be considered later. The use of two such distributed mirrors instead of two cleaved faces may help in extending the lifetime of semiconductor injection lasers in the case where catastrophic mirror damage is the dominant failure mode. When the corrugation extends along the whole length of an amplifying medium, a distributed feedback laser[4] may result. In these lasers there are no discrete mirrors and this makes them very desirable for an optical integrated circuit.

In this chapter we shall focus our attention on a laser geometry in which the distributed feedback is supplied by surface corrugation, elaborate on its modes, and conclude with a description of the first observation of such a laser in GaAs[5].

III.2 Theory

The problem of coupling by surface perturbation between TE modes in a dielectric waveguide can be treated in the same fashion as the time dependent perturbation in quantum mechanics. The solution for the perturbed guide can be expanded in terms of the modes of the unperturbed guide. Assuming that the zero order mode enters the perturbed section of the waveguide at $z = 0$ (as shown in Fig. III.2a), one can calculate "transition rates" or coupling coefficients to different guided modes, to radiation modes (modes of the continuum) and to the backward going mode. This approach was used by Marcuse[1] to calculate mode conversions and radiation losses in waveguides.

We shall apply the same approach used in Chapter II for the calculation of the coupling coefficient between the modes of two adjacent guides. We start by writing the coupled mode equations for forward (+) and backward (-) going zero order modes:

$$\frac{dA_0^{(+)}(z)}{dz} = (-i\beta_0 + \alpha)\, A_0^{(+)}(z) - iKe^{-i\eta z} A_0^{(-)}(z) \qquad \text{(III.2.1)}$$

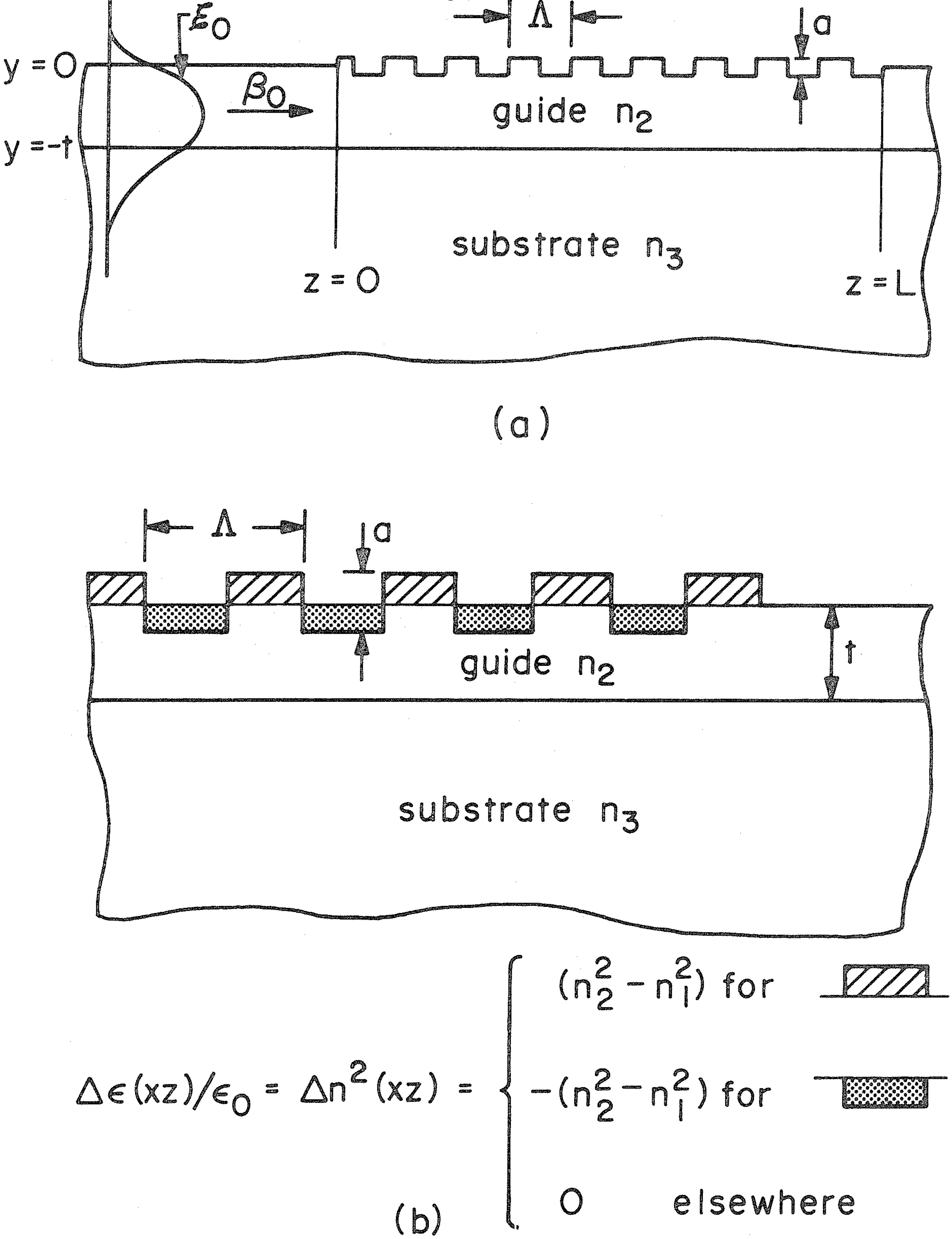

Fig. III.2. (a) Distributed mirror of length L .
(b) Definition of the perturbation in the dielectric constant caused by the corrugation.

$$\frac{dA_0^{(-)}(z)}{dz} = (i\beta_0 - \alpha)\, A_0^{(-)}(z) + iKe^{i\eta z}\, A_0^{(+)} \qquad \text{(III.2.2)}$$

where β_0 is the propagation constant of the mode, α is the gain of the medium, and K is the coupling coefficient between the modes. K appears with different signs in the two equations because the modes carry power in opposite directions (see Appendix II). In addition, K is multiplied by a phase term $e^{\pm i\eta z}$ which represents the spatial variation of the coupling perturbations. As we shall see later, η is exactly the k vector of the perturbation. $A_0^{(+)}$ and $A_0^{(-)}$ are the amplitudes of the modes

$$E_0^{(+)}(y,z) = A_0^{(+)}(z)\mathcal{E}_0(y) \qquad \text{(III.2.3)}$$

$$E_0^{(-)}(y,z) = A_0^{(-)}(z)\mathcal{E}_0(y) \qquad \text{(III.2.4)}$$

The mode profile $\mathcal{E}_0(y)$ is normalized to carry one unit of power, so that the power $P_0^{(+)}(z)$ carried by $E_0^{(+)}(y,z)$ is given by

$$P_0^{(+)}(z) = |A_0^{(+)}(z)|^2 \qquad \text{(III.2.5)}$$

The rate of growth of $P_0^{(+)}(z)$ because of the coupling can be derived from III.2.1 (we assume $\alpha = 0$ for this purpose)

$$\frac{dP_0^{(+)}(z)}{dz} = 2\,\mathrm{Re}\left\{A_0^{(+)}(z)\left[-iKe^{-i\eta z}A_0^{(-)}(z)\right]^*\right\} \qquad \text{(III.2.6)}$$

We shall derive now an expression for the power growth from a physical point of view, and by a comparison with III.2.6 find expressions for K and η.

In a similar fashion to what we did in Chapter II, we use the perturbations in the polarization of the backward going mode, caused by the index disturbance at the surface, to drive the forward going mode. Coupling can take place only between TE or TM modes but not from TE to TM, because the driving polarization is in the same direction as the field (we assume isotropic media). The driving polarization caused by a TE mode is given by:

$$[P^{(-)}_{pert}(y,z,t)]_y = \Delta\varepsilon(y,z)[E^{(-)}_0(y,z,t)]_y \tag{III.2.7}$$

where $\Delta\varepsilon(y,z)$ is the perturbation in the dielectric constant and is given in Fig. III.2b. Power generation for the $(+)$ mode in an infinitesimal volume dV is given by:

$$\frac{dP^{(+)}_0}{dV} = -\overline{E^{(+)}_0(y,z,t)\,\frac{\partial P^{(-)}_{pert}(y,z,t)}{\partial t}} \tag{III.2.8}$$

where the horizontal bar denotes time averaging. Using III.2.4 and time dependence of $e^{i\omega t}$, III.2.8 becomes after the time averaging:

$$\frac{dP^{(+)}_0}{dV} = \tfrac{1}{2}\,R_e\left\{A^{(+)}_0(z)\mathcal{E}_0(y)[-i\omega\Delta\varepsilon(y,z)\mathcal{E}_0(y)A^{(-)}_0(z)]^*\right\} \tag{III.2.9}$$

the growth of the total power $P^{(+)}_0$ can now be derived by simply integrating over x and y. We obtain

$$\frac{dP_0^{(+)}(z)}{dz} = \frac{1}{2} R_e \left\{ A_0^{(+)}(z) \left[-i\omega \iint_{-\infty}^{\infty} \mathcal{E}_0^*(y)\Delta\varepsilon(y,z)\mathcal{E}_0(y)dxdy \right]^* A_0^{(-)}(z)^* \right\} \tag{III.2.10}$$

Comparing III.2.10 with III.2.6 we find:

$$Ke^{-i\eta z} = \frac{\omega}{4} \iint_{-\infty}^{\infty} \mathcal{E}_0^2(y)\Delta\varepsilon(y,z)dxdy \tag{III.2.11}$$

The integral in III.2.11 can be simplified if the perturbation is small enough ($a \ll \lambda$) so we can approximate $\mathcal{E}_0(y)$ by $\mathcal{E}_0(0)$. We ignore for the time being the integral over x because we consider now a planar guide. (The x integral will be used when we consider a channel laser.) With the help of the mode's profile expression from Appendix I, we get after simple manipulations:

$$Ke^{-i\eta z} = \frac{h^2 a}{2\beta_0(t + \frac{1}{p} + \frac{1}{q})} \operatorname{sgn}\left[\cos(\frac{2\pi}{\Lambda} z)\right] \tag{III.2.12}$$

where

$$\operatorname{sgn}[\text{argument}] = \begin{cases} 1 & \text{for argument} > 0 \\ -1 & \text{for argument} < 0 \end{cases} \tag{III.2.13}$$

Using Fourier expansion we can rewrite III.2.12 as

$$Ke^{-i\eta z} = \frac{h^2 a}{2\beta_0(t + \frac{1}{p} + \frac{1}{q})} \left[\frac{4}{\pi} \cos(\frac{2\pi}{\Lambda} z) - \frac{4}{3\pi} \cos(3 \frac{2\pi}{\Lambda} z) + \dots \right] \tag{III.2.14}$$

Only one term from the left side of III.2.14 will give synchronous contribution when substituted into the coupled modes equations. For first order coupling from $A_0^{(+)}$ to $A_0^{(-)}$ which occurs when $\frac{2\pi}{\Lambda} \simeq 2\beta_0$

we find

$$\eta = \frac{2\pi}{\Lambda} \tag{III.2.15}$$

and the coupling coefficient for this case is

$$K = \frac{h^2\ a}{\pi\beta_0(t + \frac{1}{p} + \frac{1}{q})} \tag{III.2.16}$$

On the other hand, for third order coupling which occurs when $3\,\frac{2\pi}{\Lambda} \cong 2\beta_0$, the synchronous term is the one for which

$$\eta = 3\,\frac{2\pi}{\Lambda} \tag{III.2.17}$$

and the appropriate coefficient for the third order coupling is

$$K = \frac{h^2\ a}{3\pi\beta_0(t + \frac{1}{p} + \frac{1}{q})} \tag{III.2.18}$$

These expressions can be further simplified for a well confined zero order mode for which

$$h \simeq \frac{\pi}{t} \tag{III.2.19}$$

$$t \gg \frac{1}{p} + \frac{1}{q} \tag{III.2.20}$$

We can thus rewrite III.2.16 as

$$K = \frac{\pi a}{\beta_0\ t^3} \tag{III.2.21}$$

An additional contribution to the coupling coefficient may arise in a case where the gain (or the loss) α of the medium varies periodically[8]. The $\Delta\varepsilon$ which represent gain variations is imaginary, and the combined $\Delta\varepsilon$ becomes complex:

$$\Delta\varepsilon(y,z) = \Delta\varepsilon_{\text{corrugation}}(y,z) + i\,\frac{1}{k_0}\,\Delta\alpha(y,z) \qquad \text{(III.2.22)}$$

where k_0 is the free space propagation constant and $\Delta\alpha(y,z)$ is the variation in the gain. Using this expression for $\Delta\varepsilon(y,z)$ one has to go back to equation III.2.11 and evaluate K. This coupling coefficient will have the following form

$$K = K_{\text{corrugation}} + iK_{\text{gain}} \qquad \text{(III.2.23)}$$

where $K_{\text{corrugation}}$ is the one given by III.2.16.

Now that we have obtained the value of K and η let us return to the coupled mode equations. To eliminate β_0 from the equations we redefine $A_0^{(\pm)}(z)$

$$\begin{aligned} A_0^{(+)}(z) &\longrightarrow A_0^{(+)}(z)e^{-i(\beta_0-\Delta\beta)} \\ A_0^{(-)}(z) &\longrightarrow A_0^{(-)}(z)e^{i(\beta_0-\Delta\beta)} \end{aligned} \qquad \text{(III.2.24)}$$

where $\Delta\beta$ is the phase mismatch constant

$$\Delta\beta = \beta_0 - \tfrac{1}{2}\,\frac{2\pi}{\Lambda} \qquad \text{(III.2.25)}$$

Substituting all that into III.2.2 and III.2.2 we get:

$$\frac{dA_0^{(+)}(z)}{dz} = (\alpha - i\Delta\beta)A_0^{(+)}(z) - iK\,A_0^{(-)}(z) \qquad \text{(III.2.26)}$$

$$\frac{dA_0^{(-)}(z)}{dz} = -(\alpha - i\Delta\beta)A_0^{(-)}(z) + iK\,A_0^{(+)}(z) \qquad \text{(III.2.27)}$$

This pair of coupled equations will be our starting point in the next sections. We recall that K (for a well confined zero order mode and $a \ll \lambda$) and $\Delta\beta$ are given by:

$$K = \frac{\pi a}{\beta_0 t^3} \quad ; \quad \Delta\beta = \beta_0 - \tfrac{1}{2}\,\frac{2\pi}{\Lambda} \qquad \text{(III.2.28)}$$

III.3 Distributed Mirror

We consider now the geometry described in Fig. III.2a. The (+) zero order mode propagating in the guide from left to right enters at $z = 0$ a corrugated section of length L. If $2\beta_0 \approx \frac{2\pi}{\Lambda}$ reflection occurs. The (+) mode decays while the (-) mode grows as indicated in Fig. I.5. Our aim now is to find how strong the reflection is as a function of the guide properties, and how selective the reflection is for different frequencies that propagate with different propagation constant $-\beta_0$. To do that we consider again the coupled mode equations III.2.26 and III.2.27, taking $\alpha = 0$.

$$\frac{dA_0^{(+)}(z)}{dz} = -i\Delta\beta\, A_0^{(+)}(z) \; -iK\, A_0^{(-)}(z) \tag{III.2.26}$$

$$\frac{dA_0^{(-)}(z)}{dz} = i\Delta\beta\, A_0^{(-)}(z) + iK\, A_0^{(+)}(z) \tag{III.2.27}$$

The boundary conditions that describe the case under consideration are:

$$A_0^{(+)}(0) = 1 \qquad\qquad A_0^{(-)}(L) = 0 \tag{III.3.1}$$

The solution is given by:

$$A_0^{(-)}(z) = \frac{-iK \sinh \gamma(L-z)}{\gamma \cosh \gamma L + i\Delta\beta \sinh \gamma L} \tag{III.3.2}$$

$$A_0^{(+)}(z) = \frac{\gamma \cosh \gamma(L-z) + i\Delta\beta \sinh \gamma(L-z)}{\gamma \cosh \gamma L + i\Delta\beta \sinh \gamma L} \tag{III.3.3}$$

where

$$\gamma = (K^2 - (\Delta\beta)^2)^{\frac{1}{2}} \tag{III.3.4}$$

Under phase matching conditions $(\Delta\beta = 0)$ the Bragg condition

$$2\beta_0 = \frac{2\pi}{\Lambda} \tag{III.3.5}$$

is fulfilled, and we have the strongest reflection:

$$A_0^{(-)} = -i\,\frac{\sinh K(L-z)}{\cosh KL} \tag{III.3.6}$$

$$A_0^{(+)} = \frac{\cosh K(L-z)}{\cosh KL} \tag{III.3.7}$$

A plot of the mode powers for this case is shown in Fig. I.5. The curves of $|A_0^{(-)}|^2$ and $|A_0^{(+)}|^2$ are plotted for $KL = 1.84$. According to III.2.21, it represents the reflection of a well confined mode in a guide with $t = 3\mu$ $n_2 = 3.6$ $\lambda = 0.8\mu$ $a = 500\text{Å}$ and $L = 9\text{mm}$.

The selectivity or the filtering properties of the mirror can be described in terms of $\Delta\beta$. We recall

$$\Delta\beta = \beta_0(\omega) - \tfrac{1}{2}\frac{2\pi}{\Lambda} \tag{III.2.23}$$

it can be approximated by

$$\Delta\beta \approx (\omega\frac{n_2}{c} - \tfrac{1}{2}\frac{2\pi}{\Lambda}) = \Delta\omega\frac{n_2}{c} \tag{III.3.8}$$

Thus its value represents deviation from the exact frequency for which the Bragg condition III.3.5 is fulfilled (ω_{Bragg}). Figure III.3a describes the reflection properties of a mirror with a fixed K and the phase shift associated with it. The different curves represent different lengths. As can be seen, the longer the length is, the narrower the reflection band is. For a finite mirror length the peak reflection is less than unity, but the peak is relatively wide. Its width $\Delta\beta_{refl.}$ is given approximately by

$$\Delta\beta_{refl.} = 2(K^2 + \frac{\pi^2}{L^2})^{\frac{1}{2}} \tag{III.3.9}$$

An infinitely long mirror has a flat total reflection band with a width $\Delta\beta$ of $2K$. This total reflection band is the stop band of this

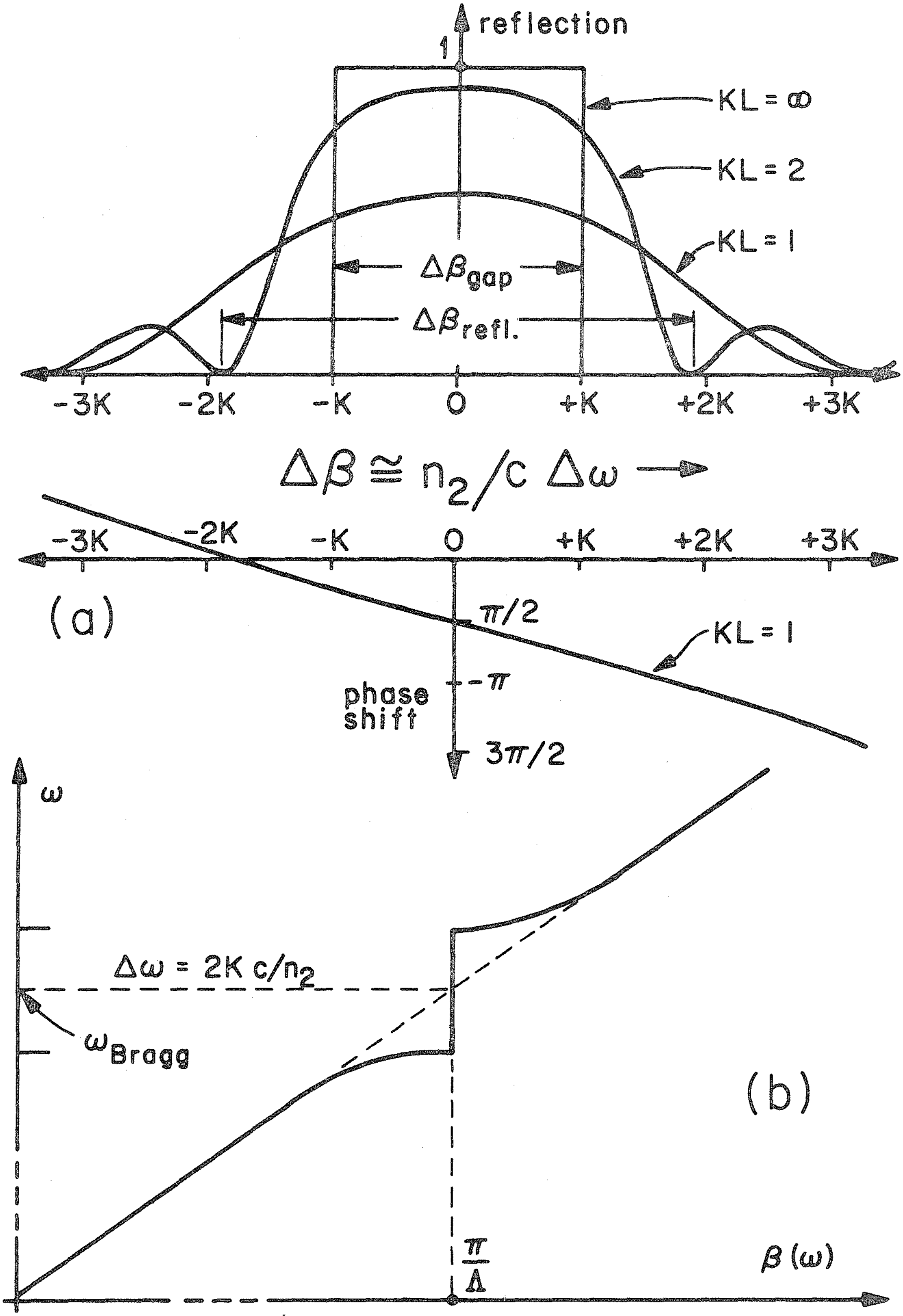

Fig. III.3. (a) Reflection intensity and phase shift from a distributed mirror as a function of $\Delta\beta$ for different values of KL.
(b) A stop band in the mode dispersion caused by the corrugation.

periodic structure, and is analogous to Bragg scattering of Bloch electron wave in a crystal, from one edge of the Brillouin zone to the other by the crystal periodicity[6]. The dispersion $(\omega - \beta)$ diagram of the waveguide thus has a stop band and is modified at its vicinity as shown in Fig. III.3b. The midgap frequency is the Bragg frequency for which

$$\beta_0(\omega_{Bragg}) = \frac{1}{2}\frac{2\pi}{\Lambda} \qquad \text{(III.3.10)}$$

The height of the energy gap is the frequency region over which the propagation constant becomes complex, and thus the propagation is forbidden. (The wave is not absorbed but reflected.) The gap region is given by

$$\Delta\beta_{gap} = 2K \qquad \text{(III.3.11)}$$

and if we take $\beta_0(\omega)$, the non-perturbed propagation constant, as approximately:

$$\beta_0(\omega) \approx \frac{\omega}{c} n_2 \qquad \text{(III.3.12)}$$

we get:

$$\Delta\omega_{gap} = 2K\frac{C}{n_2} \qquad \text{(III.3.13)}$$

In the gap the real propagation constant is fixed and is equal to $\frac{1}{2}\frac{2\pi}{\Lambda}$. Outside the stop band the propagation constant is real, but is modified somewhat to accommodate the gap, as shown in Fig. III.3b.

Two Bragg reflectors can form a laser cavity[7]. Two corrugated mirrors can, for example, be used instead of cleaved faces to form a semiconductor laser cavity as shown in Fig. III.4a. The reflection of the mirrors can be controlled by changing their length or the depth of the corrugation to supply the appropriate feedback for oscillations even for a low gain medium. We assume that the mirror's properties do not change much in the presence of a low gain, and that its length is much smaller than the laser's length (a different case where the mirrors extend all over the laser is treated in the next section).

$$L_m \ll L_\ell \tag{III.3.14}$$

This means that the spectral reflectivity of the mirrors is much wider than the spacing between the longitudinal modes of the laser. We recall that the width of the reflectivity in $\vec{k}$ space is given by III.3.9

$$\Delta\beta_{mirror} = 2(K^2 + \frac{\pi^2}{L_m^2})^{\frac{1}{2}} \tag{III.3.15}$$

For a mirror reflectivity which is close to a unity we can assume that

$$KL_m \simeq 2 \tag{III.3.16}$$

Thus a lower limit for $\Delta\beta_{mirror}$ is

$$\Delta\beta_{mirror} > 2\,\frac{\pi}{L_m} \tag{III.3.17}$$

On the other hand the spacing of the longitudinal modes is given approximately by: (we ignore dispersion because of the gain in the

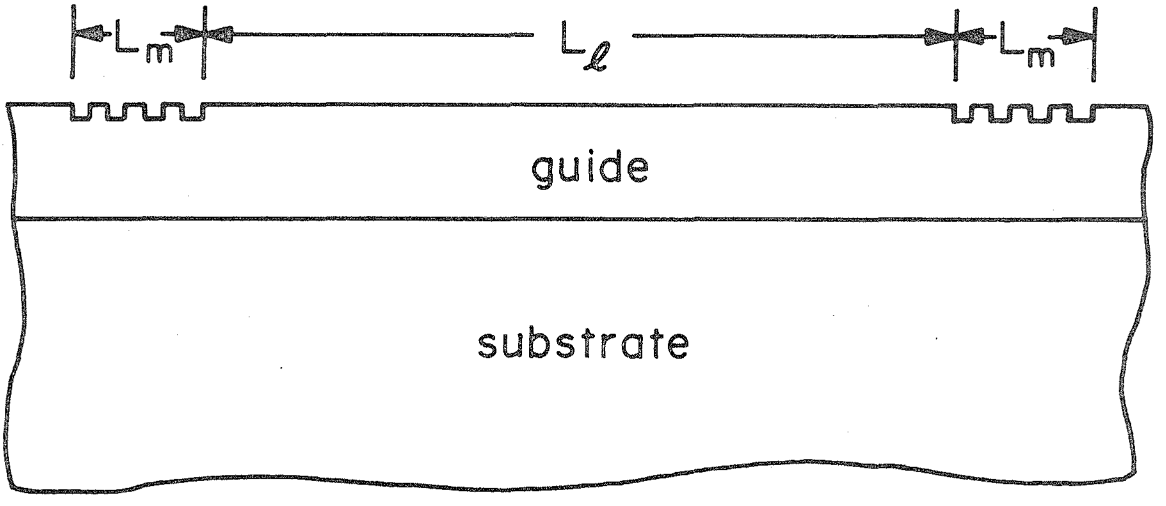

(a)

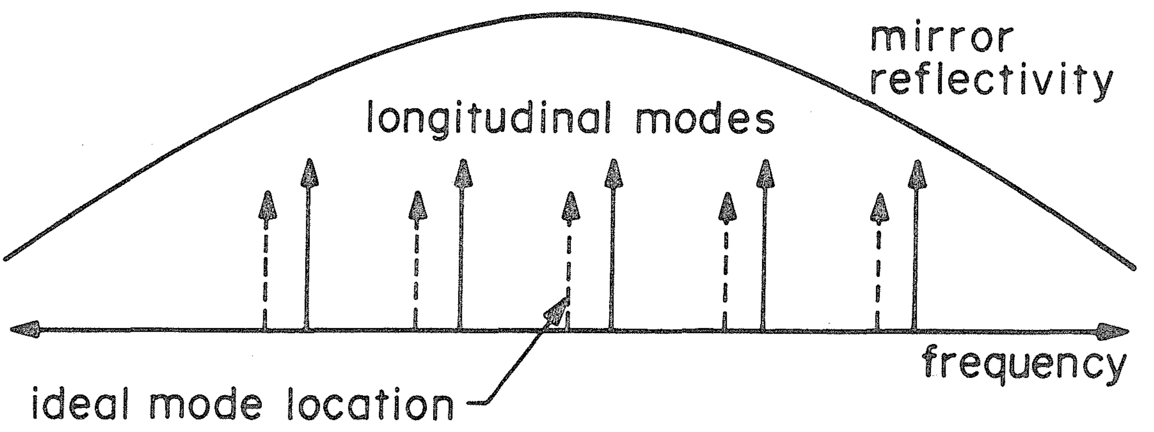

(b)

Fig. III.4. (a) A laser, formed by two distributed mirrors.

(b) Longitudinal mode spectrum of the above laser.

medium, and dispersion in the phase of the reflected beam from the mirror which is shown in Fig. III.3a and can be ignored for $L_m \ll L_\ell$) .

$$\Delta\beta_{\text{longitudinal modes}} = \frac{\pi}{L_\ell} \tag{III.3.18}$$

The longitudinal modes distribution is shown in Fig. III.4b. The location of the modes with respect to the center of the mirror reflectivity, which is important for longitudinal mode discrimination, depends on the exact distance between the two mirrors. According to III.3.6 the reflected wave from the mirrors suffers a phase shift of $-90°$. This means that for a longitudinal mode to coincide with the peak of the reflection, the distance between the mirrors has to be such that it compensates the $-90°$ phase shift for the Bragg frequency. This requires that

$$L_\ell = (2m+1)\,\frac{\lambda_{\text{Bragg}}}{4} = (2m+1)\,\frac{\Lambda}{2} \tag{III.3.19}$$

Another way to state this condition is that the relative phase of the two corrugations has to be $180°$. This requirement may be found difficult to fulfill especially when the propagation constant under the corrugated section may not be exactly the same as the one in the bulk of the guide. In addition the flatness of the reflectivity curve close to the center, reduces the ability to discriminate between close longitudinal modes.

When the corrugation is extended over the total length of the laser, a distributed feedback laser[4] results, and a better control of the longitudinal modes becomes possible.

III.4 Distributed Feedback Laser

We consider now the geometry shown in Fig. III.5a. The corrugation extends from $z = -\frac{1}{2}L$ to $z = \frac{1}{2}L$ and we assume that the waveguide has a gain of α. In the previous section we have discussed the reflection properties of a corrugated structure. In this section we shall discuss its lasing properties and inquire about the modes of oscillation, their frequencies and threshold gains.

Our starting point is the coupled modes equation derived in Section III.2.

$$\frac{dA_0^{(+)}(z)}{dz} = (\alpha - i\Delta\beta)A_0^{(+)}(z) - iKA_0^{(-)}(z) \tag{III.2.26}$$

$$\frac{dA_0^{(-)}(z)}{dz} = -(\alpha - i\Delta\beta)A_0^{(-)}(z) + iKA_0^{(+)}(z) \tag{III.2.27}$$

The corrugation is responsible for the coupling mechanism and the coupling coefficient was found to be (for a well confined zero order mode and corrugation depth $a \ll \lambda$)

$$K = \frac{\pi a}{\beta_0 t^3} \tag{III.2.21}$$

where t is the thickness of the guide. We recall that $\Delta\beta$ is the deviation of the unperturbed propagation constant of the guided mode from π/Λ.

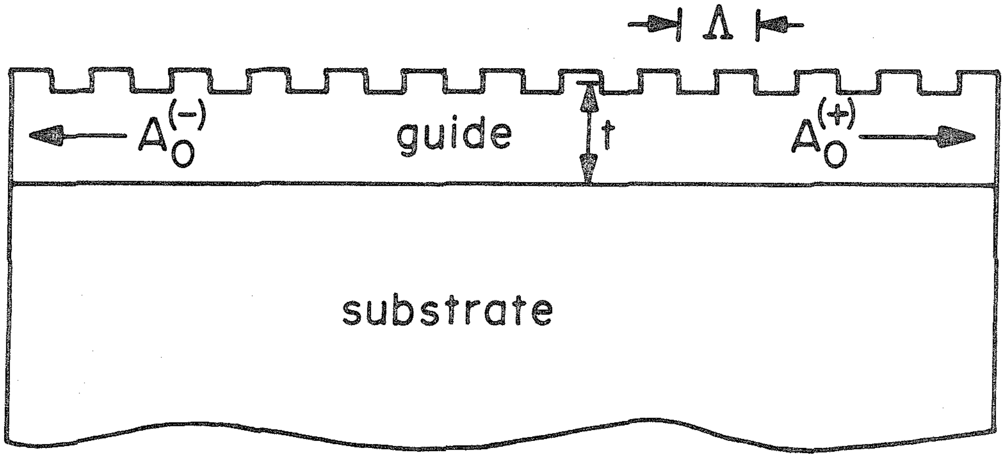

(a)

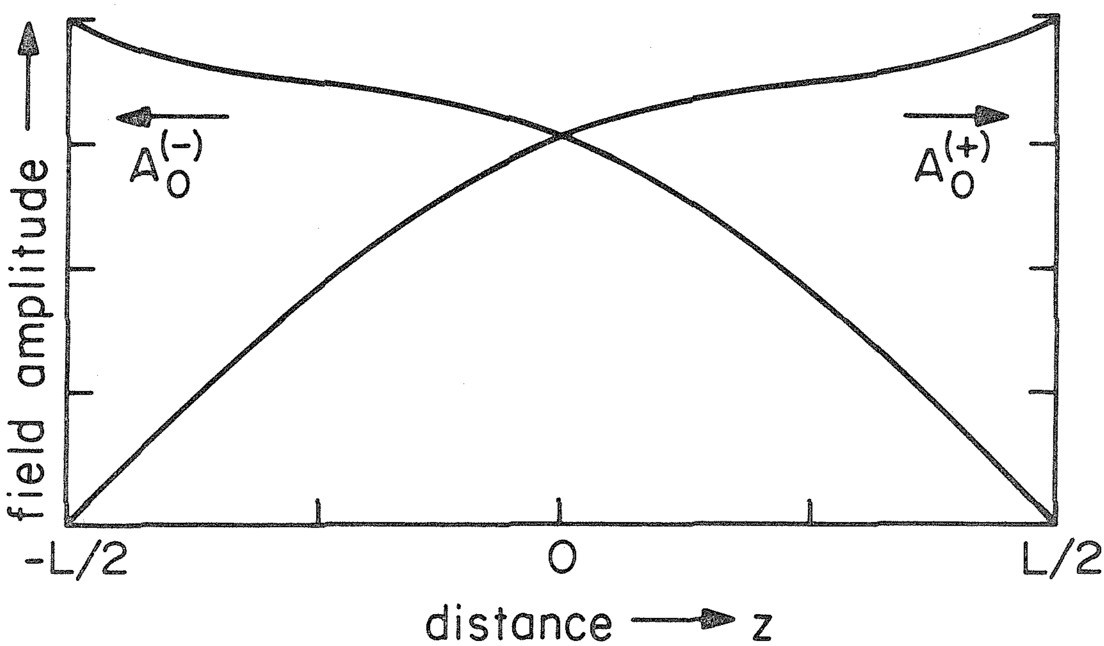

(b)

Fig. III.5. (a) A distributed feedback laser of length L .

(b) Plot of the amplitudes of the propagating modes in the laser.

$$\Delta\beta = \beta_0(\omega) - \tfrac{1}{2}\,\frac{2\pi}{\Lambda} \qquad \text{(III.2.25)}$$

From this point on we follow the original discussion of the distributed feedback laser by Kogelnik and Shank[8]. We start by imposing the appropriate boundary conditions. Since this is an oscillator we assume that there are no incoming waves. Thus the boundary conditions are:

$$A_0^{(+)}(-\tfrac{1}{2}L) = 0 \quad , \qquad A_0^{(-)}(\tfrac{1}{2}L) = 0 \qquad \text{(III.4.1)}$$

A solution with such boundary conditions exists only when the following relation is fulfilled[8]

$$\alpha - i\Delta\beta = \gamma\coth(\gamma L) \qquad \text{(III.4.2)}$$

where

$$\gamma \equiv [(\alpha - i\Delta\beta)^2 + K^2]^{\frac{1}{2}} \qquad \text{(III.4.3)}$$

The complex equation III.4.2 which can also be written as

$$\frac{-\gamma + (\alpha - i\Delta\beta)}{\gamma + (\alpha - i\Delta\beta)}\, e^{2\gamma L} = 1 \qquad \text{(III.4.4)}$$

determines for a given K and L the eigenvalues of $\Delta\beta$ (the shift in the modes frequency) and the corresponding α (the threshold gain) for which oscillations can take place. The solution for $A_0(z)$ is given by

$$A_0^{(+)}(z) = \sinh\gamma(z + \tfrac{1}{2}L) \qquad \text{(III.4.5)}$$

$$A_0^{(-)}(z) = \sinh \gamma(z - \tfrac{1}{2}L) \qquad \text{(III.4.6)}$$

and is shown in Fig. III.5b. As can be seen in the figure, each wave starts with a zero amplitude, at a different side of the laser. The wave grows as it propagates because of the energy continuously fed into it by the other wave and because of the gain which exists in the medium.

In the experimental cases to be discussed later $\alpha \gg K$ so we confine our attention now to this high gain situation. Thus, γ, which is given by III.4.3, can be expanded as

$$\gamma \approx (\alpha - i\Delta\beta) + \frac{K^2}{2(\alpha - i\Delta\beta)} \qquad \text{(III.4.7)}$$

and Equation III.4.4 can be written approximately

$$\frac{-K^2}{4(\alpha - i\Delta\beta)^2}\, e^{2\gamma L} = 1 \qquad \text{(III.4.8)}$$

The phases of this equation give us the phase constants and thus the frequencies of the modes of oscillation (by quantizing $\Delta\beta$), while the absolute value of this equation gives the threshold conditions for the different modes (by solving for α). The distinct values of $(\Delta\beta)_m$ for which oscillations are possible are thus given by:

$$2(\Delta\beta)_m L - \arctan \frac{2\alpha_m(\Delta\beta)_m}{\alpha_m^2 - (\Delta\beta)_m^2} - \frac{1}{2}\,\frac{K^2(\Delta\beta)_m L}{\alpha_m^2 + (\Delta\beta)_m^2} = (2m+1)\pi \qquad \text{(III.4.9)}$$

where m is an integer which denotes the longitudinal mode number.

This equation is not in a closed form because α_m has not been determined yet. However, if we assume that K , $\Delta\beta \ll \alpha$ we immediately get

$$(\Delta\beta)_m = \frac{m\pi + \frac{1}{2}\pi}{L} \qquad \text{(III.4.10)}$$

Using III.3.8 we find that for such a laser, the spacing of the longitudinal modes is approximately the same as the spacing of a regular two-mirror laser of length L . We have

$$\text{Frequency spacing of longitudinal modes} = \frac{c}{2n_2 L} \qquad \text{(III.4.11)}$$

We also find that we do not have a mode for which $\Delta\beta = 0$. This means that the laser will not oscillate with a frequency which is exactly the Bragg frequency. A physical explanation of this effect will be discussed later.

The threshold gain for the m^{th} longitudinal mode can be derived from III.4.8 by taking the absolute value of the equation. It yields

$$\frac{e^{2\alpha_m L}}{\alpha_m^2 + (\Delta\beta)_m^2} = \frac{4}{K^2} \qquad \text{(III.4.12)}$$

The value of the gain can be found either by using the approximate value of $(\Delta\beta)_m$ (III.4.9) or, more accurately, by solving III.4.12 in conjunction with III.4.9 for $(\Delta\beta)_m$ and α_m . The broken lines in Fig. III.6 describes a specific example of a distributed feedback laser of length $L = 1$ mm and $K = 2\ \text{cm}^{-1}$. It shows the required threshold

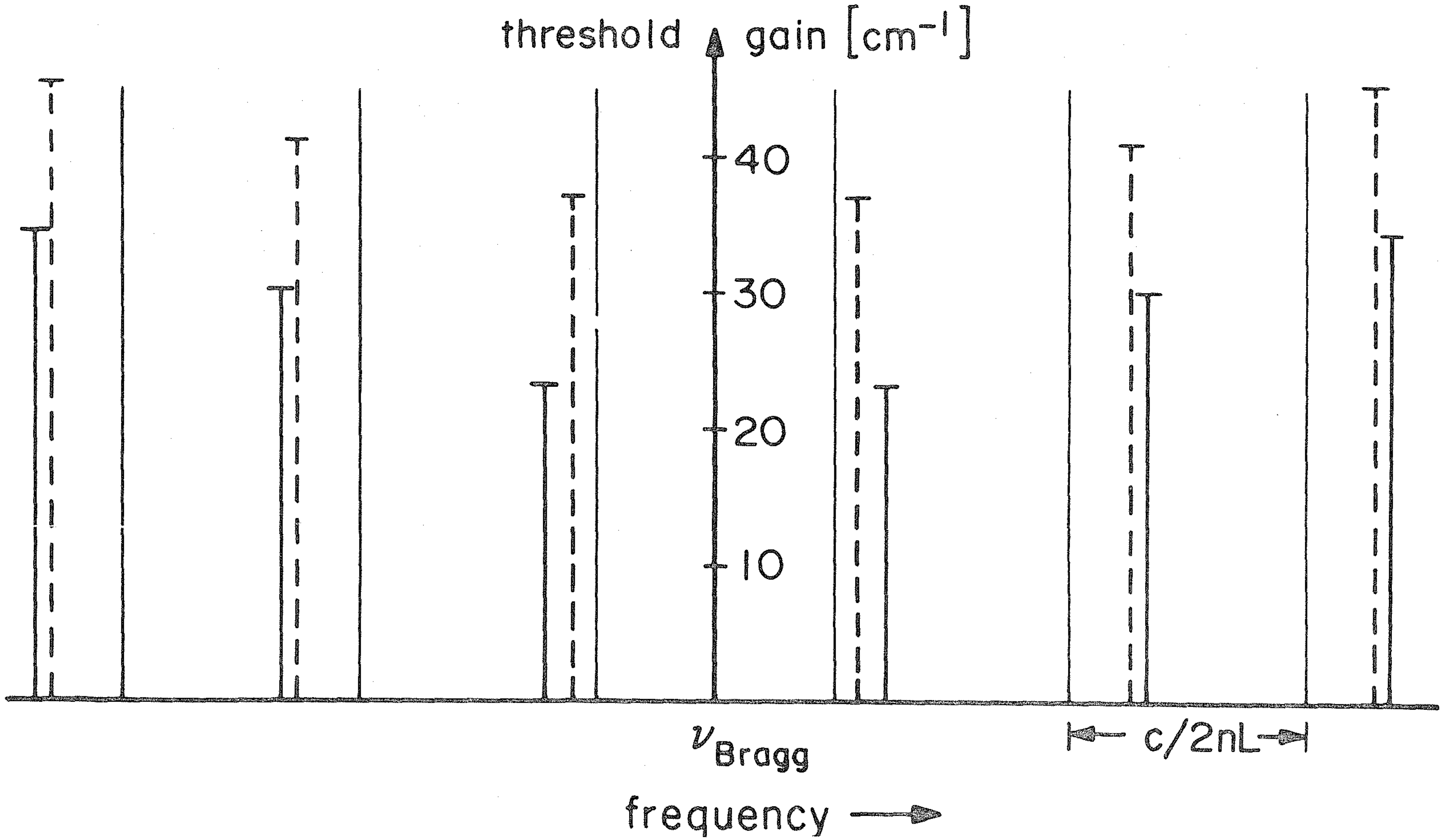

Fig. III.6. Longitudinal mode spectrum and required threshold gain for a distributed feedback laser. Broken lines $K = 2\ cm^{-1}$ $L = 1mm$, solid lines $K = 6\ cm^{-1}$ $L = 1mm$.

gain and the deviation of different longitudinal modes from the Bragg frequency. Since $\Delta\beta$ is not much smaller than α the modes do not coincide with the c/2nL spacings, but are further pushed to the sides. The selectivity of the device is evident from higher threshold gain needed for the higher order modes.

As we have observed, the laser does not have a mode for which $\Delta\beta = 0$. This can be explained in the following manner. We recall that according to III.3.6 the reflected wave from a distributed mirror suffers a phase shift of -90° , when its frequency is exactly $\omega_{Bragg}(\Delta\beta = 0)$. Thus, if we consider as an example a wave propagating to the right, the fraction of it which is reflected backward and then reflected again forward will suffer a total phase shift of -180° . This means that it will interfere destructively with the original wave, and prevent oscillation at that particular frequency.

It is interesting to note that this problem does not exist when the coupling mechanism is provided by periodic gain variation. According to III.2.22, in this case K is imaginary, giving rise to a zero phase shift, and oscillation exactly at the Bragg frequency is allowed[8]. This mode, for which $\Delta\beta = 0$, would clearly have the lowest threshold gain.

We have noted earlier that a corrugated waveguide has a stopband of frequencies (Fig. III.3b), in which propagation is not allowed. The gap increases with increasing K . When it becomes comparable to the c/2nL spacings, it starts pushing the longitudinal modes to the sides, preventing oscillations inside the stop band. A small amount of pushing is evident in the second example in Fig. III.6. The solid lines describe the modes of a laser with $K = 6\ cm^{-1}$ and $L = 1$ mm . Also evident are the lower threshold gains and the better selectivity of the laser.

III.5 Distributed Feedback Laser in GaAs - Experiment

Fundamental Bragg coupling of a waveguide laser requires a corrugation with a period of $\sim \lambda / 2n_2$ where λ is the free space oscillation wavelength and n_2 the index of refraction of the waveguide. For $n_2 \sim 3.6$ and $\lambda = .82\mu$ the requisite period is $\sim 0.11\mu$.

A technique for the fabrication of such small period gratings in solid substrates was developed. It consists of ion milling a photoresist grating into the substrate, which is GaAs in this case. The grating in the photoresist is formed by exposing it with an interference pattern of two laser beams. In order to achieve the small period grating U.V. laser (HeCd λ = 3250Å) was used and the wavelength was further reduced by sending the beams through a prism ($n \simeq 1.5$) (the prism is attached to the photoresist with index machining oil between them). A scanning electron microscope photograph of a corrugated GaAs crystal is shown in Fig. III.7. The period is 0.115μ . Further details on the fabrication are given in Chapter V.

In this section we shall give a short description of the first observation of a distributed feedback laser in GaAs[5]. The data were obtained by M. Nakamura and H. W. Yen. A more detailed description of the experiment and its analysis will thus be given in H. W. Yen's thesis.

The GaAs dielectric waveguide used in the experiment was

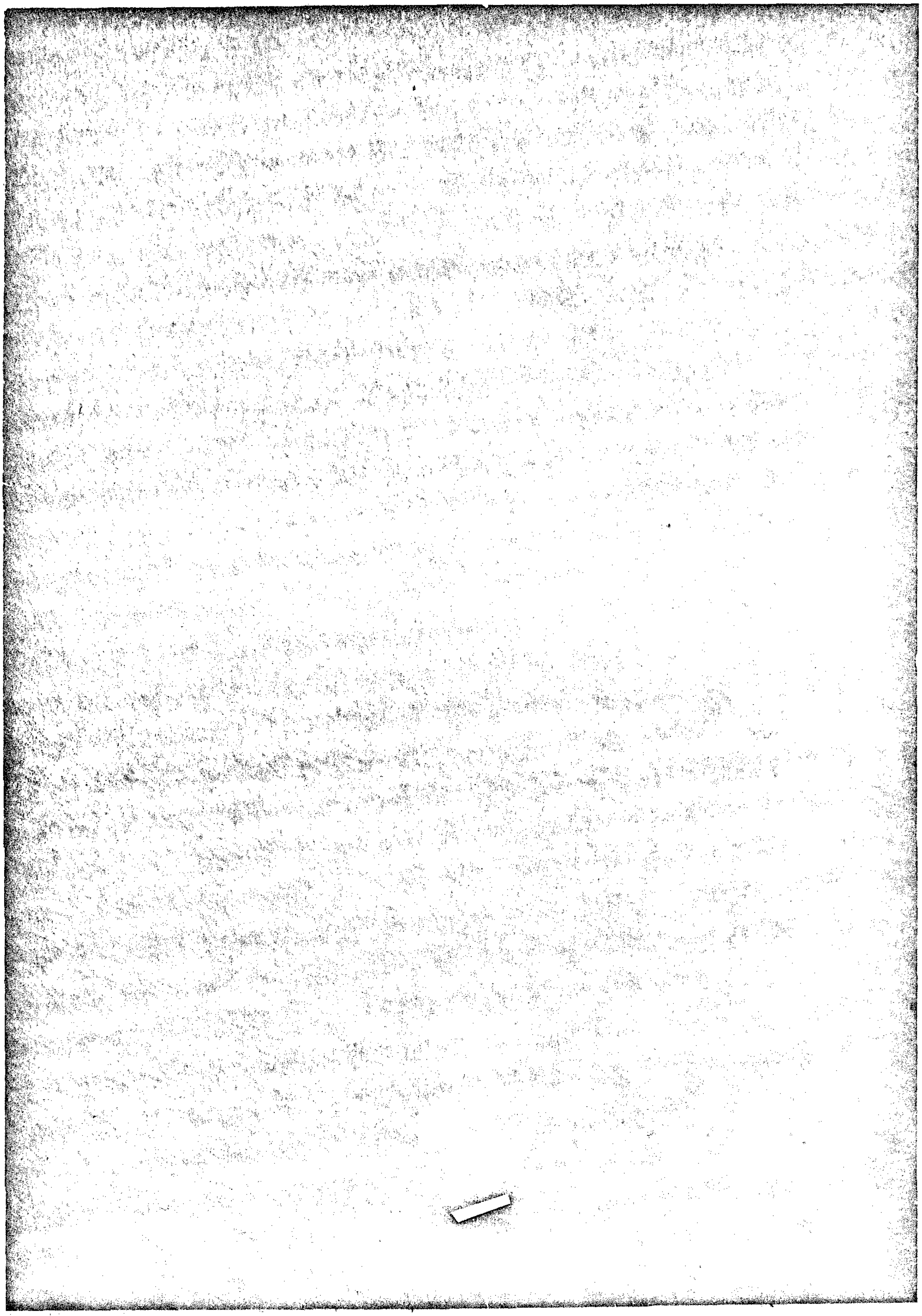

Fig. III.7. A Scanning Electron Micrograph of the surface corrugation on a GaAs crystal. The period is 0.115μ produced by growing an undoped $Ga_{1-x}Al_xAs$ $(x \sim 0.3)$ and a GaAs double layer on a GaAs substrate. The thickness of the guiding GaAs layer was 2μ. The samples were pumped optically at $77°K$ using a pulsed dye-laser (Rhodamine B) tuned to $\lambda_p = 6300Å$. The individual pumping pulses had a duration of 7×10^{-9} sec and a peak power of $\sim 2kW$. Cylindrical lenses were used to pump a rectangular strip 0.33mm wide and of a variable length, as shown in Fig. III.8. The output beam of the laser emerged through a side surface and was guided into a spectrometer.

A spectrum of the laser output is shown in Fig. III.9. The pumping intensity was 1.1 times the threshold intensity I_{th} and the length of the pumped region was 150μ.

The width of the oscillation spectrum of Fig. II.9 is less than 1Å and is within the resolution of the spectrometer. It corresponds to a single longitudinal mode oscillation. By increasing the pumping intensity and the length of the pumped region, multi-longitudinal-mode oscillation was observed as shown in Fig. III.10. The length of the pumped region was 700μ, and the pumping intensity was $1.4\ I_{th}$.

The existence of only one longitudinal mode in Fig. III.9 rather than the two symmetrical lowest order longitudinal modes about 5Å apart, predicted by the theory (Fig. III.6) for a corrugated structure, may indicate that there exists some sort of periodic gain variation in the sample, which contributes to the distributed feedback. In addition the fact that close to the center of the spectrum in Fig. III.10, the modes' spacings are smaller than at the edges of the spectrum

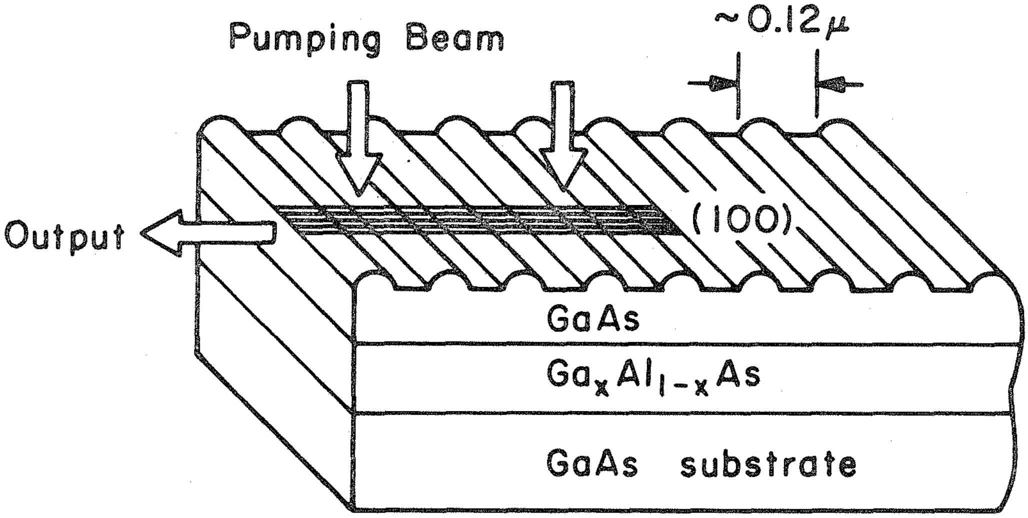

Fig. III.8. Illustration of the laser crystal and the configuration used.

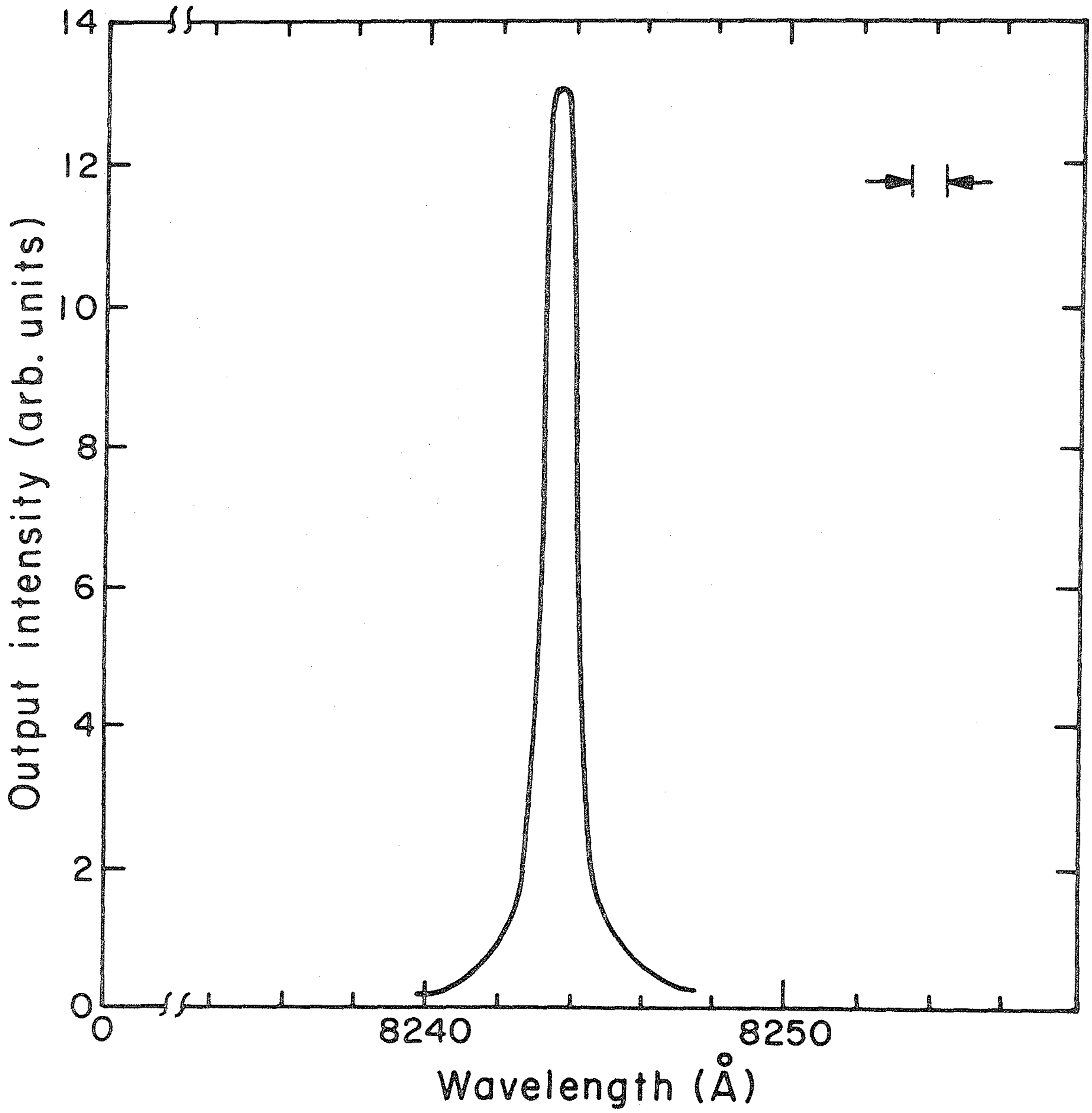

Fig. III.9. The oscillation spectrum of a GaAs waveguide laser. The length of the pumped region was 150μ and $I/I_{th} = 1.1$ (after Ref. 5).

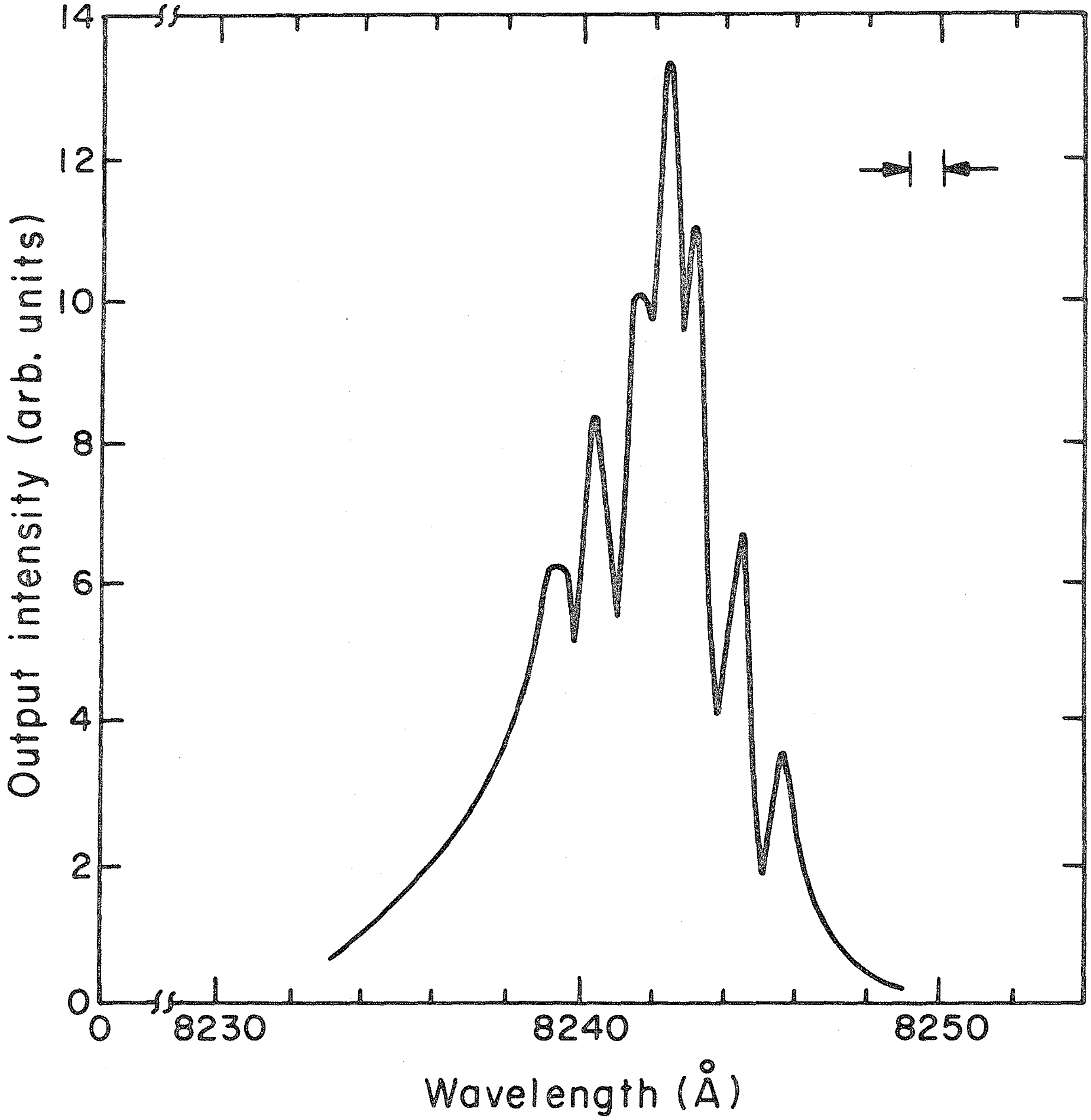

Fig. III.10. The emission spectrum of laser oscillation. The length of the pumped region was 700μ . $I/I_{th} = 1.4$ (after Ref. 5).

supports the above assumption.

As discussed in the previous section the spacings between the modes are quite similar to those of a regular laser of length L . For a regular laser, because of index dispersion, the longitudinal mode spacing $\Delta\lambda$ is given by

$$\Delta\lambda \approx \frac{\lambda^2}{2(n - \lambda \frac{dn}{d\lambda}) L} \qquad (III.5.1)$$

where λ is the vacuum oscillation wavelength, n is the guide's index of refraction, and L the length of the pumped region. If we take $n - \lambda \frac{dn}{d\lambda} = 4.5$, a value obtained from a Fabry-Perot laser using a similar waveguide, we obtain $\Delta\lambda \sim 1$Å . This agrees with the spacing in Fig. III.10.

As we have seen earlier, in a distributed feedback laser the wavelength of the oscillation is determined by the period of the mechanical corrugation

$$\lambda = 2n_2\Lambda \qquad (III.5.2)$$

where Λ is the period of the corrugation and we have assumed $(t \gg \lambda / n_2)$.

By varying Λ it is possible to tune the frequency of oscillation. A number of waveguides were thus prepared with a different corrugation period. The measured oscillation wavelength λ of the samples is plotted as a function of the period in Fig. III.11. The tuning range shown is about 45Å . The mechanical period in this experiment is three times larger than the one required by III.5.1 and the Bragg

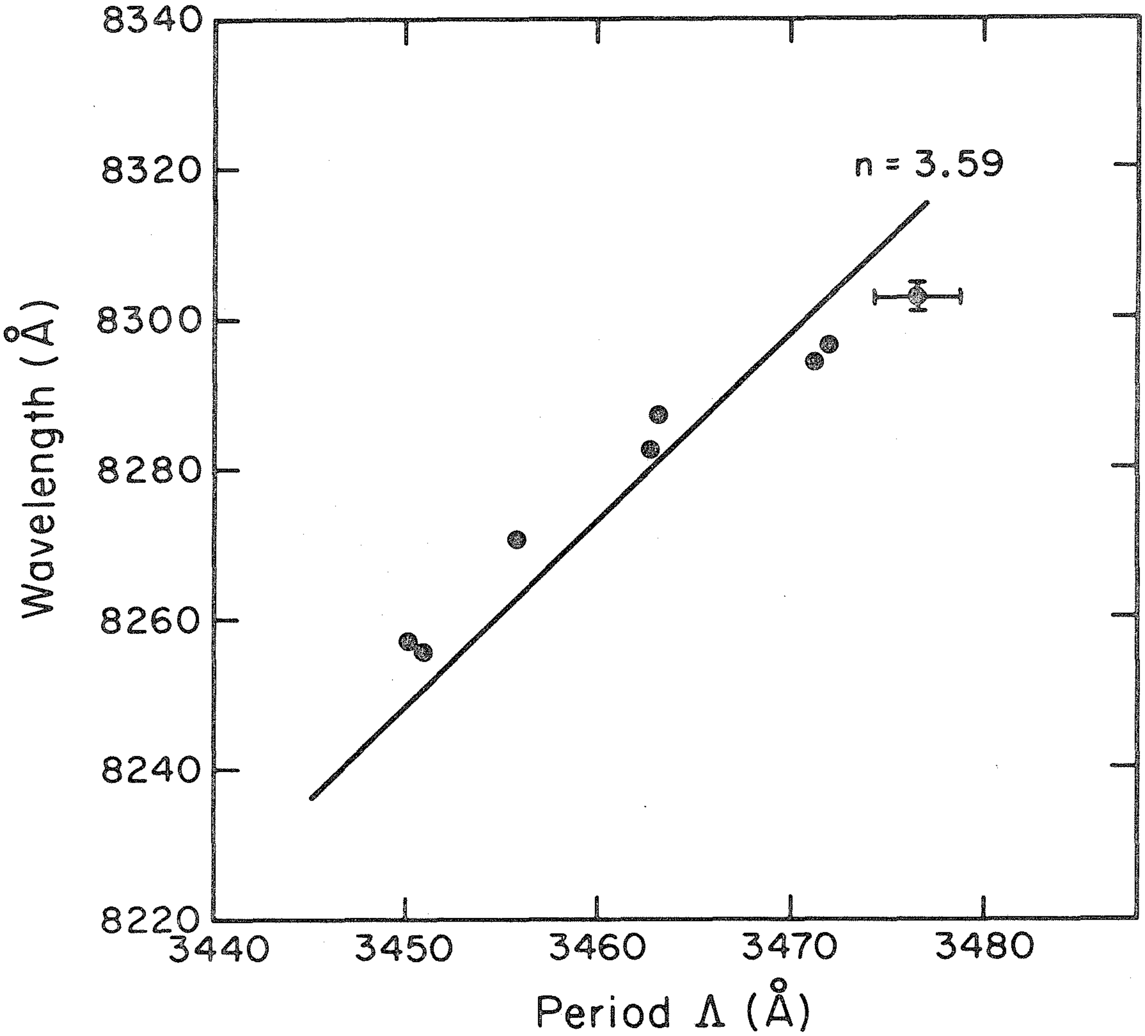

Fig. III.11. Oscillation wavelength as a function of corrugation period. The third order component of the corrugation is the Bragg reflector (after Ref. 5).

reflection is provided by the third order Fourier component of corrugation. Fig. III.11 indicates that the laser feedback is indeed caused by the corrugations and that their use leads to a stabilization of the output wavelength.

III.6 The Merits of Distributed Feedback Semiconductor Lasers

The previous section describes the operation of an optically pumped GaAs distributed feedback laser. It is evident now that the fabrication of such a laser is much more difficult than that of the conventional one (which uses two cleave faces as mirrors). Furthermore, it seems as if the fabrication of a distributed feedback injection laser would be considerably more complicated.

The heterostructure GaAs lasers, which combine low threshold current at room temperature[9] with relatively long life time[10], are multilayer structures. The propagating mode is confined to the inner layers and does not reach the surface. It is thus quite difficult to perturb the mode by corrugating the surface, and another mean would have to be found. Corrugating one of the inner layers by performing the epitaxial growth of the layers in two separate steps is a possibility. However this solution may tamper with the not so well understood life time problem of these lasers.

Because of the above reasons I would like to conclude this chapter by discussing the advantages of the distributed feedback lasers.

The first advantage is the capability to predetermine the wavelength around which the laser will oscillate. As we have discussed earlier the laser wavelength, λ , is given approximately by:

$$\lambda \approx 2\, n_2\, \Lambda \tag{III.5.1}$$

where Λ is the corrugation period and n_2 is the guide's index of refraction. It is thus possible to vary the laser wavelength by varying the corrugation period.

The second advantage is the discrimination of the distributed feedback mechanism between different longitudinal modes. Figure III.6 describes mode spectrum and required threshold gain for a corrugated distributed feedback laser. There are two symmetrical longitudinal modes with the lowest threshold gain. The differences in the required gain between the modes is a function of the parameters of the laser and can be enhanced. In a laser where the distributed feedback is supplied by gain variation the discrimination is even better, because there is only one mode with the lowest threshold gain.

The limited number of longitudinal modes of the laser is important for optical communications via optical fibers. The dispersion which exists in these fibers tends to limit the information rate capabilities when the bandwidth of the radiation is not narrow enough. In a waveguide laser the width of its radiation depends in addition to the number of longitudinal modes on the number of lateral modes. Let us therefore, devote our attention to these modes and their control.

The lateral modes of a rectangular waveguide were discussed in Chapter II. As an example Figure III.12a describes the (0,0) (1,0) and (2,1) modes of a rectangular laser (the mode's notation (m,n) is such that m+1 and n+1 denote the number of field extrema in the x direction and the y direction respectively). The thickness (t) of the guide is usually 1μ or less, while the width (w) is a few tens of microns or more. This means that the phase constant in the y direction is much larger than the one in the x direction. In the following we shall see how this large phase constant discriminates between an (m,0) and an (m,n>0) modes. Later on we shall describe a method that discriminates between a (0,0) and an (m>0,0) modes. This will allow the operation of a distributed feedback laser that combines narrow bandwidth with lowest order transverse mode operation.

In a rectangular guide the propagation vector is given by the vectorial sum of the phase constants in the three orthogonal directions x,y,z . The phase constant in the z direction is β , while $\pm h_x$ and $\pm h_y$ are the phase constants in the x and y directions. The absolute value of the $\vec{k}$ vector in the guide is thus given by

$$|\vec{k}| = (\beta^2 + h_x^2 + h_y^2)^{\frac{1}{2}} \qquad \text{(III.6.1)}$$

The vacuum wavelength of the laser radiation λ , therefore is

$$\lambda = \frac{2\pi n_2}{(\beta^2 + h_x^2 + h_y^2)^{\frac{1}{2}}} \qquad \text{(III.6.2)}$$

where n_2 is the guide's index.

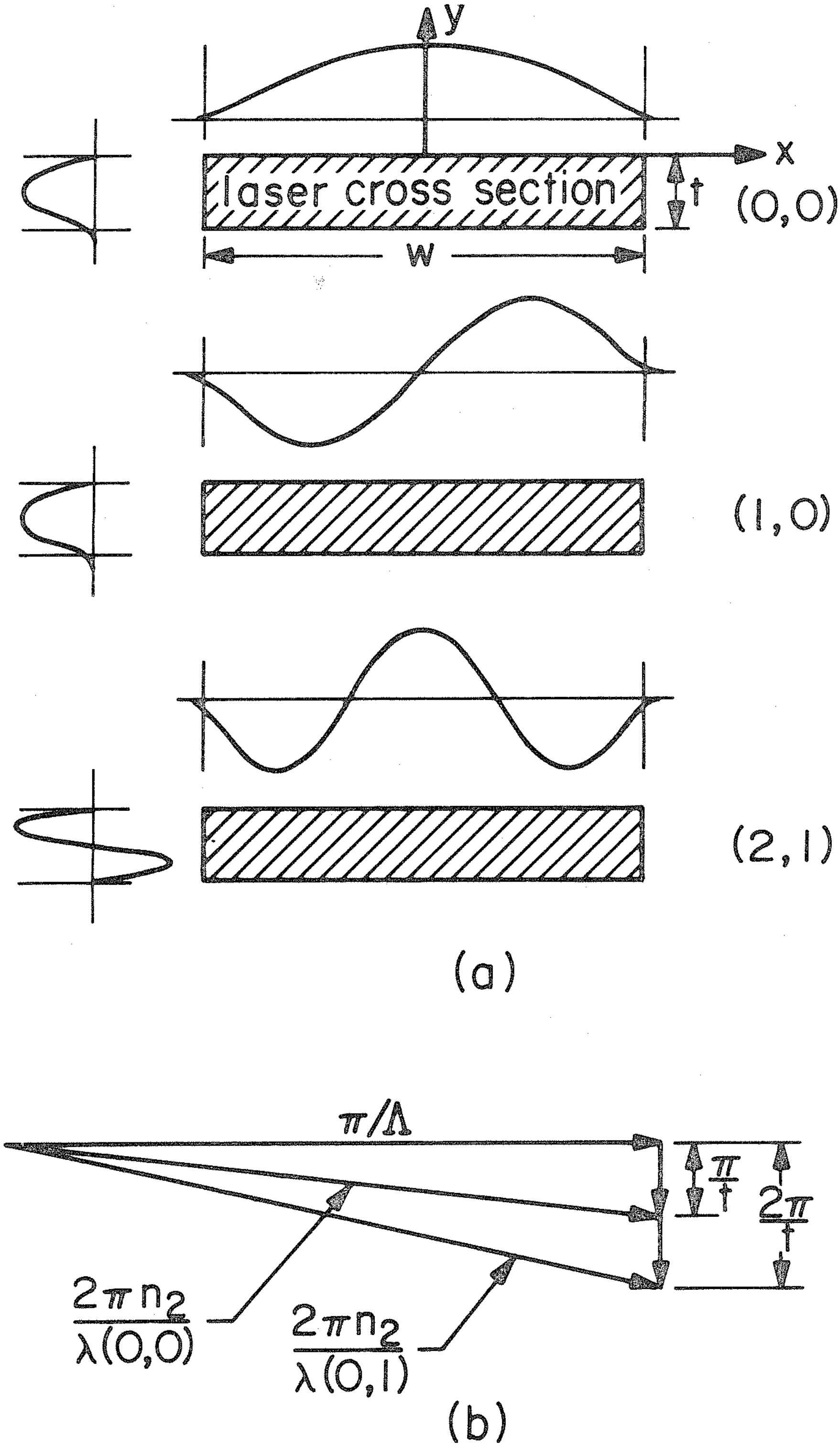

Fig. III.12. (a) Different transverse modes in a rectangular cross section laser.
(b) $\vec{k}$ vector diagram in a distributed feedback laser of thickness t .

As was discussed in the previous sections, in a distributed feedback laser the phase constant in the z direction of the oscillating modes, is determined by the corrugation period. The β's of the lowest threshold modes are given approximately by:

$$\beta \approx \frac{\pi}{\Lambda} \qquad \text{(III.6.3)}$$

As we have noted above since $t \ll w$

$$h_y \gg h_x \qquad \text{(III.6.4)}$$

and we can ignore h_x in III.6.2 and take m as being 0 .

Using III.6.3, III.6.4 and III.6.2 we can express the vacuum wavelength as a function of the mode number $(0,n)$.

$$\lambda_{(0,n)} = \frac{2\pi n_2}{\left[\left(\frac{\pi}{\Lambda}\right)^2 + (h_y)_n^2\right]^{\frac{1}{2}}} \qquad \text{(III.6.5)}$$

$(h_y)_n$ is phase constant in the y direction for a particular mode number, which for well confined modes is given by

$$(h_y)_n = \frac{(n+1)\pi}{t} \qquad \text{(III.6.6)}$$

Substituting III.6.6 in III.6.5 immediately yields the different oscillation wavelength of the different thickness transverse modes in a distributed feedback laser.

$$\lambda_{(0,n)} = \frac{2\pi n_2}{\left[\left(\frac{\pi}{\Lambda}\right)^2 + \frac{(n+1)^2\pi^2}{t^2}\right]^{\frac{1}{2}}} \qquad \text{(III.6.7)}$$

As an example we consider two transverse modes (0,0) and (0,1) . The $\vec{k}$ vectors diagram for that particular case is shown in Fig. III.12b. The expressions for $\lambda(0,0)$ and $\lambda(0,1)$ are given by III.6.7 as

$$\lambda_{(0,0)} = \frac{2\pi n_2}{\left[\left(\frac{\pi}{\Lambda}\right)^2 + \frac{\pi^2}{t^2}\right]^{\frac{1}{2}}} \qquad \lambda_{(0,1)} = \frac{2\pi n_2}{\left[\left(\frac{\pi}{\Lambda}\right)^2 + \frac{4\pi^2}{t^2}\right]^{\frac{1}{2}}} \qquad \text{(III.6.8)}$$

Using typical values such as $\Lambda = 0.115\mu$, $t = 1\mu$ and $n_2 = 3.6$ we find

$$\Delta\lambda = \lambda_{(0,0)} - \lambda_{(0,1)} = 8226 - 8070\text{Å} = 156\text{Å}$$

This separation between the two modes is larger than half the width of the fluorescence spectrum in GaAs! If Λ is chosen properly so that $\lambda_{(0,0)}$ corresponds to the center of gain curve, $\lambda_{(0,1)}$ will automatically be placed outside the gain curve and the (0,1) mode will not oscillate.

It is important to realize that the effect described above is due to the fact, that in a distributed feedback laser the phase constant of the longitudinal mode is clamped to a value of $\frac{\pi}{\Lambda}$. In a conventional laser, on the other hand, β can take different values and thus allow oscillation of the (0,1) mode[11].

The wavelength separation between two different width transverse modes is not large (because $w \gg t$) , and therefore does not allow discrimination in the fashion described above. However the wavelength separation is enough to widen the bandwidth of the laser and should be avoided. In addition the existence of high order transverse modes affects the far field radiation pattern of the laser by causing the beam to diverge strongly. We shall use another property of the distributed feedback laser to show how it is possible to increase the threshold gain required for higher order width transverse modes.

Let us consider again equation III.2.11, which expresses the value of the coupling coefficient in terms of an overlap integral between the propagating mode and the perturbation in the dielectric constant.

$$K\, e^{-i\eta z} = \frac{\omega}{4} \iint_{-\infty}^{\infty} \Delta\varepsilon(x,y,z)\mathcal{E}^2_{(m,0)}(x,y)dxdy \qquad \text{(III.2.11)}$$

The surface corrugation thus perturbs the propagating mode the most where it overlaps the peak of the mode's power profile. Figure III.13a describes the power profile of well confined (0,0) , (1,0) and (2,0) modes. As can be seen, in the (0,0) case most of the power propagates close to the center of the laser's width, while in the higher order modes a smaller fraction of the power propagates close to the center. For a high mode number the power distribution tends to be uniform over the whole width.

A corrugation extending only over a central portion, say 1/3 of the laser width, would be felt mainly by the (0,0) mode because of its unique power distribution. This will cause the (0,0) mode to

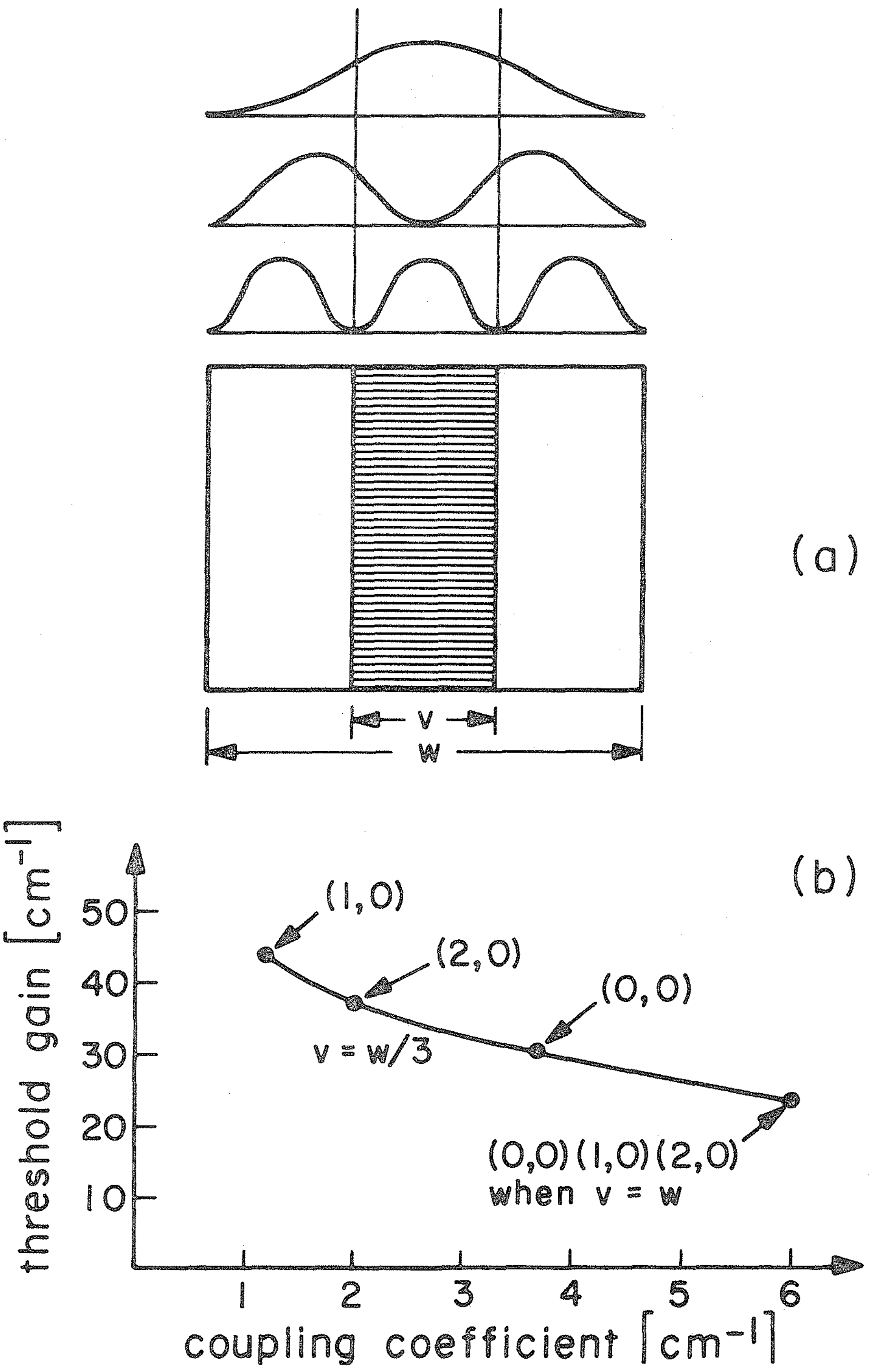

Fig. III.13. (a) Power profile distribution for different width-transverse modes.

(b) Diagram of the coupling coefficient and threshold gain for the above modes for $v = w$ and $v = w/3$.

have a higher K and thus a lower threshold gain than the rest of the modes. A complete transverse mode control will thus be achieved.

Let us calculate now the degree of discrimination between the modes. We first note that the mode profile in the x direction for well confined modes is given by

$$\mathcal{E}_{(0,m)}(x) = \left(\frac{2}{w}\right)^{\frac{1}{2}} \cos \frac{(m+1)\pi}{w} x \qquad \text{for even } m$$

$$\mathcal{E}_{(0,m)}(x) = \left(\frac{2}{w}\right)^{\frac{1}{2}} \sin \frac{(m+1)\pi}{w} x \qquad \text{for odd } m \qquad \text{(III.6.9)}$$

where w is the width of the guide and $\left(\frac{2}{w}\right)^{\frac{1}{2}}$ is a normalization factor. We can express now the coupling coefficient for the different modes in terms of K and an overlap integral in the x direction. K is the coupling coefficient for the case where the corrugation extends all over the guide and is given by III.2.16. We can thus write

$$K_{(m,0)} = K \int_{-v/2}^{v/2} \cos^2 \left[\frac{(m+1)\pi}{w} x\right] dx \qquad \text{for even } m$$

$$K_{(m,0)} = K \int_{-v/2}^{v/2} \sin^2 \left[\frac{(m+1)\pi}{w} x\right] dx \qquad \text{for odd } m \qquad \text{(III.6.10)}$$

According to III.6.10 one finds that for $v = \frac{1}{3} w$

$$K_{(0,0)} = 0.6K, \quad K_{(1,0)} = 0.2K, \quad K_{(2,0)} = 0.33K \qquad \text{(III.6.11)}$$

Considering the same example discussed in section 4 (Fig. III.6) with $K = 6\ cm^{-1}$ and $L = 1mm$, we can calculate now the threshold gains for the lowest order longitudinal mode but with the different lateral modes. The results are shown in Fig. 13b and indicate quite an effective discrimination between the transverse modes.

The last advantage of a distributed feedback laser which should be mentioned is its compatibility with the concept of integrated optical circuits. The conventional GaAs laser is cleaved on both ends. The high index of refraction of GaAs provided enough reflection at the interface to sustain oscillations. It is difficult, however, to incorporate this method into the fabrication of an optical circuit. One possibility is the replacement of the cleave with a sharp step in the guide's thickness, which will provide enough reflection for the oscillation. Such a step was fabricated by ion milling and is shown in Fig. III.14. The distributed feedback laser on the other hand has no discrete mirrors at all and therefore is highly compatible with optical circuits.

Figure III.15a describes a configuration in which a large optical cavity GaAs laser (LOC)[12] is incorporated into a guiding structure. The guiding layer is the $Al_yGa_{1-y}As$ while the active layer is the upper GaAs layer. (For this purpose we must require that $x > y$ and that the GaAs layer be too thin to support a guided mode of its own.) The gain is provided in this case by the optical pumping while the feedback is supplied by the corrugation. To avoid absorption by the GaAs layer outside the laser area, it is removed from there by

Top

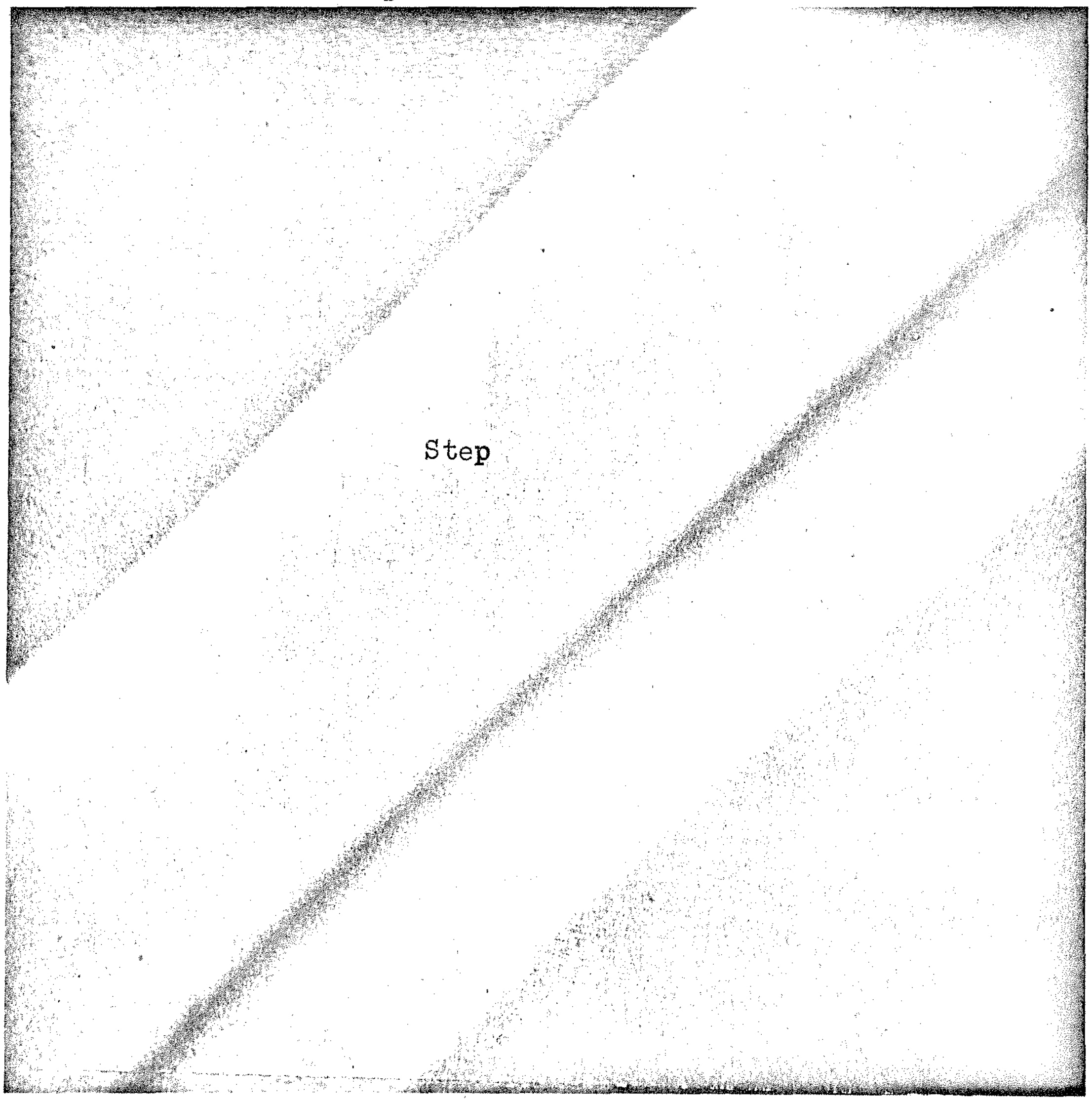

Bottom

Fig. III.14. A scanning electron micrograph of a 3μ deep step ion milled in GaAs.

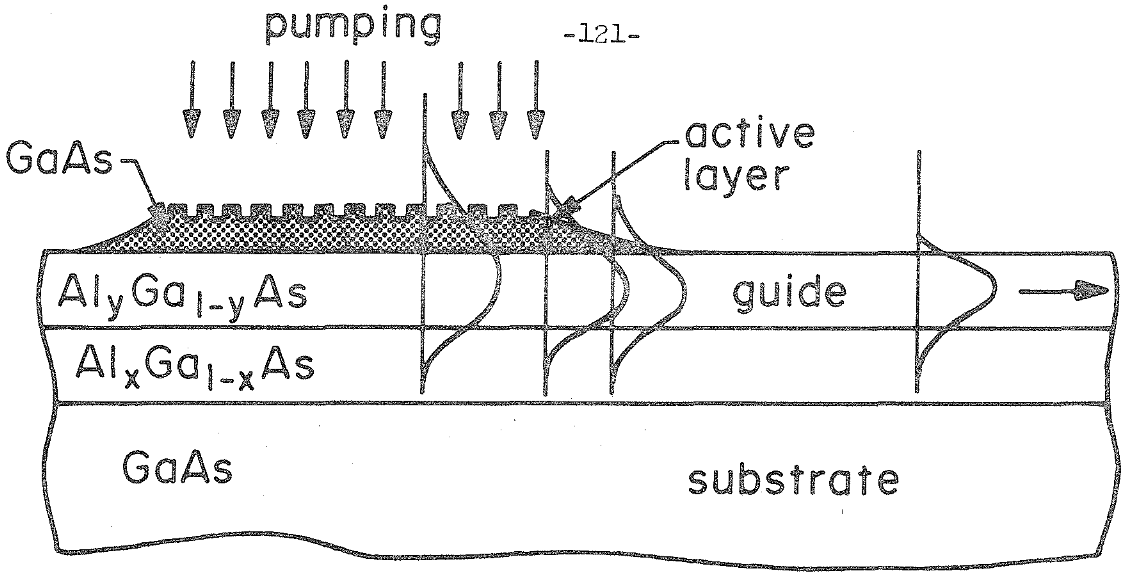

(a)

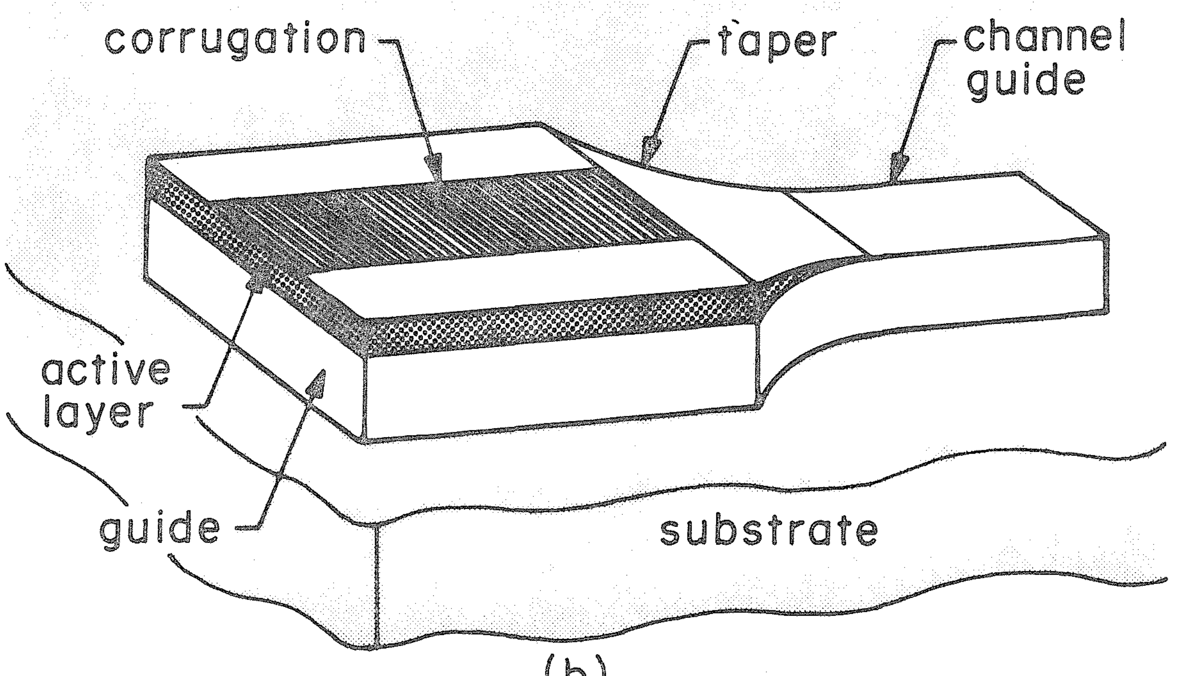

(b)

Fig. III.15. (a) A configuration for a distributed feedback large optical cavity GaAs laser.

(b) The above configuration with a tapered width for matching the elliptical output beam to a square channel guide.

gradually tapering its thickness to zero. As opposed to the sharp step discussed above and shown in Fig. III.14, in a taper the mode gradually adapts itself to the variation in the thickness and does not suffer severe reflection or loss[13] (provided that the final thickness guide can support that mode).

Ion milling, which is described in detail in Chapter V, can also be used to taper the width of the laser and thus turn the elliptical output beam into a more round one. This is shown in Fig. III.15b. The laser is a distributed feedback LOC laser. The corrugation extends over the central portion only for transverse mode control. The width of the laser as well as the active layer are tapered to fit the cross section of a square channel guide. Such a configuration can incorporate a single or two longitudinal modes together with a round lowest order transverse mode operation.

It can thus be concluded that the advantages of the GaAs distributed feedback laser encourage an attempt to implement it in an injection laser configuration.

References for Chapter III

1. D. Marcuse, "Mode Conversion Caused by Surface Imperfections of a Dielectric Slab Waveguide," Bell System Technical Journal 48 3187 (1969).

2. M. L. Dakss, L. Kuhn, P. F. Heidrich and B. A. Scott, "Grating Coupler for Efficient Excitation of Optical Guided Waves in Thin Films," Appl. Phys. Lett. 16, 523 (1970).

3. K. Ogawa, W. S. C. Chang, B. L. Sopori, and F. J. Rosenbaum, "A Theoretical Analysis of Etched Grating Couplers for Integrated Optics," IEEE J. of Quantum Electronics, 9, 29 (1973).

4. H. Kogelnik and C. V. Shank, "Stimulated Emission in a Periodic Structure," Appl. Phys. Lett. 18, 152 (1971). Also, C. V. Shank, J. E. Bjorkholm and H. Kogelnik, "Tunable Distributed Feedback Dye Laser," Appl. Phys. Lett. 18, 395 (1971). Also, D. P. Schinke, R. G. Smith, E. G. Spencer and M. F. Galvin, "Thin-Film Distributed Feedback Laser Fabricated by Ion Milling," Appl. Phys. Lett. 21 494 (1972).

5. M. Nakamura, A. Yariv, H. W. Yen, S. Somekh and H. L. Garvin, "Optically Pumped GaAs Surface Laser with Corrugation Feedback," Appl. Phys. Lett. 22, 515 (1973). Also, M. Nakamura, H. W. Yen, A. Yariv, E. Garmire, S. Somekh and H. L. Garvin, "Laser Oscillation in Epitaxial GaAs Waveguides with Corrugation Feedback," to be published in Appl. Phys. Lett. Also, H. W. Yen, M. Nakamura, E. Garmire, S. Somekh, A. Yariv, and H. L. Garvin, "Optically Pumped GaAs Waveguide Lasers with a Fundamental 0.12μ Corrugation

Feedback," to be published in Optics Communications.

6. C. Kittel, Introduction to Solid State Physics, John Wiley and Sons, Inc., 4th ed., Chapter 9.

7. I. P. Kaminow, H. P. Weber and E. A. Chandross, "A Poly (Methyl Methacrylate) Dye Laser with Internal Diffraction Grating Resonator," Appl. Phys. Lett. 18, 497 (1971).

8. H. Kogelnik and C. V. Shank, "Coupled-Wave Theory of Distributed Feedback Lasers," J. Appl. Phys. 43, 2327 (1972).

9. M. B. Panish, H. C. Casey, Jr., S. Sumski, and P. W. Foy, "Reduction of Threshold Current Density in GaAs-$Al_xGa_{1-x}As$ Heterostructure Laser by Separate Optical and Carrier Confinement," Appl. Phys. Lett. 22, 590 (1973).

10. B. C. DeLoach, "Reliability of GaAs Injection Lasers," presented at the Conference on Laser Engineering and Applications, Washington, D. C., May 30-June 1, 1973.

11. T. L. Paoli, J. E. Ripper, T. H. Zachos, "Resonant Modes of GaAs Junction Lasers, II: High-Injection Levels," IEEE J.Q.E, QE-5, 271 (1969).

12. H. F. Lockwood, H. Kressel, H. S. Sommers, Jr., and F. Z. Hawrylo, "An Efficient Large Optical Cavity Injection Laser," Appl. Phys. Lett. 17, 499 (1970).

13. D. Marcuse, "Radiation Losses of Tapered Dielectric Slab Waveguides," Bell Systems Technical Journal, 49, 273 (1970).

IV. NONLINEAR OPTICAL INTERACTIONS IN PERIODIC THIN FILMS

IV.1 Introduction

Optically isotropic materials have, to date, not been used in nonlinear optical applications because the conventional technique of birefringent phase matching[1] cannot be applied. This has, so far, precluded the use of many highly nonlinear materials, such as GaAs, from practical utilization in second-harmonic generation, parametric oscillation, and frequency upconversion.

One approach to phase matching in optically isotropic materials involves the use of dimensional dispersion in thin-film waveguides[2]. Another suggestion[3,4,5] utilizes periodically laminated structures. The realization of this last approach involves a fractional wavelength control of the lamination period and has not yet been demonstrated. In this chapter we wish to discuss two new approaches to phase matching which involve a periodic corrugation of the surface of the thin-film waveguide, or a periodic modulation of the nonlinear optical properties of the propagation medium. The latter approach is capable, in principle, of yielding effective nonlinear coefficients approaching the bulk value while affecting little the propagation characteristics of the propagating modes. Techniques for implementing both ideas in a thin dielectric waveguide are also described.

IV.2 Theory

Let us consider, for the sake of simplicity, a second harmonic generation in the dielectric waveguide shown in Fig. IV.1. The electric field of the n^{th} TE guided mode, as an example, is given by the following expression:

$$E_n^{\omega}(x,z,t) = A_n^{\omega}\mathcal{E}_n^{\omega}(x)\ e^{i(\omega t - \beta_n^{\omega} z)} \qquad \text{(IV.2.1)}$$

The propagation phase constant β_n^{ω} as well as the lateral mode profile $\mathcal{E}_n^{\omega}(x)$ are determined by the frequency ω, the mode number n ($n+1$ is the number of extrema), the guide index $n_2(\omega)$, the substrate index $n_3(\omega)$ and the guide thickness t. The mode profile $\mathcal{E}_n^{\omega}(x)$ is normalized to carry one unit of power per unit length in the y direction, so that the power carried by the field is:

$$P_n^{\omega} = |A_n^{\omega}|^2 W \qquad \text{(IV.2.2)}$$

where W is the width of the waveguide in the y direction. β_n^{ω} varies between its value for the bulk guide material and that of the substrate

$$n_3(\omega)k_0 < \beta_n^{\omega} < n_2(\omega)\ k_0 \qquad \text{(IV.2.3)}$$

where $k_0 \equiv 2\pi/\lambda_0$ is the free space wave number. For large t and small mode number β_n^{ω} approaches the upper limit, while the lower limit is approached by reducing the thickness t or choosing a higher number mode. The electric field of the second harmonic m^{th} mode is given similarly:

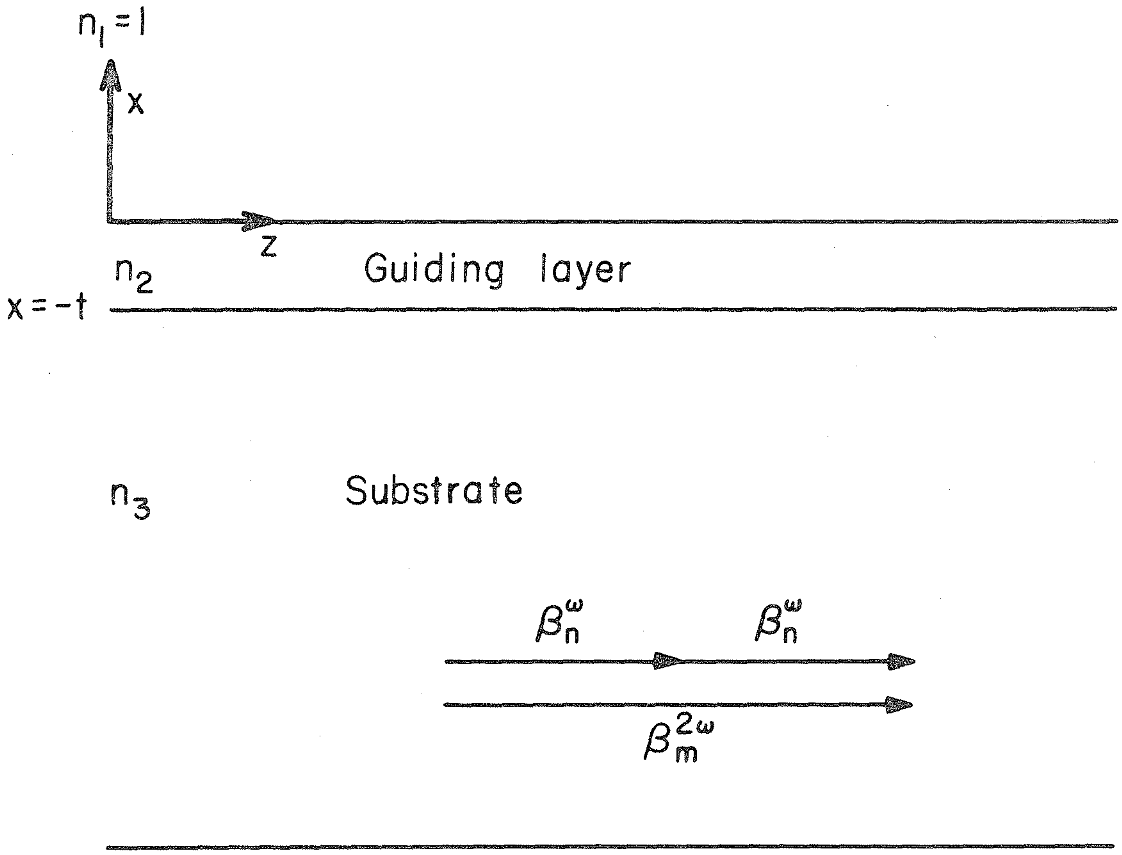

Fig. IV.1 The basic configuration of a dielectric waveguide and the required phase matching condition for second harmonic generation.

$$E_m^{2\omega}(x,z,t) = A_m^{2\omega}\mathcal{E}_m^{2\omega}(x)\ e^{i(2\omega t\ -\ \beta_m^{2\omega}z)} \qquad \text{(IV.2.4)}$$

and the value for $\beta_m^{2\omega}$ is confined between the two limits

$$n_3(2\omega)\ 2k_0 < \beta_m^{2\omega} < n_2(2\omega)2k_0 \qquad \text{(IV.2.5)}$$

The second harmonic polarization generated by the fundamental $E_n^{\omega}(x,z,t)$ is taken as

$$P^{2\omega}(x,z,t) = d_{NL}(x)(A_n^{\omega})^2[\mathcal{E}_0(x)]^2 e^{i(2\omega t-2\beta_n^{\omega}z)} \qquad \text{(IV.2.6)}$$

where $d_{NL}(x)$ is the appropriate bulk nonlinear tensor element. This polarization drives the second harmonic radiation, thus the power generation per unit volume in the m^{th} second harmonic mode at a given point is given by the same expression II.4.6 used in Chapter II:

$$\frac{dP_m^{2\omega}}{dv} = -\ \overline{E_m^{2\omega}\ \frac{\partial P^{2\omega}}{\partial t}} \qquad \text{(IV.2.7)}$$

where the horizontal bar denotes time averaging. Performing the time averaging and integrating over x and y yields the rate of power growth in the m^{th} second harmonic mode:

$$\frac{dP_m^{2\omega}}{dz} = \omega W\ \mathrm{Im} \int_{-\infty}^{\infty} E_m^{2\omega}(P^{2\omega})^* dx \qquad \text{(IV.2.8)}$$

Substituting IV.2.4 and IV.2.6 in IV.2.8 yields

$$\frac{dP_m^{2\omega}(z)}{dz} = \omega W \ \mathrm{Im} \left\{ (A_n^{\omega})^2 A_m^{2\omega}(z) \ e^{-i(\beta_m^{2\omega}-2\beta_n^{\omega})z} \int_{-\infty}^{\infty} d_{NL}(x)(\mathcal{E}_n^{\omega}(x))^2 \mathcal{E}_m^{2\omega}(x)dx \right\} \tag{IV.2.9}$$

Equation IV.2.9 readily gives the two requirements needed for effective nonlinear interaction (so we shall not switch to the coupled mode formalism in this case). The first requirement is the well known phase matching condition which arises from the need to eliminate the oscillating exponential term in the differential equation IV.2.9. The condition is:

$$\Delta\beta \equiv \beta_m^{2\omega} - 2\beta_n^{\omega} = 0 \tag{IV.2.10}$$

The second requirement for a high rate of second harmonic power growth is a large value for the overlap integral of the fundamental intensity mode profile and the second harmonic field profile in equation IV.2.9.

$$\int_{-\infty}^{\infty} d_{NL}(x)(\mathcal{E}_n^{\omega}(x))^2 \mathcal{E}_m^{2\omega}(x) \ dx \tag{IV.2.11}$$

Under certain conditions, namely, $n_2(\omega) > n_3(2\omega)$ it is possible to compensate for the normal dispersion of the material and to phase match by choosing the right thickness t and the mode numbers n and m. However, this usually requires accurate control of the thickness[2] and for $n \neq m$ (especially when $m > 1$) involves a large decrease in the magnitude of the overlap integral IV.1.11 thus reducing the effective nonlinear coefficient for the interaction.

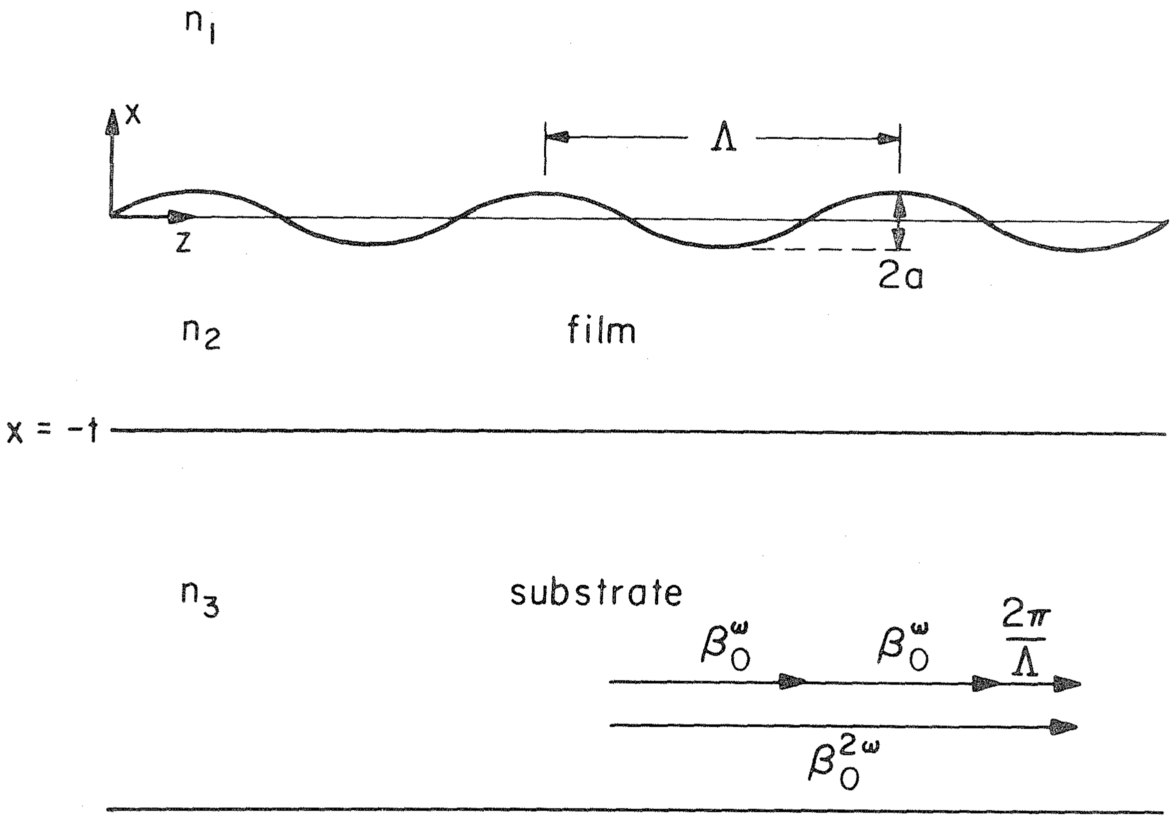

Fig. IV.2 A waveguide with a periodic corrugation of its surface, and the required phase matching condition for second harmonic generation.

To overcome the problem of $\Delta\beta \neq 0$ in a thin film structure, let us consider the waveguide shown in Fig. IV.2[7]. The corrugation on the waveguide's boundary defines a periodic structure with a period of Λ that modifies the propagating modes. The perturbed field has a Floquet form and can be written as

$$E_n^{\omega}(xzt) = A_n e^{i(\omega t - \beta_n^{\omega} z)} \mathcal{E}_n^{\omega}(x) \sum B_{n\ell}^{\omega}(x) e^{-i\ell \frac{2\pi}{\Lambda} z} \qquad \text{(IV.2.12)}$$

The mode, thus, consists of a number of space harmonics, each with its phase constant

$$\beta_{n\ell}^{\omega} = \beta_n^{\omega} + \ell \frac{2\pi}{\Lambda} \qquad \ell = \pm 1 \ \pm 2 \ldots \qquad \text{(IV.2.13)}$$

We assume that the period Λ is large enough so that the space harmonics of the low orders do not couple into the continuum ("leaky") modes[6], and the x dependence of $B_{n\ell}$ can be ignored. Phase matched interactions are thus no longer limited to the principal value of β but can involve the space harmonics. As an example, second-harmonic generation can be achieved by matching the fundamental $(\ell = 0)$ space harmonic at ω to the first $(\ell = \pm 1)$ space harmonic at 2ω, so that

$$\beta_0^{2\omega} = 2\beta_0^{\omega} \pm (2\pi/\Lambda) \qquad \text{(IV.2.14)}$$

The penalty for using the space harmonics is that the conversion efficiency is reduced relative to the phase-matched interaction in the bulk by a factor which in the example just quoted is approximately equal to $|B_{01}^{2\omega}|^2$.

An approximate[7] and a more accurate[8] estimate of the factor for a typical example of second harmonic generation in GaAs at 10.6μ , shows an efficiency reduction around the factor of 20. This quite large reduction in the effective nonlinearity still keeps GaAs comparable to $LiNbO_3$, one of the best phase-matchable materials. However, one would like to take a greater advantage of the high nonlinear coefficient of a material such as GaAs. Let us therefore consider the following method of phase matching in thin films.

IV.3 Phase Matching by Periodic Modulation of the Nonlinear Optical Properties

We consider now the waveguide shown in Fig. IV.3. The nonlinear coefficient of the guiding layer is modulated periodically with a period Λ , while the index of refraction is assumed to remain unchanged. To analyze the new situation we note that the nonlinear coefficient d_{NL} in IV.2.9 is now a function of z as well as of x . We limit ourselves to the case where the fundamental and the second harmonic are well confined zero order modes. This makes it possible to neglect the x dependence of d_{NL} so that IV.2.9 can be written as

$$\frac{dP_0^{2\omega}(z)}{dz} = \omega W \ \mathrm{Im} \left\{ (A_0^{\omega})^2 A_0^{2\omega}(z) \left[\int_0^t (\mathcal{E}_0^{\omega}(x))^2 \mathcal{E}_0^{2\omega}(x) dx \right] e^{i\Delta\beta z} d_{NL}(z) \right\} \quad \text{(IV.3.1)}$$

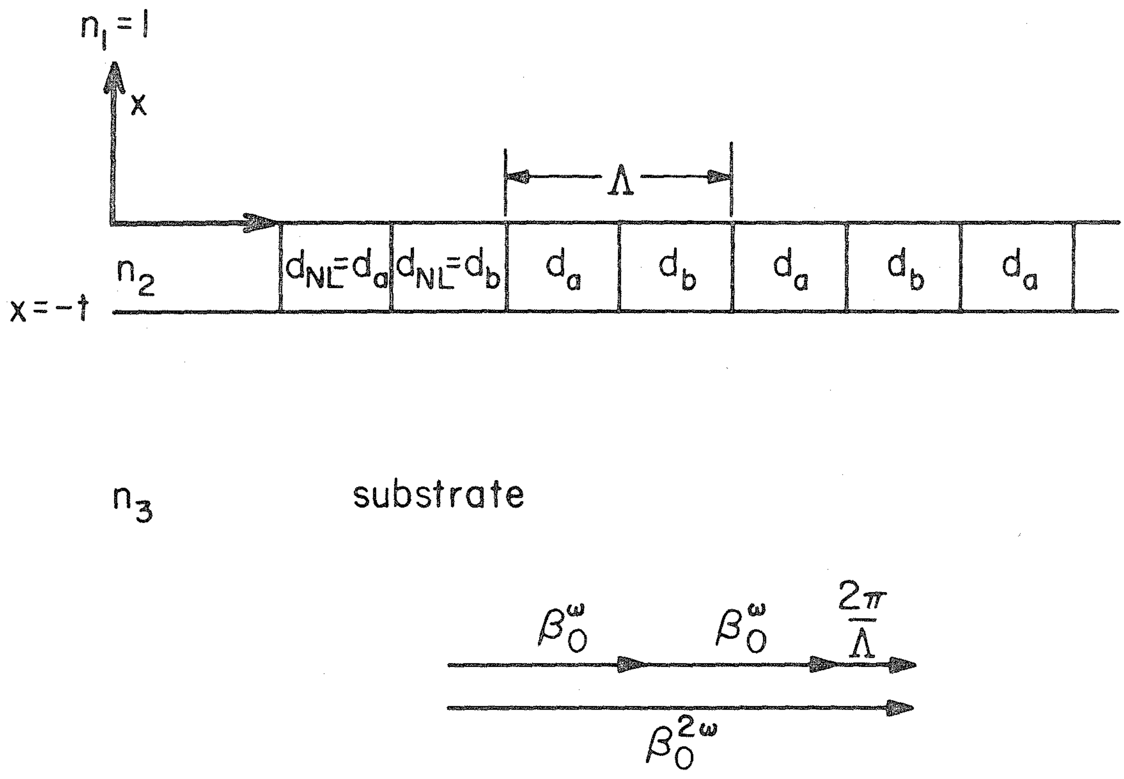

Fig. IV.3 A waveguide with a periodic modulation of the nonlinear coefficient d_{NL}, and the required phase matching condition for second harmonic generation.

If the spatial modulation period Λ is chosen equal to

$$\frac{2\pi}{\Lambda} = \Delta\beta \tag{IV.3.2}$$

the fundamental component in the Fourier expansion of $d_{NL}(z)$ will provide a term with an exponential dependence of $e^{-i\Delta\beta z}$. This term, by multiplying the $e^{i\Delta\beta z}$ in IV.3.1 gives rise to a synchronous contribution that allows the cumulative buildup of the second harmonic power. The amplitude of this particular term in the expansion of $d_{NL}(z)$ determines the effectiveness of the interaction. To be specific, consider an example with

$$d_a = d_{NL} \quad , \quad d_b = 0 \tag{IV.3.3}$$

where d_{NL} is the original nonlinear coefficient of the guiding layer, and where the period Λ is chosen so that IV.3.2 is satisfied. The Fourier expansion of this rectangular form nonlinear coefficient is:

$$d_{NL}(z) = \frac{d_{NL}}{2} + \sum_{m \text{ odd}} \frac{2\, d_{NL}}{m\pi} \sin \frac{2\pi m}{\Lambda} z \tag{IV.3.4}$$

Using IV.3.4 and IV.3.2 in IV.3.1 and keeping the synchronous term only leads to

$$\frac{dP_0^{2\omega}}{dz} = \omega W(A_0^{\omega})A_0^{2\omega}(z) \left[\int_0^t (\mathcal{E}_0^{\omega}(x))^2 \mathcal{E}_0^{2\omega}(x)dx \right] \frac{d_{NL}}{\pi} \tag{IV.3.5}$$

The mode overlap integral reaches an optimum value when the modes are well confined. It approaches the value

$$\int_0^t (\mathcal{E}_0^{\omega}(x))^2 \mathcal{E}_0^{2\omega}(x)dx = \frac{(2\omega\mu)^{3/2}}{\beta_0^{\omega}(\beta_0^{2\omega})^{\frac{1}{2}}\ t^{\frac{1}{2}}} \tag{IV.3.6}$$

Using IV.2.2 to express A_0^{ω} and $A_0^{2\omega}$ in terms of the respective mode powers, IV.3.5 becomes

$$\frac{dP_0^{2\omega}(z)}{dz} = \frac{\sqrt{8}\omega^{5/2}\mu^{3/2}P_0^{\omega}}{\beta_0^{\omega}(\beta_0^{2\omega})^{\frac{1}{2}}(Wt)^{\frac{1}{2}}}\ \frac{d_{NL}}{\pi}\left(P_0^{2\omega}(z)\right)^{\frac{1}{2}} \tag{IV.3.7}$$

A solution of IV.3.6 where β_0^{ω} and $\beta_0^{2\omega}$ are assumed to be equal to the bulk propagation constants gives in the nondepleted pump approximation:

$$\frac{P_0^{2\omega}(\ell)}{P_0^{\omega}} = \frac{2\ \omega^2\ d_{eff}^2\ \ell^2}{(n_2(\omega))^2 n_2(2\omega)}\left(\frac{\mu_0}{\varepsilon_0}\right)^{3/2}\ \frac{P_0^{\omega}}{(Wt)} \tag{IV.3.8}$$

This result is of a form identical to the bulk interaction[9] except that here the effective nonlinear coefficient is

$$d_{eff} = \frac{d_{NL}}{\pi} \tag{IV.3.9}$$

The conversion efficiency from ω to 2ω is seen to be proportional to the mode power density $P_0^{\omega}/(Wt)$. Since W and t can be made comparable to λ this power density can become very large even for small power input. The penalty for modulating d_{NL} in order to phase match is a reduction of the effective nonlinear coefficient by a factor of $\frac{1}{\pi}$.

A physical picture of the way in which the spatial modulation of d_{NL} overcomes the problem of phase matching is the following: When $\Delta\beta \neq 0$ the generated second harmonic wave and the second harmonic polarization wave driving it drift gradually (with distance) apart in phase. When $\Delta\beta z = \pi$ the accumulated phase shift is $\pi/2$ and power begins to flow back from the second harmonic to the fundamental. This happens after one coherence length $\ell_c \equiv \frac{\pi}{\Delta\beta}$. By having d_{NL} equal to zero between $z = \ell_c$ and $z = 2\ell_c$ the reversal of power flow is prevented. By $z = 2\ell_c$ the accumulated phase shift has returned to the favorable region $(-\frac{\pi}{2} < \phi < \frac{\pi}{2})$ and the nonlinear interaction is "turned on" $(d_{NL} \neq 0)$ again*. The reduced value of d_{eff} as given by IV.3.9 reflects the fact that not all the physical length of the structure partakes in the interaction.

IV.4 Implementation of the Phase Matching Methods

The implementation of first method which uses surface corrugation for phase matching is relatively simple. It is possible to use the same fabrication technique which was developed for the fabrication

---

*It is clear from this picture that a reversal of the sign of d_{NL} in the second half of each period will lead to a doubling in the value of d_{eff}.

of the distributed feedback laser, and which is described in detail in Chapter V.

The implementation of the modulation of the nonlinear coefficient method is more difficult but seems possible, since the guiding layer extends only a few microns below the surface and therefore is readily accessible. One approach is to use ion-milling to fabricate a series of grooves normal to the propagation direction in a single crystal thin film guide and then sputter-fill the grooves with a polycrystalline form of the film material (for which $d_{NL} = 0$) or with some other material with a similar index of refraction.

Another approach is to try and deposit a thin film that will have the above property. For example we have sputtered GaAs on the (100) face of a hot (370°C) GaAs substrate and found the film to be in a crystalline form. On the other hand when GaAs is sputtered on SiO_2 it has a $\langle 111 \rangle$ preferred orientation[10]. This raises the possibility of achieving the appropriate structure, by sputtering GaAs on a GaAs (or $Al_xG_{1-x}As$ which has a lower index) substrate which is covered periodically with very thin stripes of SiO_2.

Experiments in both approaches are presently carried on. The availability of such techniques plus the fast evolving technology of GaAlAs epitaxy should make possible the development of tunable optical parametric oscillators, upconverters, and second-harmonic generators using thin films.

References for Chapter IV

1. J. A. Giordmaine, "Mixing of Light Waves in Crystals," Phys. Rev. Lett. 8, 19 (1972). Also, P. D. Maker, R. W. Terhune, M. Nisenoff, and C. M. Savage, "Effects of Dispersion and Focusing on the Production of Optical Harmonics," Phys. Rev. Lett. 8, 21 (1962).
2. D. B. Anderson and J. T. Boyd, "Wideband CO_2 Laser Second Harmonic Generation Phase Matched in GaAs Thin Film Waveguides." Appl. Phys. Lett. 19, 266 (1971). Also, P. K. Tien, "Light Waves in Thin Films and Integrated Optics," Appl. Optics 10, 2395 (1971).
3. A. Ashkin and A. Yariv, Bell Telephone Laboratories Technical Memorandum, November 13, 1961.
4. N. Bloembergen and A. J. Sievers, "Nonlinear Optical Properties of Periodic Laminar Structures," Appl. Phys. Lett. 17, 493 (1970).
5. C. L. Tang and P. P. Bey, "Phase Matching in Second Harmonic Generation Using Artificial Periodic Structures," IEEE Journal of Quantum Electronics QE-9, 9 (1973).
6. D. Marcuse, "Mode Conversion Caused by Surface Imperfections of a Dielectric Slab Waveguide," Bell System Tech. Journal, 48, 3187 (1969). Also, D. Marcuse, "Higher-Order Scattering Losses in Dielectric Waveguides," Bell System Tech. Journal 51, 1801 (1972).
7. S. Somekh and A. Yariv, "Phase-Matchable Nonlinear Optical Interactions in Periodic Thin Films," Appl. Phys. Lett. 21, 140 (1972).
8. A. Gover and A. Yariv, "Periodically Perturbed Dielectric Waveguides," to be published.

9. A. Yariv, Introduction to Optical Electronics, New York: Holt, Rinehart and Winston, 1971, p.190.

10. B. Molnar, J. J. Flood, and M. H. Francombe, "Fibered and Epitaxial Growth in Sputtered Films of GaAs," Journal of Appl. Phys. 35, 3554 (1964).

V. FABRICATION OF INTEGRATED OPTICS COMPONENTS

V.1 Introduction

All the integrated optics components and devices which we have discussed above demand high quality edge smoothness and high resolution formation in dimensions down to submicron sizes. As an example we recall that for a first order distributed feedback laser in GaAs a corrugation with a period of 0.115μ has to be fabricated on the surface of the GaAs.

These require state of the art performances of the most sophisticated microfabrication methods such as electron beam lithography and ion beam milling (etching or machining). Following the description of these methods we[1] shall detail another method that was developed for the fabrication of very small period corrugations in a solid substrate. This method utilizes holographic exposure of photoresist. The fabrication of channel waveguides (embedded and ridged) as well as directional couplers will be discussed. We shall also include in this chapter a description of the use of holographic exposure and ion milling in the fabrication of excellent wire grid polarizers for infrared radiation.

Since in all of these fabrications ion milling was used, we devote the next section to the description of this process.

V.2 Ion Beam Milling*

The sputtering process provides a convenient method for thin film deposition and removal which can be applied to a wide variety of materials. The term sputtering refers to the ejection of atoms from a target surface by bombardment with energetic particles (usually ions with energies in the range of 0.6 to 20 keV). The ejected atoms can be either removed from a target substrate or deposited on an opposing substrate. Plasma sputtering is widely used in the microelectronics industry[(2)] and has also been used in the fabrication of glass wave-guides[(3)]. The plasma is usually created in an inert gas (at 10^{-1} to 10^{-3} Torr) by a dc or rf discharge and the sputtering occurs by ion bombardment from the plasma. Ion beam sputtering is performed by bombarding the target surface with a collimated ion beam in high vacuum. This type of sputtering has proved to be a useful alternative in instances where high vacuum conditions are desired for film deposition, or when control and direction of micromachining is important[(4)].

For fabrication purposes an inert gas ion beam is produced in a duoplasmatron-type ion source (as shown in Fig. V.1), accelerated through a high vacuum chamber and directed (with or without final focusing) to impinge on a target surface. The high energy (typically 3 to 10 keV) impact of the ions causes sputtering ejection of the target material. By means of contact masking or by shadow masking, patterns can be machined (milled) into the surface of the target.

---

*Also referred to as "back sputtering" or "ion beam machining."

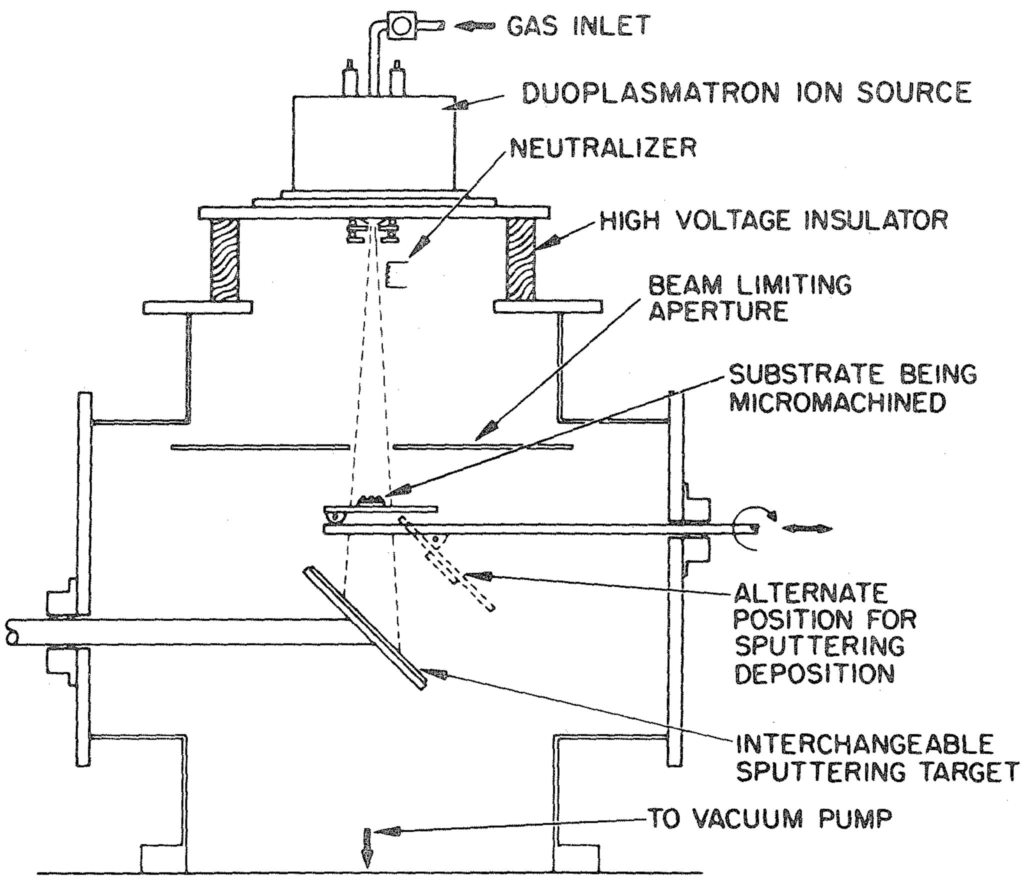

Fig. V.1 Schematic diagram of the duoplasmatron ion beam sputtering system. (after Ref. 1)

The directed beam permits etching of patterns which are more sharply defined than those of chemical etching and, because no material is impervious to the sputtering attack, high resolution patterns can be produced in a broad variety of thin film materials.

A broad ion beam bombarding a target is used to accomplish high vacuum deposition of the sputtered target material onto an opposing substrate. This is illustrated by the alternate substrate position shown in Fig. V.1. Electrons provided by the neutralizing filament are trapped in the potential of the ion beam and are available for continuous neutralization of any positive surface charge which may tend to accumulate. Therefore, dc bombardment suffices for sputtering deposition or removal of either metallic or insulating materials.

Since the back-sputtering rate proceeds uniformly in a given homogenous material, the three-dimensional shape of a contact mask will be fairly well replicated in the substrate if sputtering continues until the mask is just etched away. Some distortion of the cross-sectional detail occurs because the sputtering rate varies with the angle of incidence. Also, the depth of etching into the substrate may differ from the depth of the photoresist removed if the sputtering yields of the two materials differ.

V.3 Periodic Corrugation in Optical Waveguides

Periodic structures in optical waveguides can be made by corrugation of the waveguide surface. As we have discussed, when choosing the right periodicity it is possible to convert power from one mode to another,[5] or couple power between a confined guided mode and an unconfined radiation mode, thus forming a grating coupler(6). Mode conversion from a forward propagating mode to a backward propagating mode forms a distributed mirror. This kind of a mirror may help in extending the lifetime of semiconductor injection lasers in the cases where mirror damage is the dominant failure mode. As was discussed in Chapter III, if the corrugation extends along the length of an amplifying medium a distributed feedback laser results(7). In general, corrugating the surface of an optical thin film waveguide produces space harmonics with phase velocities which depend on the corrugation period. These can be used in interactions which require phase matching such as in nonlinear optics experiments and devices(8).

The periods of the corrugations needed for these applications vary from as low as approximately 0.11μ for a distributed feedback laser in GaAs to tens of microns for the phase matching of $10.6\mu m$ second harmonic generation in GaAs.

We have employed two approaches for fabricating gratings and found them both successful. In the first approach a computer-programmed scanning electron microscope* (SEM) was used to "write" a grating pattern of 0.1μ wide lines with a period of 0.37μ in a masking material of polymethyl methacrylate (PMM). After dissolving away (developing) the material in the exposed (or written) areas, a broad-

---

*We wish to express our appreciation to Dr. E. D. Wolf and W. E. Perkins of the Hughes Research Laboratories for the electron lithography work.

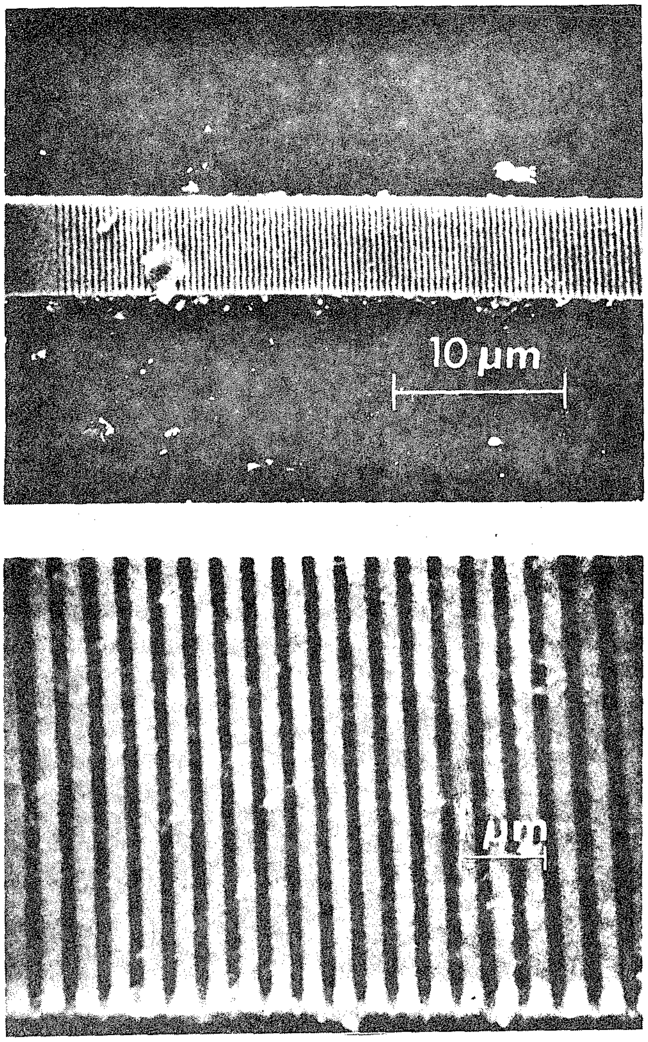

Fig. V.2 Planar phase grating coupler with 1000 Å grooves ion-beam machined into an optical waveguide. Periodicity is 3700 Å. (after Ref. 1) area argon ion beam was used to etch the grooves into the substrate (in this case ZnS) using the PMM as a sputter mask. Figure V.2 shows the resulting grating in a 10μ wide by 2μ thick waveguide of ZnS. The depth of the etching is 500Å .

Since an SEM beam can be focused down to 100Å and that size is compatible with the PMM resolution(9), it is reasonable to assume that the 1100Å period grating (which is needed for the GaAs distributed feedback laser) can be fabricated using this method. The area on which such a grating can be written is limited by the depth of field of the electron beam. This problem can be overcome by mounting the substrate on an interferometer controlled table, and moving it in steps in order to cover a larger area (such tables are available with resolution of about 300Å). However, the SEM writing process is relatively slow and expensive. Thus an alternative approach for the fabrication of periodic structures had to be developed.

In this new approach the grating mask pattern was produced by laser holographic techniques. The surface of the guiding layer was spin-coated with a photosensitive resist material (both KPR or Shipley 1350 resists* were used). Argon laser (λ = 4580Å) beams from a common source were projected onto the resist at an angle, as shown in Fig. V.3a. The interference of these two beams caused exposure with a sinusoidal variation across the surface at a period of

---

*Manufacturers are, respectively, Eastman Kodak Company and Shipley Company, Inc.

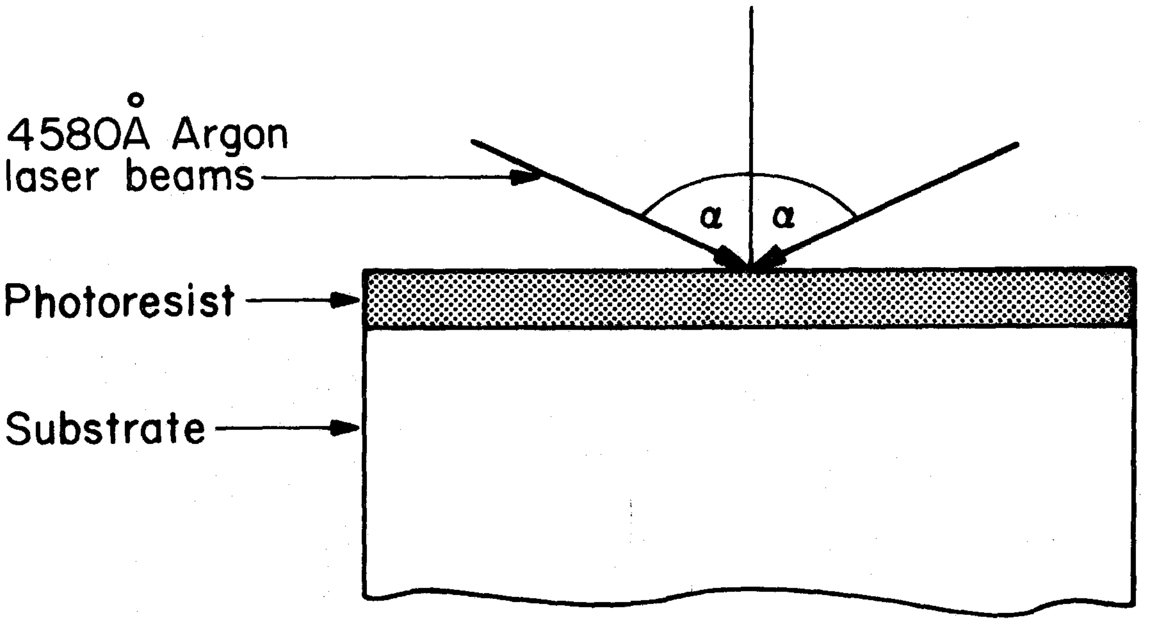

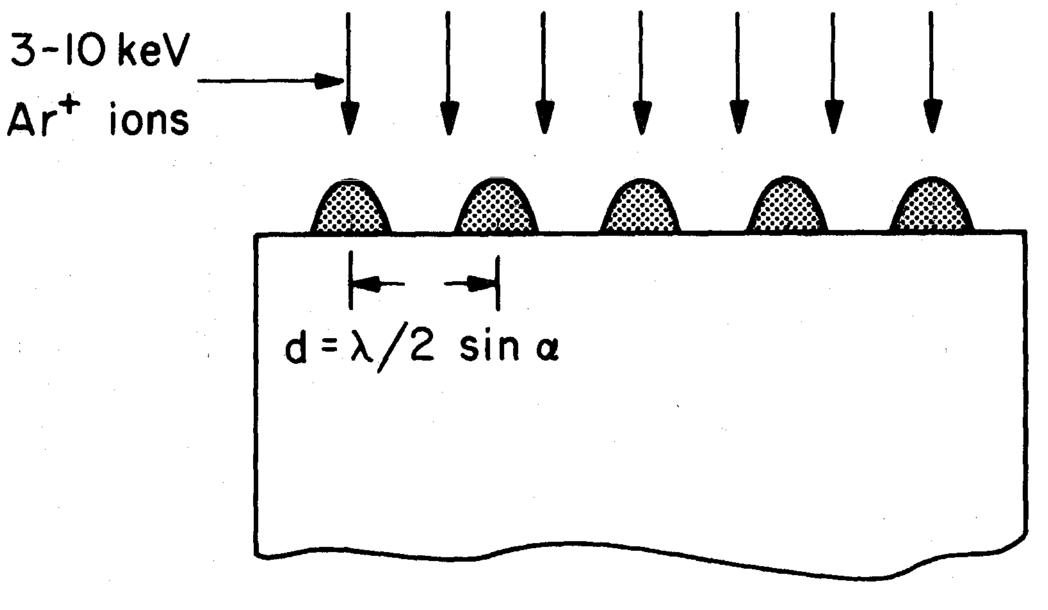

Fig. V.3 (a) Holographic exposure of photoresist.

(b) Ion machining of photoresist after development.

$$d = \frac{\lambda}{2 \sin \alpha} \tag{V.3.1}$$

By adjusting the exposure and development parameters the pattern is left as a partial coverage on the surface of the substrate (Fig. V.3b). Although lower exposure and development leaves the undulating pattern on the surface of the resist layer(10) and, in principle, the material can be ion machined away leaving a replica of the undulations in the substrate surface, this approach is difficult to control if the resist material contains volatile components. This is because the ion beam heats the resist material and gas evolution causes bubbles and blisters which lift the pattern and stretch it to eventual destruction. It is more desirable to develop the pattern as clearly defined and separated stripes which provides for local gas evolution without bubble formation.

We have produced grating patterns with periods of 0.28μ, 0.35μ, 0.41μ, 1.4μ, and 3.0μ using the holographic technique described above. Ion beam machining was then employed to etch these structures into the surface of silicon and GaAs substrates. The 0.41μ pattern was etched to a depth of 0.12μ into the surface of GaAs as can be seen from the SEM cross-section photograph (Fig. V.4). Figures V.5a and b show lower magnification photographs of the $1.4\mu m$ grating. Figure V.6 shows the smallest period grating produced in the configuration shown in Fig. V.3a, 0.28μ. This period was determined by the laser wavelength rather than the photoresist resolution. Equation V.3.1 indicates that the lowest period possible (for $\alpha = 90^\circ$) is $\lambda/2$.

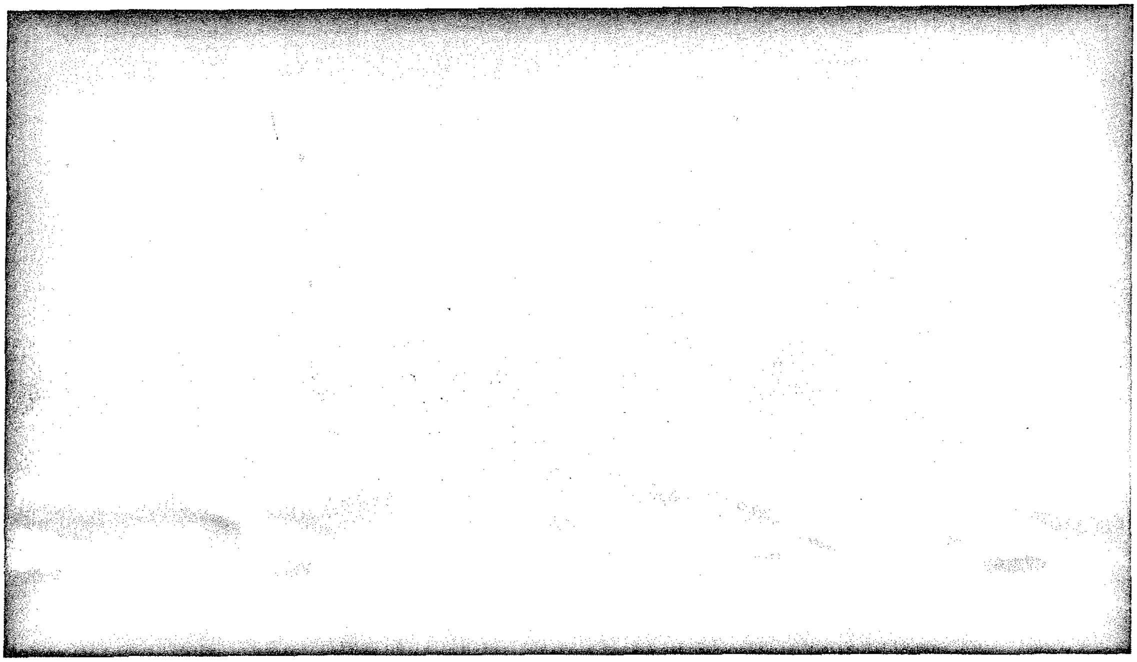

Fig. V.4 Cross section of grating pattern (0.41 μm periodicity) in GaAs. Scanning electron microscope magnification is 75,000 X.

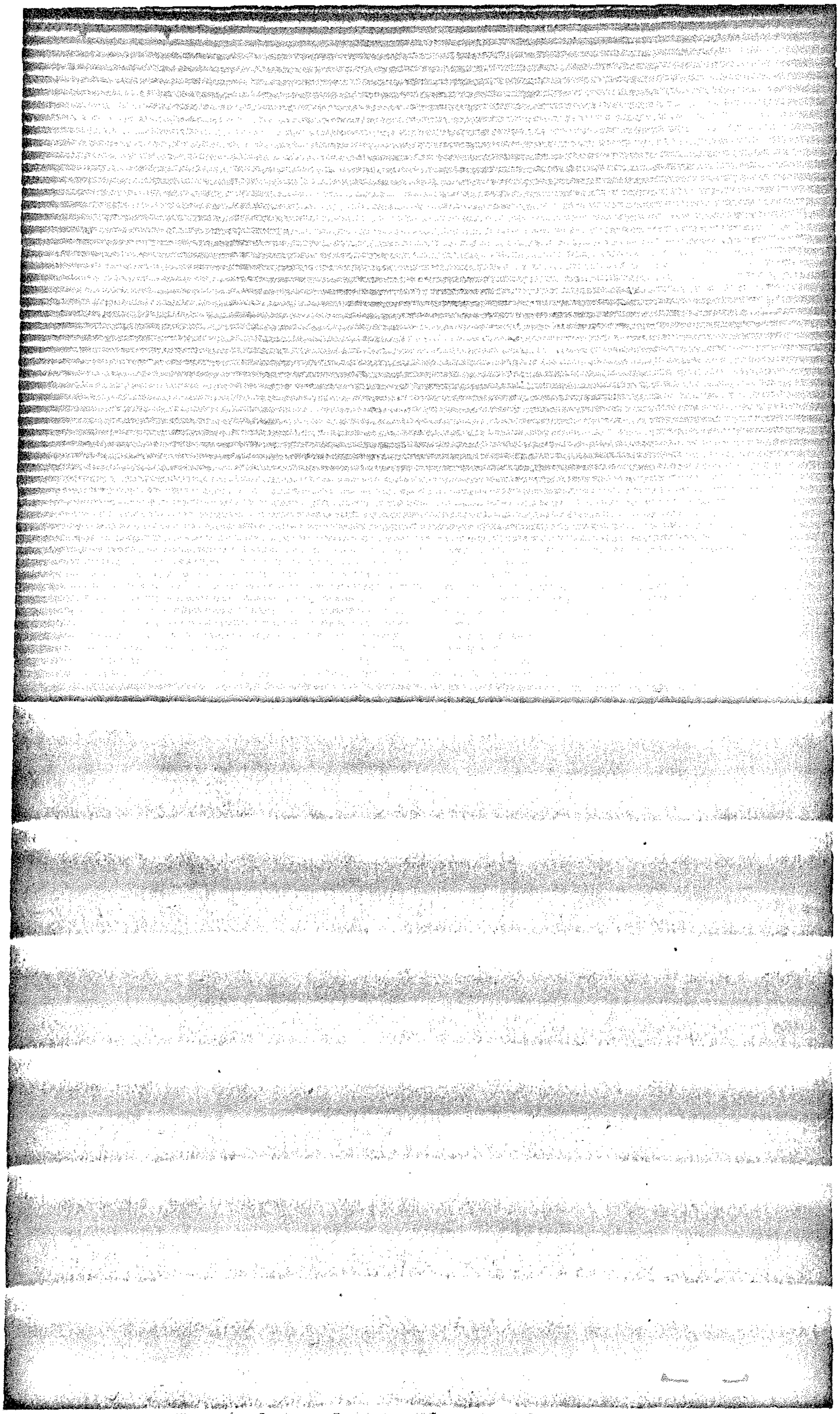

Fig. V.5 SEM photographs of 1.4 μm grating in GaAs.

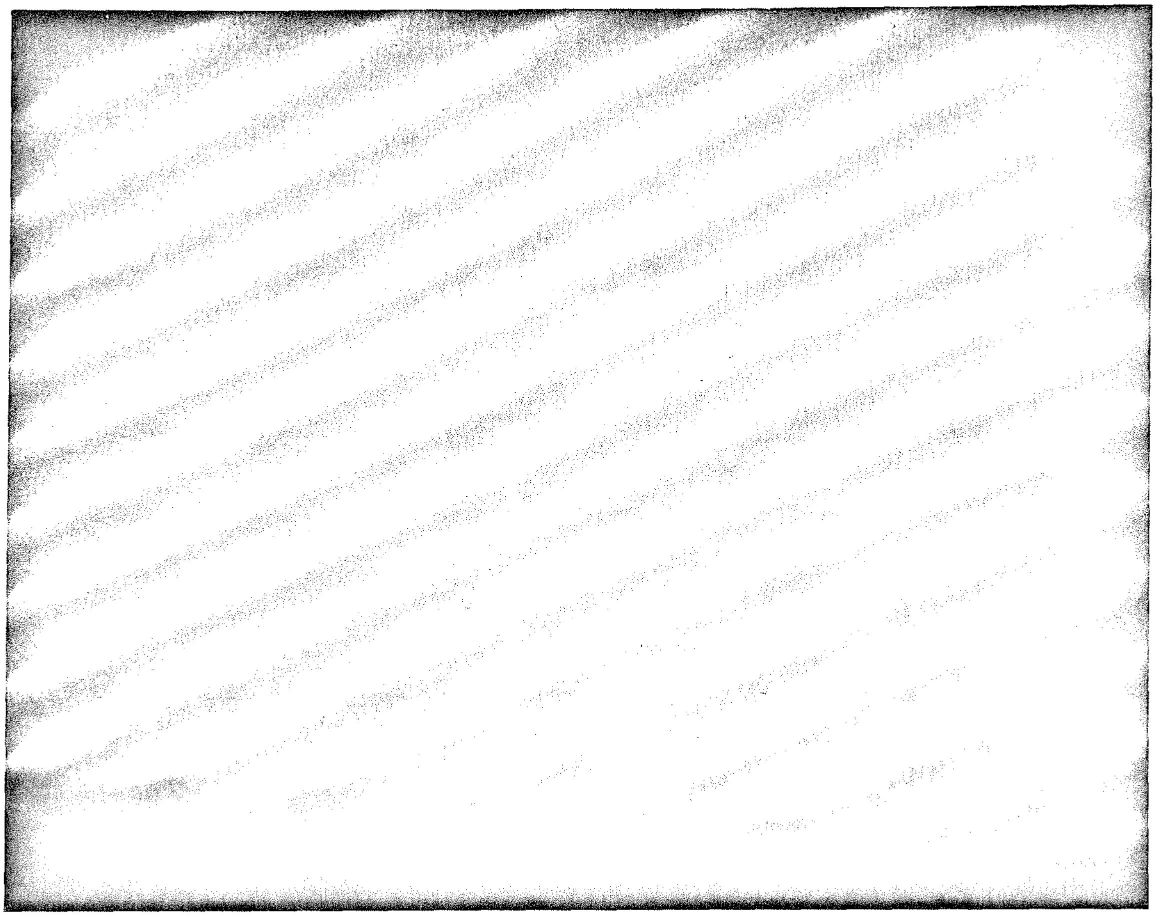

Fig. V.6 SEM photograph of a 0.28μ grating.

The smallest wavelength continuous laser available is an HeCd (λ = 3250Å). Since even this wavelength is not short enough for the fabrication of the 1100Å grating, the light beam had to be sent through a quartz block ($n \approx 1.5$) to further reduce the wavelength. The configuration used is shown in Fig. V.7. HeCd laser beams incident on both sides of the quartz block reach the photo resist by passing through an index matching oil at the bottom of the block. This configuration has enabled us to produce a 1150Å grating which was shown in Fig. III.7. (Special care had to be taken to remove the oil from the photoresist before development by dipping in xylene.)

The exact period of a given grating was measured after the exposure by shining a laser beam on it and calculating the period from the laser wavelength and the diffraction angle. In the case of the 1150Å grating the HeCd beam must be sent again through the quartz in order to obtain a diffracted beam. Thus the index of the quartz entered into the calculation and it had to be measured accurately. This was done by first measuring the period of a grating with a medium size period, using HeCd laser in air. Then the third order diffraction from this 0.3465μ grating was measured by shining the HeCd through the quartz. From these measurements it was possible to derive accurately the index of the quartz block ($n = 1.544$), and with it the shorter periods were determined.

The combination of ion milling and holographic exposure offers also a very successful means for fabricating wire grid polarizers. The wire grid polarizer consists of a pattern of fine gold lines spaced

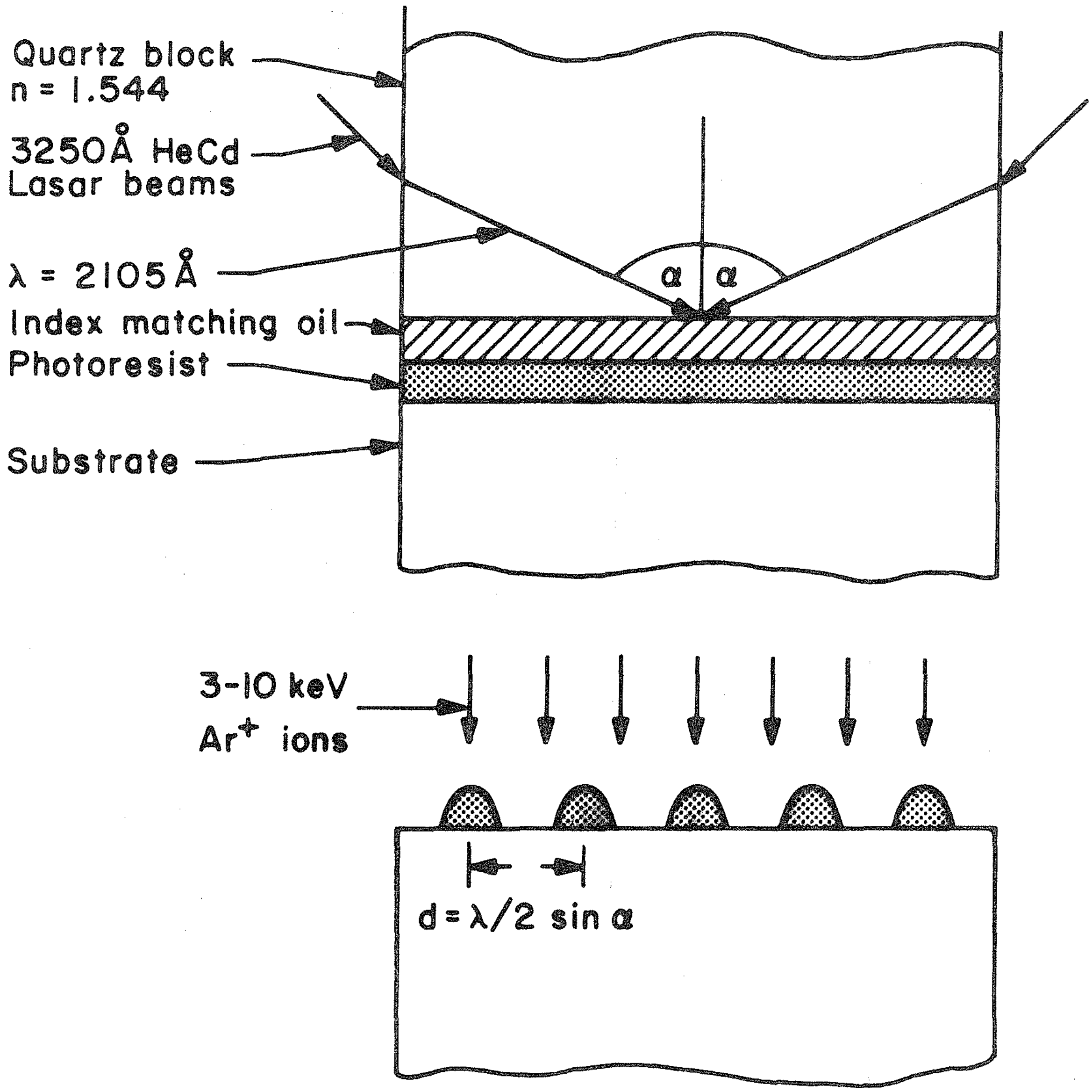

Fig. V.7 (a) Holographic exposure of photoresist through a quartz block.

(b) Ion machining of photoresist after development.

in intervals much smaller than the wavelength of the radiation to be polarized. Such a wire grid transmits radiation which has its electric field perpendicular to the lines, and reflects the radiation which is polarized parallel to the wires[15].

H. L. Garvin et al[16] have fabricated wire grid polarizers by depositing a gold film on an antireflection coated CdTe substrate. Then a photoresist mask was applied by the techniques described above, and ion beam milling was used to etch through the exposed gold down to the substrate material. The performance of this 1.1μ wire grid polarizer is shown in Fig. V.8. The polarizer has a transmission of 93% for the one polarization, an extinction ratio of 550, and a reflection of more than 99% for the other polarization.

The holographic exposure offers the advantage of small periods together with the possibility of fabrication of such a polarizer on a curved substrate to be used as a mirror. Two such mirrors in a laser cavity could form a tunable output coupling mechanism by rotating the direction of one against the other. In such a case the laser will oscillate with a polarization given by the bisector of the angle between the direction of the two polarizers, and the strength of the output coupling will be determined by the size of that angle. The wavelength at which these polarizers operate can be extended to a shorter region by the use of the super small periods described above.

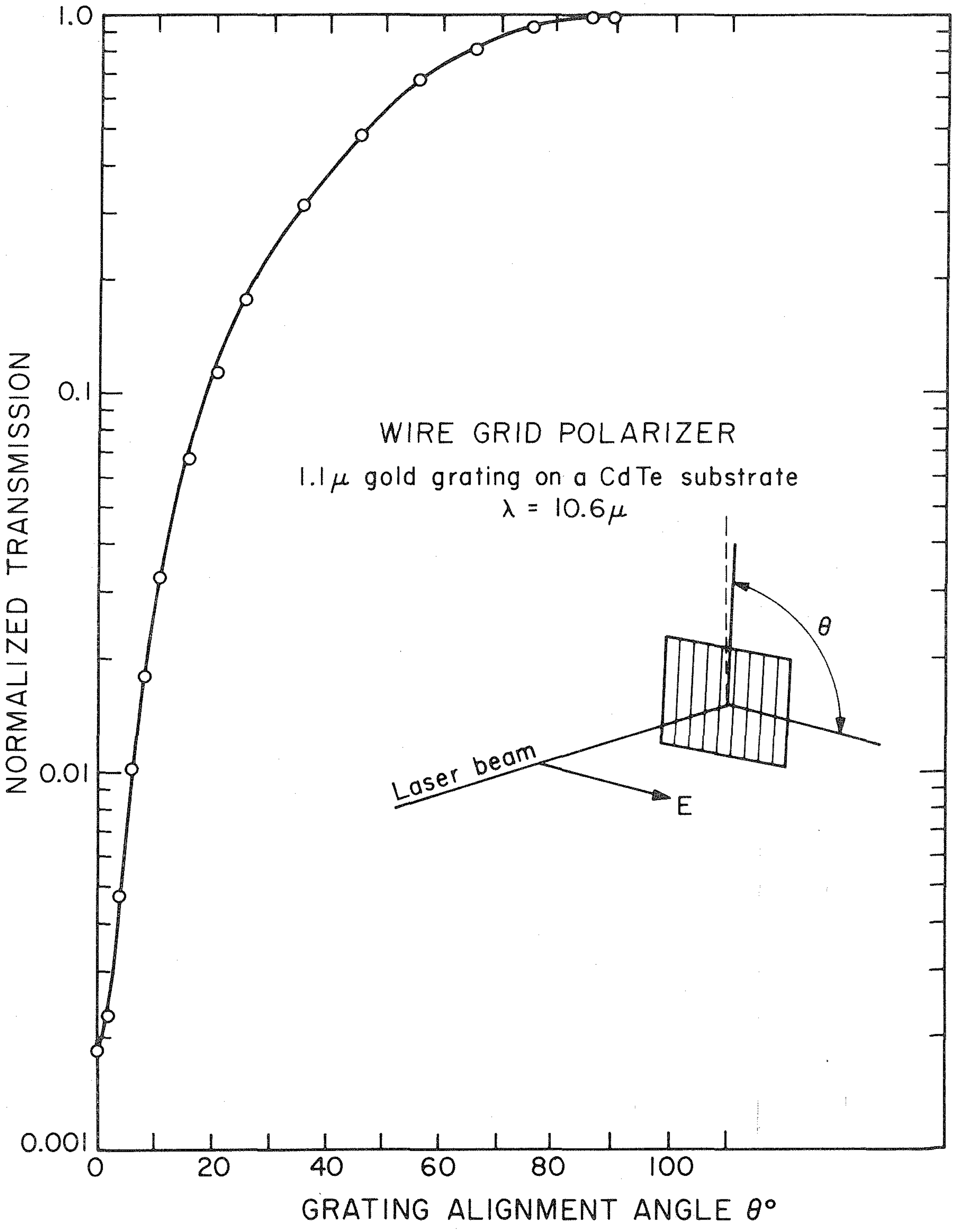

Fig. V.8 Wire grid polarizer (after Reference 16).

V.4 Optical Circuitry

Ion machining combined with either conventional photo-lithography or scanning electron lithography is very useful in the fabrication of optical circuitry. Components such as straight and curved channel waveguides, directional couplers, thin film analogs of lenses and prisms(11), etc. can be constructed by this technique. The ion beam can be used to copy structures in the exposed photoresist (or electron resist) into the guiding material, or into a specific masking material that is used whenever the guides are made by ion implantation(12,13) or diffusion(14). We shall describe here the fabrication of embedded and ridged channel guides in GaAs.

Bombardment of high free carrier concentration GaAs with protons causes defect centers in the material, which traps the free carriers and thus produces a compensated layer. The thickness of the layer is related to the energy of the protons, and for the 300 keV protons used it is 3μ. The presence of charge carriers leads to a depression of the optical dielectric constant. The difference $N_g - N_s$ in carrier density between the guide and substrate causes the dielectric constant of the guide to exceed that of the substrate by:

$$\Delta\varepsilon = \frac{(N_s - N_g)e^2}{m^* \omega^2} \qquad \text{(V.4.1)}$$

where N_s and N_g are the carrier densities in the substrate and in the guide respectively. m^* and e are the effective mass and charge of the carriers and ω is the radian optical frequency. As we shall see later this plasma contribution seems to dominate for wavelength away from the bandgap of the material. Since a gold layer 1.5μ thick can completely block the 300 keV protons used, an optical circuit can be implanted if a suitable gold mask is constructed on the surface of the GaAs substrate.

In the fabrication of channel waveguides closely spaced so as to allow directional coupling between them, we have used a conventional photographic mask. A GaAs substrate was sputter coated with a 1.8μ thick gold layer. Finally, a photoresist layer (2μ) was spin deposited and was exposed through a mask of appropriate transparent stripes. The exposed resist was developed down to the gold, to form stripes of resist with a ridge shape. The succeeding step was ion machining of the clear areas of gold down to the substrate. Figures II.4a and II.4b show the resulting gold stripes with the remainder of the photoresist on top of them. The distance between the centers of adjacent channels is about 6.3μ. The clear areas between the gold stripes are where the proton implantation takes place and the channel waveguides are formed. After the implantation the gold was removed and the samples annealed at 500°C for 10 minutes in order to reduce the optical attenuation. The optical measurements of these guides and the coupling between them is described in Chapter II.

One of the important parameters that influences these measurements is the dielectric discontinuity between the substrate and the implanted region. An estimate for this dielectric discontinuity is the plasma contribution given by (V.4.1). However according to it, the change in the index of refraction at $\lambda = 1.06\mu$ should be smaller than at $\lambda = 1.15\mu$. The measured values of the coupling coefficient K (see Chapter II) contradict that, and indicate an increase in $\Delta\varepsilon$ at 1.06μ rather than a decrease with respect to 1.15μ. Because of that, an attempt was made to measure and compare the values of the dielectric discontinuities at both wavelengths. Since it is quite difficult to measure small changes in the index of refraction that take place in such small dimensions the following method was used. The multichannel sample shown in Fig. II.4b was polished from the substrate side, and used as a phase grating by shining the laser light perpendicular to the channels. The geometry and the resulting diffraction orders are shown in Fig. V.9. Using the amplitudes of the diffraction orders for 1.15μ and 1.06μ it is possible to find the ratio between $\Delta n_{1.06\mu}$ and $\Delta n_{1.15\mu}$. It was found that

$$\frac{\Delta n_{1.06\mu}}{\Delta n_{1.15\mu}} \approx 1.1 \qquad \text{(V.4.2)}$$

This means that as the wavelength approaches the bandgap of GaAs (0.9μ) the plasma contribution is not the dominant contribution to Δn, and that additional contribution (probably because of increased bandgap tail absorption in the implanted region) starts to increase Δn. In order to derive the absolute change in the index from this measurement an estimate of the channel dimensions has to be made. Using the mask shape as shown in Fig. II.4b (width 2.4μ separation 3.9μ) and

Δn measurement

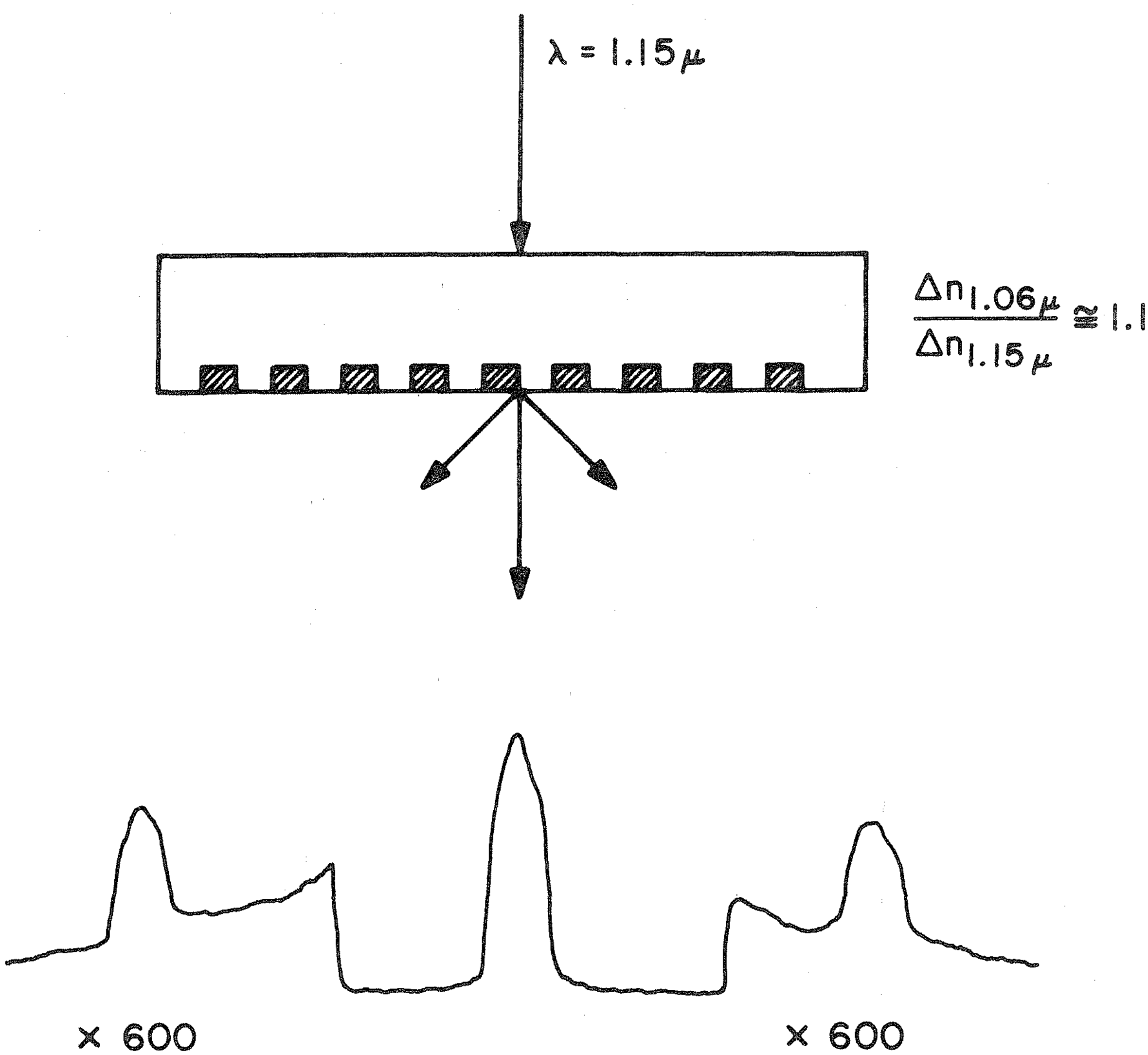

Fig. V.9 Δn measurement by use of a multichannel directional coupler as a phase grating.

a penetration depth of 3μ for the protons, the approximate values for Δn are:

$$\Delta n_{1.06} = 5.5\cdot 10^{-3} \qquad \Delta n_{1.15} = 5\cdot 10^{-3}$$

while the value calculated using the plasma contribution V.4.1 for a substrate concentration of $N_s = 2.10^{18}\ cm^{-3}$ are

$$\Delta n_{1.06} = 3.7\cdot 10^{-3} \qquad \Delta n_{1.15} = 4.3\cdot 10^{-3}$$

The agreement thus is adequate for 1.15μ only.

As can be seen in Fig. II.4b the side walls of the gold stripes are quite rough. The reason is the limited quality of the photographic mask. A better wall definition can be achieved by using one of the methods described earlier, namely, scanning electron lithography, or the holographic technique. The fact that the attenuation of the channel guides is about that of planar guides fabricated in the same substrate (about 5 cm^{-1}) indicates that the walls are smoothed out by the nature of the proton implantation and the subsequent annealing. However, rough walls are a major limitation in the fabrication of ridged guides. Therefore in the fabrication of these guides (which is shown in Fig. V.10) a mask produced by the holographic technique was used to expose the photoresist on top of the GaAs. Towards the end of the machining the sample was tilted at various angles with respect to the ion beam to ensure the effect of "ion polishing." Two examples of ridged guides are shown in Fig. II.15. The rough

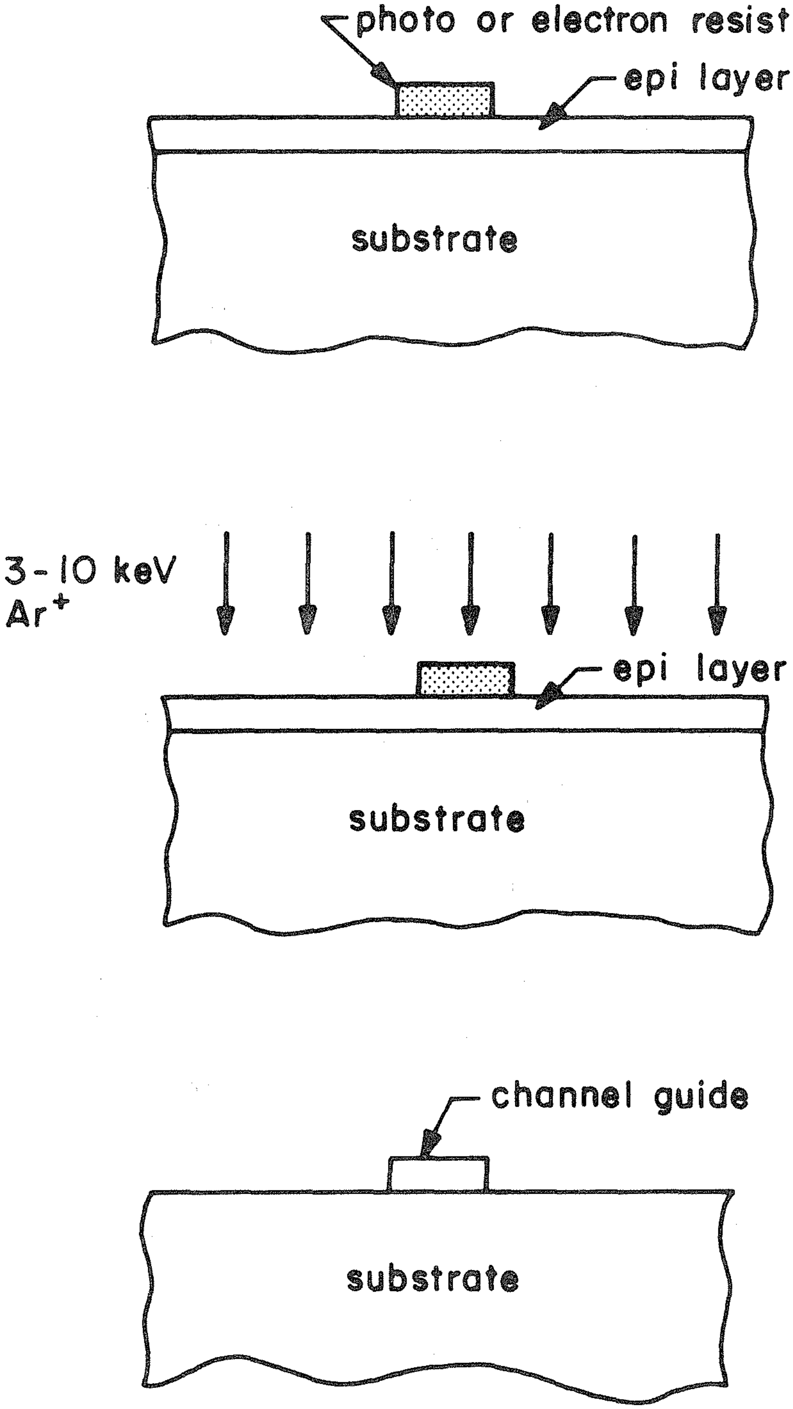

Fig. V.10 Channel waveguide fabrication by removal of superfluous sections of an epilayer by ion milling.

channel was fabricated with a conventional mask and, as can be seen in the photograph, with a photoresist which was not thick enough to protect the top of the channel. Figure II.15b on the other hand describes a guide fabricated with the use of a holographic mask and an "ion polish" at the end of the machining. The smoothness of the walls in this figure as well as of the step in Fig. III.14 indicates that ion milling can be used to fabricate optical resonators for surface lasers and terminations for waveguides (in materials that do not cleave too well) for input, output and coupling.

References for Chapter V

1. H. L. Garvin, E. Garmire, S. Somekh, H. Stoll, and A. Yariv, "Ion Beam Micromachining of Integrated Optics Components," Appl. Optics 12, 455 (1973).

2. Many applications have been cited at the Symposia on the Deposition of Thin Films by Sputtering, sponsored by the University of Rochester and Bendix Corporation, Rochester, New York, held in 1966, 1967, and 1969, and at the Conference and School Sessions on "The Elements, Techniques and Applications of Sputtering," sponsored by the Materials Research Corp., Orangeburg, New York.

3. J. E. Groell and R. D. Standley, "Sputtered Glass Waveguides for Integrated Optical Circuits," BSTJ 48, 3445 (1969).

4. H. L. Garvin, "Ion Beam Sputtering for Thin Film Deposition and High-Precision Micromachining," Proc. 3rd Symposium on the Deposition of Thin Films by Sputtering, Rochester, N. Y., pp. 4-11, September 7-10, 1969.

5. D. Marcuse, "Mode Conversion Caused by Surface Imperfections of a Dielectric Slab Waveguide," BSTJ 48, 3177 (1969).

6. M. L. Dakss, L. Kuhn, P. F. Heidrich, and B. A. Scott, "A Grating Coupler for Efficient Excitation of Optical Guided Waves in Thin Films," Appl. Phys. Lett. 16, 523 (1970).

7. H. Kogelnik and C. V. Shank, "Stimulated Emission in a Periodic Structure," Appl. Phys. Lett. 18, 152 (1971).

8. S. Somekh and A. Yariv, "Phase-Matchable Nonlinear Optical Interactions in Corrugated Thin Films," Appl. Phys. Lett. 21, 140 (1972).

9. E. D. Wolf et al, "Response of Elvacite 2041," Proc. 11th Symposium on Electron, Ion and Laser Beam Technology, Boulder, Colorado 1971.

10. R. G. Brandes and R. K. Curran, "Modulation Transfer Function of AZ111 Photoresist," Appl. Optics 10, 2101 (1971).

11. R. Shubert and J. H. Harris, "Optical Guided-Wave Focusing and Diffraction," JOSA 61, 154 (1971). Also, R. Ulrich and R. J. Martin, "Geometrical Optics in Thin Film Light Guides," Appl. Optics 10, 2077 (1971).

12. E. Garmire, H. Stoll, A. Yariv, and R. G. Hunsperger, "Optical Waveguiding in Proton-Implanted GaAs," Appl. Phys. Lett. 21, 87 (1972).

13. R. D. Standley, W. M. Gibson, and J. W. Rodgers, "Properties of Ion-Bombarded Fused Quartz for Integrated Optics," Appl. Optics 11, 1313 (1972).

14. W. E. Martin and D. B. Hall, "Optical Waveguides by Diffusion in II-VI Compounds," Appl. Phys. Lett. 21, 325 (1972).

15. J. P. Auton, "Infrared Transmission Polarizers by Photolithography," Appl. Optics 6, 1023 (1967).

16. H. L. Garvin, J. E. Kiefer, and S. Somekh, "Wire Grid Polarizers for 10.6μ Radiation," presented at the Conference on Laser Engineering and Applications, Washington, D. C., May 30 - June 1, 1973.

Appendix I: The Modes of a Planar Waveguide

The modes of the waveguide are derived by solving the wave equation and requiring the transverse components of the electric and magnetic field to be continuous across the waveguide discontinuities. In the case of the planar guide there are two kinds of solutions, TE in which the electric field is transverse and TM in which the magnetic field is transverse. For a given frequency the guide's thickness and dielectric discontinuity determines the number of guided modes. These guided modes peak inside the guide and decay exponentially outside the waveguide region. A different sort are the so-called "radiation modes" which do not decay outside the guide, but extend from $x = -\infty$ to $x = +\infty$ and are capable of carrying power away from the waveguide[1]. Let us describe now the different guided modes of the geometry shown in Fig. A.1a.

TE Modes

The field components of these modes are E_y, H_x and H_z. The field component E_y obeys the wave equation

$$\nabla^2 E_y = \frac{n_i^2}{c^2} \frac{\partial^2 E_y}{\partial t^2} \qquad i = 1,2,3 \tag{A.I.1}$$

We take $E_y(xzt)$ in the form

$$E_y(xzt) = \mathcal{E}(x)\, e^{i(\omega t - \beta z)} \tag{A.I.2}$$

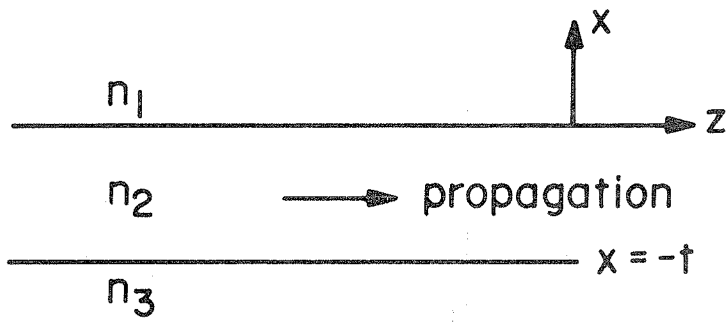

(a)

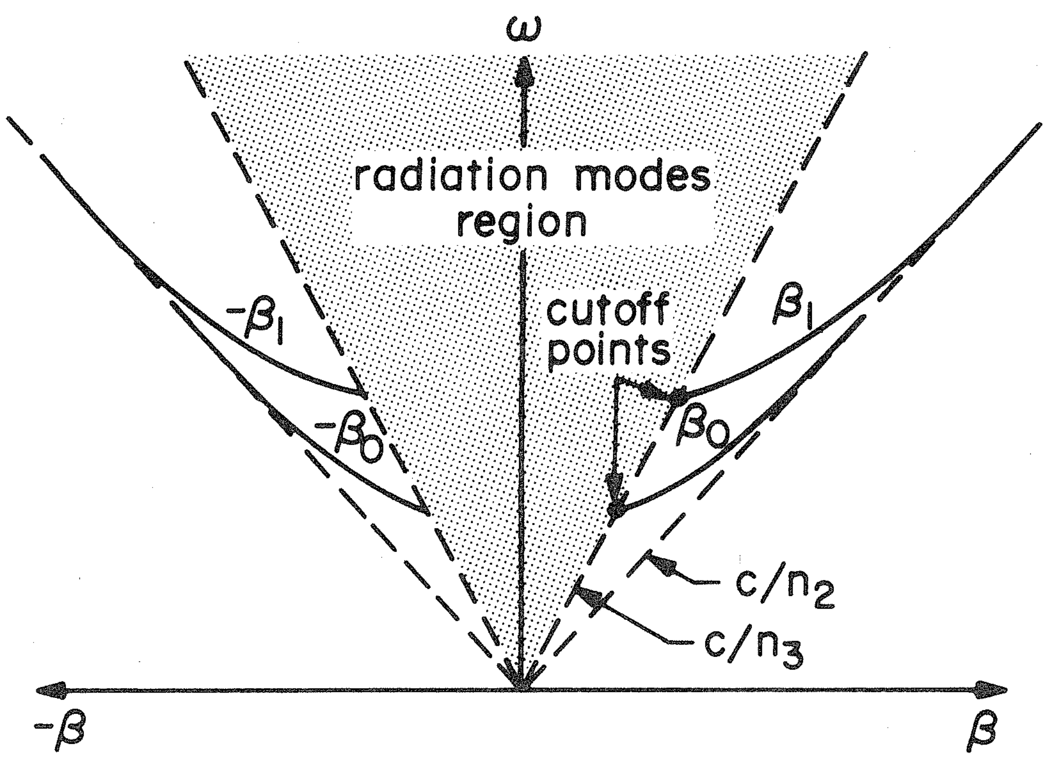

(b)

Fig. A.1 (a) The basic configuration of a planar dielectric waveguide.

(b) Mode dispersion in the above waveguide.

The mode profile $\mathcal{E}(x)$ of a guided mode is taken as:

$$\mathcal{E}(x) = \begin{cases} C\, e^{-qx} & 0 \le x < \infty \\ C[\cos(hx) - \frac{q}{h}\sin(hx)] & -t \le x \le 0 \\ C[\cos(ht) + \frac{q}{h}\sin(ht)]e^{p(x+t)} & -\infty < x \le -t \end{cases} \qquad \text{(A.I.3)}$$

which applying A.I.1 to region 1,2,3, yields

$$h = (n_2^2 k_0^2 - \beta^2)^{\frac{1}{2}} \qquad q = (\beta^2 - n_1^2 k_0^2)^{\frac{1}{2}}$$

$$p = (\beta^2 - n_3^2 k_0^2)^{\frac{1}{2}} \qquad k_0 \equiv \frac{\omega}{c} \qquad \text{(A.I.4)}$$

H_x and H_z are given by:

$$H_x = -\frac{\beta}{\omega\mu_0} E_y \qquad H_z = \frac{i}{\omega\mu_0}\frac{\partial E_y}{\partial x} \qquad \text{(A.I.5)}$$

The continuity of E_x and H_z at the interfaces requires that the various propagation constants obey the eigenvalue equation

$$ht = (m+1)\pi - \tan^{-1}\frac{h}{p} - \tan^{-1}\frac{h}{q} \qquad \text{(A.I.6)}$$

where m is the mode number ($m+1$ is the number of extrema in the mode). We would like to normalize the mode profile in such a way that it carries one unit of power (per unit length in the y direction). We thus write

$$\frac{1}{2}\int_{-\infty}^{\infty} E_y H_x^* dx = \frac{\beta}{2\omega\mu}\int_{-\infty}^{\infty} |E_y(x)|^2 dx = 1 \qquad \text{(A.I.7)}$$

Using A.I.3 we determine

$$C = 2h\left[\frac{\omega\mu}{\beta(t+\frac{1}{q}+\frac{1}{p})(h^2+q^2)}\right]^{\frac{1}{2}} \qquad \text{(A.I.8)}$$

TM Modes

The field components of these modes are H_y, E_x and E_z .

$$H_y(xzg) = \mathcal{H}(x)\ e^{i(\omega t - i\beta z)}$$

$$E_x(xzt) = \frac{i}{\omega\varepsilon}\ \frac{\partial H_y}{\partial z} = \frac{\beta}{\omega\varepsilon}\ \mathcal{H}(x)e^{i(\omega t - i\beta z)}$$

$$E_z(xzt) = -\frac{i}{\omega\varepsilon}\ \frac{\partial H_y}{\partial x}$$

The mode profile $\mathcal{H}(x)$ is taken as

$$\mathcal{H}(x) = \begin{cases} C\,\frac{h}{q}\,e^{-qz} & 0 \le x < \infty \\ C\left[\frac{h}{q}\cos(hx) - \sin(hx)\right] & -t \le x \le 0 \\ C\left[\frac{h}{q}\cos(ht) + \sin(ht)\right] & -\infty < x \le -t \end{cases} \qquad \text{(A.I.9)}$$

The eigenvalue equation is

$$ht = (m+1)\pi - \tan^{-1}\frac{h}{p} - \tan^{-1}\frac{h}{q} \qquad \text{(A.I.10)}$$

where

$$\bar{p} \equiv \frac{n_2^2}{n_3^2}\, p \qquad \bar{q} \equiv \frac{n_2^2}{n_1^2}\, q$$

The normalization condition is again

$$\tfrac{1}{2}\int_{-\infty}^{\infty} H_y E_x^{*} dx = \frac{\beta}{2\omega\varepsilon}\int_{-\infty}^{\infty} \frac{H_y^2(x)}{n^2}\, dx = 1 \qquad \text{(A.I.11)}$$

This condition determines the value of C as[2]

$$C = 2\left[\frac{\omega\varepsilon_0}{\beta\, t_{eff}}\right]^{\frac{1}{2}}$$

$$t_{eff} = \frac{-\bar{q}^2+h^2}{\bar{q}^2}\left[\frac{t}{h_2^2} + \frac{q^2+h^2}{\bar{q}^2+h^2}\,\frac{1}{h_1^2 q} + \frac{p^2+h^2}{\bar{p}^2+h^2}\,\frac{1}{h_3^2 p}\right]$$

ω-β Diagram

From the above solutions it is evident that the propagation constant in the z direction $-\beta$ of a guided mode varies between the two limits

$$n_3 k_0 \le \beta \le n_2 k_0 \qquad \text{(A.I.12)}$$

(We have assumed that $n_3 > n_1$ which is usually the case.) β is less than $n_2 k_0$ in order to allow the cosine or sine variation along the x direction inside the waveguide. Outside the waveguide the mode profile should fall exponentially and this, according to A.I.4, means $\beta > n_3 k_0$. The exact value of β as we have seen, is determined for a given frequency by the guide's thickness and the dielectric discontinuity. At cutoff β equals n_3k_0 and as the frequency increases β approaches n_2k_0. This behavior is illustrated in Fig. A.1b, for propagation in the $\pm z$ directions.

Also described in this Figure A.1b is a continuum of radiation modes whose β is less than n_3k_0. This means that the p of these modes is imaginary $(p = (\beta^2 - n_3^2 k_0^2)^{\frac{1}{2}})$ and therefore the mode does not decay exponentially in the x direction but rather oscillates from $-\infty$ to $+\infty$. Any mechanism that couples power from a guided mode into a radiation mode will thus cause a power leak from the guide[1].

References

1. D. Marcuse, "Mode Conversion Caused by Surface Imperfections of a Dielectric Slab Waveguide," Bell Syst. Tech. J. 48, 3187 (1969).
2. A. Gover, private communication.

Appendix II: The Relative Signs of the Coupling Coefficient

Let us consider two lossless modes a and b, whose amplitudes A and B are related by:

$$\frac{dA}{dz} = -i\beta_a A + k_{av} B \tag{A.II.1}$$

$$\frac{dB}{dz} = -i\beta_b B + k_{ba} A \tag{A.II.2}$$

We consider first the case where both modes carry power in the same direction. The conservation of total power at any given z is expressed by

$$\frac{d}{dz} = (AA^* + BB^*) = 0 \tag{A.II.3}$$

where

$$P_a = AA^* \qquad P_b = BB^* \tag{A.II.4}$$

Because of the plus sign in A.II.3, it is satisfied when

$$K_{ab} = -K_{ba}^* \tag{A.II.5}$$

Next we consider a case in which the two modes carry power in opposite directions. The conservation of power is described now by:

$$\frac{d}{dz}(AA^* - BB^*) = 0 \tag{A.II.6}$$

Because of the minus sign the equation is satisfied only when:

$$K_{ab} = K_{ba}^* \tag{A.II.7}$$